Proposal for the Construction of a Gamma-Ray Beam Line at the Spanish Synchrotron ALBA

December 2004

Coordination:

J.L. Taín
Instituto de Física Corpuscular, C.S.I.C.-Univ.Valencia
(email: Jose.Luis.Tain@ific.uv.es, Tel: +34 963543497, Fax: +34 963543488)

A.M. Lallena
Departamento de Física Moderna, Univ. Granada
(email: lallena@ugr.es Tel: +34 958243216, Fax: +34 958249487)

Contributors:

Institut de Ciències Fotòniques, Barcelona
M. Ebrahim

Institut d'Estudis Espacials de Catalunya, Barcelona
J.M. Alvarez, M. Hernanz, G. Martínez-Pinedo

Institut de Tècniques Energètiques, Univ. Politècnica de Catalunya
F. Calviño, M.A. Duch, Yu. Kubyshin, A. Poch, J. Sempau, F. Verdera

Departamento de Física Moderna, Univ. Granada
M. Anguiano, A.M. Lallena, J. Nieves

Departamento de Física Aplicada, Univ. de Huelva
I. Martel

Instituto Tecnológico e Nuclear, Sacavem
P. Vaz

Centro de Investigaciones Energéticas Medioambientales y Tecnológicas, Madrid
D. Cano-Ott, E. González-Romero, C. Guerrero, T. Martínez

Instituto de Estructura de la Materia, C.S.I.C., Madrid
M.J.G. Borge, C. Fernández-Ramírez, E. Moya de Guerra, O. Tengblad

Departamento de Física Teórica, Univ. Autónoma de Madrid
A. Jungclaus

Departamento de Física Atómica, Molecular y Nuclear, Univ. Complutense de Madrid
L.M. Fraile, J. López-Herraiz, J.M. Udías, J.R. Vignote

Departamento de Física Teórica, Univ. Complutense de Madrid
F.J. Llanes-Estrada

Dipartimento di Fisica, INFN-Università di Lecce
G. Co', T.M.C. Maiolo

Departamento de Física, Univ. de Salamanca
L. Roso, A. Valcarce, J. Vijande

Departamento de Física de Partículas, Univ. de Santiago de Compostela
J. Benlliure, D. Cortina, E. Casarejos, I. Durán

Departamento de Física Atómica, Molecular y Nuclear, Univ. de Sevilla
J. Gómez-Camacho, J.M. Espino, F.J. Santos-Arévalo

Centre d'Etude Spatiale des Rayonnements, Toulouse
P. von Balmoos

Instituto de Física Corpuscular, C.S.I.C.-Univ.Valencia
A. Faus, S. Martí, E. Oset, B. Rubio, J.L. Taín

Contents

List of Figures

List of Tables

Executive summary

The aim of this proposal is the construction of a beam-line at ALBA which extends the range of photon sources into the hard gamma-ray energy range. Such a beam will be used for research in Nuclear Physics and Astrophysics and for applications. Gamma-rays up to 530 MeV will be produced by Compton backscattering of laser photons on the electrons circulating in the synchrotron ring. Intensities as high as $10^7 - 10^9\ \gamma/s$ can be achieved without affecting the machine performance. The beam will have a high degree (80-100 %) of linear or circular polarization and energy resolutions of 1.5 % can be achieved. These beam characteristics can be exploited to study photo-nuclear processes of interest in basic nuclear physics, ranging from nuclear structure at low energies to sub-nucleonic degrees of freedom at high energies, and astrophysics. Additionally the beam can be used to obtain nuclear data relevant to the fields of dosimetry, radiation shielding and radiation therapy. Other applications are the non-destructive inspection of objects and their elemental analysis.

The proposed installation offers specific advantages in terms of energy range, energy resolution, intensity and polarization over existing photon facilities, of either bremsstrahlung or laser backscattering type. In particular in Europe there is no other laser backscattering installation working in this energy range.

Another benefit of the proposed installation is related to the development of the experimental nuclear physics community in Spain, which has been hampered by the lack of any installation until now.

The document is organized as follows. The first chapter presents the physics case, a selection of the proposed experiments and measurements, related to nuclear physics and astrophysics, and the industrial and medical applications. More specific details of some experiments are found in the Appendices A to F. The second chapter describes the design of the installation and the parameters of the beam which can be obtained with the present design, and these are compared to other installations. More specific details of the installation are found in the Appendices G to J. Finally, Appendix K includes a list of Spanish users of the proposed beam line.

Chapter 1

Interest of the gamma-ray source

Gamma rays are present in Nature as a consequence of natural processes. They are produced on earth in natural or induced radioactive processes. Gamma rays are also produced in astrophysical processes, reaching eventually enormous energies. They constitute in fact a signature of the processes occurring during the evolution of stars. Due to their multiple applications, methods of artificially producing γ-ray beams have been developed.

One of the more important characteristics of high energy photons is their high penetration power, which is related to their neutrality and the nature of the electromagnetic force. This is the reason for their usefulness as a tool to inspect bulky materials or industrial processes. This also explains why they may represent, directly or indirectly, a hazard to the health which has to be understood and controlled. At the same time γ-rays constitute one of the more extended and powerful methods of cancer therapy. New ways of producing high energy photons may lead to improvements of this technique.

Gamma rays may have their origin in atomic nuclei, as is the case of artificial radioactive sources employed in medicine and industry. On the other hand γ-rays can be used to explore the nucleus. As a probe of the structure and dynamics of atomic nuclei and their constituents they show many appealing properties. Intense sources of energetic γ-rays have been developed and employed to study a variety of phenomena at the nuclear and sub-nucleonic level throwing light on important questions in basic Nuclear Physics. Gamma ray induced processes in nuclei play also an important role in the understanding of stellar and explosive scenarios in Astrophysics.

The relatively weak strength of their interaction with nuclei, which is an attractive feature because in this way they perturb little the system under study, makes the experiments with photons difficult. In spite of the past efforts, there is still a lack of photo nuclear data and many questions remain open. The development of new intense sources of high energy photons with improved properties can contribute strongly to the progress in this field of research.

The γ-ray beam line that we are proposing, with its high intensity, good energy resolution and high degree of polarization opens up the possibility to conduct a wide range of experiments and measurements in basic Nuclear Physics and Astrophysics, some of which are described below and detailed in the Appendices. At the same time the installation has particular characteristics which make it useful for Industrial Applications and research on Medical Applications.

1.1 Studies in Nuclear Physics and Astrophysics

High energy photons as a probe of the structure and dynamics of atomic nuclei have particularly interesting features, consequence of the character of the electromagnetic force.

The strength of the electromagnetic interaction is much weaker than the characteristic intensity of the nuclear force, which is responsible for the major part of the nuclear properties. As a consequence, it is possible to carry out measurements without greatly disturbing the structure of the target nucleus. This constitutes a great advantage with respect to hadronic probes because, in this case, it is very complicated to separate, in a clear way, the reaction mechanism from the proper nuclear structure and dynamics. This is obviously due to the important role played by the strong interaction in both aspects.

Another characteristic of the photon-nucleus interaction is the detailed knowledge that we have about the electromagnetic interaction. Quantum electrodynamics, being the best theory we have at present, describes this interaction in an almost "exact" manner and thus one can extract quantitative, and not just qualitative, information about nuclear properties.

All these characteristics are common to both photon reactions and electron scattering. *A priori* the latter appears to be more powerful since, contrary to what happens for photon-nucleus processes, in which the momentum transferred to the nucleus is unequivocally determined by the nuclear excitation energy, electron-nucleus processes permit to vary this momentum without varying the excitation energy, and thus mapping the nuclear response over a wider phase space. On the other hand, photons are purely transverse and the nuclear response to them is of transverse character only. The longitudinal responses present in electron-nucleus scattering do not appear in photon-nucleus reactions and the interpretation of the results is easier.

Over the wide range of photon energies covered by the proposed beam line, from few MeV to more than 500 MeV, the response of the nuclear system varies considerably.

At few MeV, photons induce the movement of nucleons giving information on the nuclear wave function. This is also the energy regime of interest in Nuclear Astrophysics, around the particle evaporation thresholds important for the understanding of nuclear reactions in stars and explosive stellar events. MeV photons are at the same time a signature of the ongoing nucleosynthesis in the Universe.

Around 10-15 MeV, photons induce a strong collective motion of nucleons, the so called Giant Dipole Resonance, which dominates the response at low energies. De-excitation proceeds mainly by neutron emission, but also by charged particles. It constitutes an important contribution to the radiation hazard at accelerators.

At higher energies the photon field couples to individual nucleons and also to the mesons exchanged between nearby nucleons, carriers of the strong interaction. The latter feature is a prelude to the non-nucleonic degrees of freedom in atomic nuclei.

At still higher energies photons reveal the internal quark structure of the nucleons. In our energy window, it manifests through the excitation of the Delta resonance, which then de-excites by pion and nucleon emission.

This plethora of interesting phenomena is reflected in the range of experiments presented below.

1.1.1 Nuclear Structure and Astrophysics

The availability of an intense quasi-monochromatic and highly polarized γ-ray source of few MeV (< 10 MeV) would be extremely useful for the study of important aspects of nuclear structure and astrophysics. In principle a laser backscattering source, at difference with a bremsstrahlung source, is able to provide such a beam. Unfortunately the present design of the proposed beam line at ALBA does not allow to produce monochromatic beams below 15 MeV. This will require the development of laser sources with variable wavelength in the range 10-100 μm. The experiments presented in this subsection are not feasible at ALBA at present, but together with the desirable extension to lower energies of other experiments (see Appendix B and C) should provide a motivation for such a development.

Nuclear resonance fluorescence experiments: The Nuclear Resonance Fluorescence (NRF) or (γ,γ') reaction on bound levels maps essentially the electromagnetic dipole response of nuclei. A detailed knowledge of this response is of interest both from the nuclear physics point of view as well as with respect to astrophysics. In nuclear physics, the study of dipole properties lead to the discovery of collective modes of excitation such as the "scissors" mode or more recently the "pygmy" resonance. Of course, the NRF technique is not restricted to the investigation of collective excitations and indeed many recent NRF experiments focused on the study of two-phonon dipole excitations and their decays to one-phonon states.

In nuclear astrophysics, nuclear survival rates in hot thermal photon baths (for example in supernova explosions) are crucial for the understanding of the process of nucleosynthesis. In many cases these rates depend on photoparticle evaporation cross sections close to the threshold for (γ, n), (γ, p) or (γ, α) processes. Since most photonuclear reactions have dipole character due to the low momentum transfer of the photon, the understanding of the nuclear dipole response, especially near particle emission threshold, is of crucial importance.

Up to now, most of the NRF studies have been performed using electron generated bremsstrahlung beams. These beams suffer from the serious drawback that the photon energy spectrum is continuous and moreover has an exponentially increasing intensity with decreasing photon energy. A photon beam produced by laser backscattering with collimation in the appropriate energy range would offer three major advantages [1]: i) the nearly monochromatic photon energies would allow to selectively populate the resonant states of interest with much less uncertainty due to feeding from higher-lying states, ii) the background from nonresonant scattering would be much lower in the energy region where branches to lower-lying excited states would occur and iii) the essentially 100% linear polarization of the photon beam would lead to a much greater sensitivity of parity measurements. This latter point is the most important one since parity information is crucial for the interpretation of the observed states and the use of Compton polarimeters is limited to γ-rays below 3-4 MeV due to the energy dependence of the analyzing power of the Compton scattering process.

Photo-disintegration experiments: The study of the charged particles (mainly protons and α-particles), emitted by nuclei as a result of the absorption of gamma rays, has important implications in the study of nuclear structure, nuclear reactions and astrophysics. We shall focus

here on two specific applications (see Appendix A for more details): the investigation of the low energy continuum of weakly bound nuclei, and the investigation of reaction rates which are relevant to the astrophysical *p*-process.

In the last decade, an important fraction of the research in nuclear physics has been directed to the study of exotic nuclei. These nuclei have an excess of protons or neutrons, and therefore are unstable. The binding energies of the exotic nuclei are considerably smaller than that of the stable nuclei. This makes that the continuum of break-up states plays a very important role in the structure and in the reactions induced by exotic nuclei. In particular, the knowledge of the structure of the low-energy continuum (scattering states which are up to a few MeV above the break-up threshold) is essential to understand the properties of exotic nuclei [2]. The investigation of the break-up states in exotic nuclei is done through nuclear reactions, in which the observed cross sections are related to the continuum structure through intricate reaction mechanisms where coulomb and nuclear forces play important roles.

The experimental study of reactions such as (γ, p) and (γ, α) give direct information on the structure of the continuum. These experiments are relatively clean, in the sense that they depend only on the electro-magnetic interactions, and thus they are not sensitive to the nuclear forces. Presently, it is not possible in a facility such as ALBA to perform photo-absorption experiments on exotic nuclei. However, there is a variety of stable nuclei, which are weakly bound, such as the deuteron, ^{6,7}Li, ^{9}Be, etc. The investigation of their low-energy continuum through (γ, p) and (γ, α) reactions, complemented with their reaction cross sections, can be used to reduce the uncertainties in the theoretical models used to investigate the properties of exotic nuclei.

The study of proton-rich nuclei heavier than iron (*p*-nuclei) has a special relevance for the astrophysical *p*-process [3]. This process is responsible for the synthesis of neutron-deficient nuclei that are blocked from formation by either the *r* or *s* processes [4]. The *p*-process is essentially a sequence of (γ, n), (γ, p) or (γ, α) photo-disintegrations reactions, possibly complemented by captures of neutrons, protons or α-particles at energies typically far below 1 MeV of the Coulomb barrier in the case of charged particles.

Recent experiments have provided direct measurements of some (γ, n) reactions at the low energies of interest for the *p*-process, i.e close to the photo-disintegration threshold. One of the techniques is based on the construction of a quasi-thermal photon spectrum from a superposition of bremsstrahlung spectra with different endpoint energies [5]. As an alternative, a laser backscattering γ-ray beam could be employed. An important advantage of this approach over the bremsstrahlung approach is their more intense peaking in the energy window of astrophysical interest.

Direct measurements of photo-disintegration cross sections constitute therefore an independent set of data and the most straightforward way to constrain the calculation of the corresponding astrophysical rate. Improving the theoretical predictions for photo-disintegration rates will put *p*-process nucleosynthesis calculations on a firmer ground. As mentioned before the *p*-process takes place at very high temperatures but the nuclei involved are in a region of the nuclear chart where basic quantities like masses or β-decay rates are either known or rather reliably estimated. Experimental data on photo-reaction cross sections, even scarce, are therefore a very precious ingredient to test the validity of Hauser-Feshbach cross section calculations in the nuclear region of interest. Measurements of (γ, n) reactions on many more nuclei are certainly

necessary, but the investigation of (γ,α) and (γ,p) reactions in the energy range of interest is still a challenging prospect. In addition, the E1 and M1 γ strength functions below the particle thresholds should be addressed in direct relation to photo-reactions on nuclear excited states under stellar conditions.

1.1.2 Photo-neutron cross section measurements

Photonuclear reaction data are very important for understanding the structure and dynamics of the atomic nucleus. Moreover, photo-induced reaction cross sections are also of importance for a variety of current or emerging applications [6] like: radiation shielding design and radiation transport analysis (of particular concern are photoneutrons), calculations of absorbed dose in the human body during radiotherapy, physics and technology of fission reactors (influence on neutron balance) and fusion reactors (plasma diagnostics and shielding), activation analysis including safeguards and inspection technologies for identification of materials through radiation induced by photonuclear reactions and nuclear waste transmutation, among others.

Inspection of the "Handbook on photonuclear data for applications" [6] reveals that photonuclear data are scarce and, in many cases, discrepant. Most of the data is quite old and the discrepancies can in some cases be traced back to inaccuracies of the employed technique [7], in particular the lack of truly monochromatic γ-ray beams. The International Atomic Energy Agency (IAEA) has proposed a priority list of materials (43 elements) for which photonuclear data are needed: structural, shielding and bremsstrahlung materials (Be, Al, Si, Ti, V, Cr, Fe, Co, Ni, Cu, Zn, Zr, Mo, Sn, Ta, W, Pb), biological materials(C, N, O, Na, S, P, Cl, Ca), fissionable materials (Th, U, Np, Pu) and other materials (H, K, Ge, Sr, Nb, Pd, Ag, Cd, Sb, Te, I, Cs, Sm, Tb).

The OECD Nuclear Energy Agency has set up a Task Force for the Shielding Aspects of Accelerators, Targets and Irradiation Facilities (SATIF) which between other commitments assesses the needs of experimental data, and which in a recent meeting in Lisboa [8] recognized the value of the proposed beam line at ALBA.

Due to the lack of electric charge, neutrons are easily emitted after the absorption of photons with energies above the threshold. Accordingly this process represents a large fraction of the reaction cross-section and its determination is important. We propose to undertake a systematic revision of photoneutron measurements according to their relevance. The characteristics of the γ-ray beam line proposed at ALBA allow to measure the photoneutron cross section in the range between 15 MeV and the largest γ-ray energy of $\sim$ 500 MeV. Such a range covers down to the Giant Dipole Resonance (GDR) in the lighter nuclei (up to Cu) and extends beyond the region of excitation of the Delta nucleon resonance. It would be desirable to extend this range to lower energies in order to cover the GDR also for heavier elements. This might be possible with the development of new laser sources. See the Appendix B for details.

1.1.3 Photo-fission experiments

Fission constitutes the most clear example of a large-scale collective motion in nuclear matter where both, the nuclear structure and the dynamics of the atomic nucleus manifest. This

is the reason why fission is considered as a unique laboratory to investigate the atomic nucleus. However, the probes used to characterize the structure and the dynamics of the nucleus through fission are very often influenced by the reaction mechanism used to induce fission. In this sense, photons represent the cleanest approach since the excitation energy produced in the reaction corresponds to the initial energy of the photon, only a very small amount of angular momentum is induced and the composition of the target nucleus is not modified. However, the use of photon induced fission has been limited by the fact that the most commonly used photon facilities are based on bremsstrahlung radiation. These facilities provide a continuum spectrum of photons with a maximum energy, limiting the interest of this reaction mechanism. The quasi-monoenergetic γ-rays produced in a Compton backscattering facility overcome this limitation and justify the experimental program we propose to investigate different aspects of photo-fission that can be addressed with the present design of the γ line of ALBA. This program is organized in three experiments (see Appendix C for details):

Temperature dependence of shell effects: The different components appearing in the yields and in the kinetic-energy distributions of the fragments produced in low-energy fission are attributed to shell effects [9]. Important progress was obtained few years ago in the investigation of the influence of shell effects in fission from the electromagnetic-induced fission of more than 70 different fissile secondary beams [10]. However, very few experiments provide information on the excitation energy dependence of the different fission modes associated to shell effects. The gamma ray facility at ALBA could be used for a detailed investigation of the washing out of shell effects with excitation energy by measuring the mass or charge distributions of fission residues at different gamma energies. Since shell effects are expected to disappear around 50 MeV, the present design of the backscattering gamma line of ALBA will allow to cover the range between 16 and 60 MeV.

Multi-phonon excitations: Giant resonances in fissile nuclei decay by the competition between neutron emission and fission according to the corresponding partial decay widths, Γ_f and Γ_{xn}. Since fission probabilities increase with excitation energy, multi-phonon giant resonances should appear "enhanced" in the fission channel in comparison to single-phonon states. This effect makes multi-phonon studies in electromagnetic fission particularly attractive.

Evidences for multi-phonon giant resonances in electromagnetic fission of ^{238}U have only been presented recently [11]. However, these experiments are limited by the reconstruction of the primary excitation energy of the fissioning nucleus. The experiments proposed at ALBA can be considered as an ideal case since the primary excitation energy of the fissioning nucleus can be established with an accuracy better than 10%. In addition the high intensity of γ-rays allows to reach very low cross section processes.

Nuclear dissipation in fission: Nowadays it is well established that fission should be considered as a diffusion process above the nuclear energy-potential in the deformation coordinate. This process is not only governed by the nuclear potential but also by a dissipation coefficient representing the coupling between the intrinsic and collective degrees of freedom populated in fission [12].

The large pre-scission neutron multiplicities observed in fission induced in heavy ion collisions has been interpreted as a signature of the nuclear dissipation in fission at high excitation energies [13]. Recently a novel technique based on the use of fission induced in peripheral heavy-ion reactions at relativistic energies has been proposed [14]. The advantage of this reaction mechanism is that the excited fissioning nucleus is produced with well defined initial conditions. The γ line at ALBA offers the possibility to investigate photo-fission at high energies. The advantage of this reaction mechanism is the low amount of angular momentum induced in the collision, simplifying the description of the initial conditions of the fissioning nucleus.

1.1.4 Proton emission with polarized photons

In the last years, nucleon emission induced by electromagnetic probes, both photons and electrons scattered off nuclei, has been used as a tool to investigate the effects of different physical processes involving atomic nuclei. Among them one can mention here those due to short-range nucleon-nucleon correlations (SRC), meson-exchange currents (MEC) or final state interactions (FSI) [15].

SRC refer to those contributions which are related to the strong repulsion between two nucleons occurring when they are separated by a short distance. This effect is very well known in free nucleon-nucleon scattering and to a certain degree survives in atomic nuclei, beyond the nuclear mean field. Deviations from calculations performed in the mean field approach will inform about the role played in the nuclei by these correlations due to the nucleon-nucleon interaction.

This interaction is usually described in terms of the exchange of particles (mesons) between the nucleons. Electromagnetic probes interact with the nuclear charge and current, whose main terms are due to protons and neutrons. However, these probes can interact also with the charges and currents generated by the exchanged mesons. These are known as MEC. In light nuclei their effect is very well known. However in heavier nuclei it is obscured by the uncertainties associated to the nuclear wave function description.

FSI describe the interactions between the emitted nucleons in a given process and the residual nucleus. They are very important in many situations and in some of them they are the dominant mechanism.

Despite the interest of photon reactions for the study of the nuclear response, an analysis of the available low energy experimental data, below the pion production threshold, shows that they are old, incomplete and not accurate enough to disentangle interesting effects predicted by the theory [16]. This indicates the need of new experiments as well as theoretical efforts to implement modern realistic forces in calculations for nuclei with $A > 4$.

Photons for nuclear physics experiments are produced using *bremsstrahlung* [17] or by means of laser backscattering [18]-[21]. From the experimental point of view, one of the main problems with the photon facilities is to achieve a compromise between good energy resolution, high degree of polarization and high photon flux. This difficulty has hampered the development of the experimental programs. However, laser backscattering technique allows one to reach

simultaneously these three designing goals [22].

In the initial phase we propose a set of experiments to be done on ^{12}C and ^{16}O nuclei (see Appendix D for more details). Their nuclear structure requires, in principle, a simple description and permits a good control of the theoretical uncertainties. In particular, we are interested in one-proton emission processes with both polarized and unpolarized photons with energies in the range 60-150 MeV.

Almost all the experimental work relative to one-nucleon photo-emission in medium-heavy nuclei, has been done with unpolarized photons [15]. As far as we know, the $(\vec{\gamma}, p)$ reaction has been studied only by Yokokawa *et al.* in 1988 on the ^{12}C target at excitation energies between 40 and 70 MeV [23].

We have performed a series of calculations within a model which takes into account SRC, MEC and FSI simultaneously [24] and, as a results, we have found that the so-called asymmetry, which essentially measures the difference between the cross sections for two orientations of the polarization of the incident photons, is particularly sensitive to MEC contributions [25]. Also a certain sensitivity to SRC is observed.

At a later stage we want to extend the experimental program to study also:

- one-neutron emission, in order to elucidate the discrepancy between theory and experiment in the cross sections in comparison with those of the one-proton emission process.
- one-nucleon emission with other polarization degrees of freedom, such as the polarization of the target nucleus or the measuring of the polarization of the outgoing nucleon.
- two-nucleon emission, which, in recent years, has been investigated with unpolarized and polarized photons, and which we have found to be sensitive to the parametrization of MEC chosen [13].

1.1.5 Photon-nucleon experiments

The study of baryon excitations through pion photoproduction is of great interest from both theoretical [26, 27, 28] and experimental [29, 30] points of view. The new generation of high precision experimental facilities have provided new insight in the problem, permitting the isolation of each resonant contribution from the background due to other resonances and the non-resonant contributions (v.g. light meson exchange) and providing new data, specially in the $\Delta(1232)$ region. Because of its energy range and relatively high intensity, the proposed beam line at ALBA will be an excellent tool for this research.

In the energy range from treshold to 500 MeV, we propose the measurement of Compton scattering $(\vec{\gamma},\gamma)$ and pion photoproduction $(\vec{\gamma},\pi)$ on free protons, deuteron, ^{3}He, and ^{4}He (see Appendix E for further details).

Compton scattering and pion photoproduction on free protons would constitute a first step in the development of the experimental programme. The idea is to complete the experiments performed over the last years, specially at LEGS [31] and MAMI [32], by increasing the database

of multipoles and polarization observables in order to solve, for example, the important discrepancies between the last analysis at Brookhaven and experimental data obtained at Mainz over the last decade [31].

The use of nuclear targets instead of free protons reduces the energy transferred to the recoiling system and thus increases the energy available to excite nucleon resonances. Furthermore, the Fermi motion of nucleons inside nuclei widens up even more the range of kinematically allowed processes, for a given photon energy. Additionally, targets as ^{3}He are easily polarized, adding new observables to study. On the other hand, the recoiling system being complex, many different reaction channels are open, but suitable coincidence techniques would help isolating the particular channel of interest.

Experiments on the deuteron would permit to establish the influence of $\Delta(1232)$ in its structure [33]. A combination with previous analysis on protons allows to obtain information about the neutron. At present, the amount of experimental information is really small and the majority of the experiments were performed many years ago [30].

As far as we know, there are no pion photoproduction experiments on ^{3}He with polarized photons in the energy range of γ-ALBA. Nevertheless, this process is of great interest at present thanks to realistic three-body models [34] developed in the last years and Compton [35] and pion photoproduction models [28] with consistent $\Delta(1232)$ description. In this way we would be able to perform an acceptable theoretical analysis of the influence of the $\Delta(1232)$ in systems like ^{3}He and few body systems.

^{4}He is a high density and highly bound nucleus, compared to any other light nucleus. Thus, pion photoproduction appears as an excellent mechanism to study the pion in the nuclear medium. Because of the ^{4}He spin ($J = 0$), the contribution of photons with polarization parallel to the scattering plane is zero and the asymmetry $\Sigma = -1$ for all energies. There are experimental data in the energy range of 200 to 300 MeV [36] where no violation of $\Sigma = -1$ was found. High precission measurements of possible violations of this asymmetry in a broad energy range seem to be a suitable way to search for internal structure effects in ^{4}He.

In the energy range expected for γ-ALBA the production of further mesons can be envisioned. The threshold for two-pion production is well below 500-600 MeV. This channel has been studied in the past, but precision studies would be possible at γ-ALBA. An exotic channel is readily available through double-charged pion production $\gamma Z \to (Z-2)\pi^+\pi^+$. This isospin $I = 2$ channel cannot hold a molecular-type resonance as the strong interaction is repulsive [37], but γ-ALBA could exclude the presence of any intrinsic narrow state (automatically a tetraquark) such as the much debated pentaquark in a flavor-exotic KN wave. Exotic spectroscopy is expected to come to the forefront of research in the upcoming years [38].

On the contrary, the production of $I = 0$ pion pairs is guaranteed to give a window into the established physics of the σ resonance [$f_0(400-1200)$], a broad structure in $\pi\pi$ scattering and final states that is expected to have a large molecular-type tetraquark component [39]. The connection of this resonance to the Roper [40] can also be studied for example by the two-pion plus nucleon decay of the Roper.

1.1.6 Deeply-bound pionic atoms

It has become increasingly clear in the last few years that understanding the pion-nucleus interactions at the lowest energies is of fundamental importance. At these low energies the connection to the underlying symmetries of hadronic interactions is most direct.

There are two ways of studying the pion-nucleus interaction at low energies, pion scattering and pionic-atoms. In many ways pionic-atoms provide the cleanest information. Pions are in specific orbital angular momentum states with respect to the nucleus and the strong interaction shifts of these states and their widths provide direct information about the $\pi-$nucleus interaction in those individual $l-$states.

The production of deeply bound pionic atoms not reachable with standard $X-$ray techniques has been an experimental challenge. It has been realized for several years now that more experimental data for deeper bound levels in heavy nuclei is needed in order to understand the situation. Ideally, one would like to be able to study the 1s,2p,2s,... levels in heavy nuclei like lead. Unfortunately, as mentioned earlier, one can not hope to populate these deeply bound states by cascade. The pion is absorbed long before it gets down to these states. This problem has presented theorists and experimentalists with one of the greatest challenges in pion-physics. How to populate these states? How to identify them? How to measure their widths?

The list of suggestions to produce directly these states, without going through a cascade as in the $X-$ray technique is long: resonant production by photons or protons, several reactions as (e,e'), (n,p) , (π^-,π^+), (γ,π^+), (Σ^-,Λ), (n,d), (π^-,γ), $(d,^3\mathrm{He})$, $(p,^2\mathrm{He})$ (for details see for instance Ref. [41] and [42] and references therein). The observation of such states and the precise measurement of the energy and width would provide valuable information on the details of the pion nuclear interaction, like the density dependence or isospin dependence of the absorption mechanisms, the strength of the real part of the repulsive $s-$wave part of the pion-nucleus potential, or on the possibility of partial restoration of chiral symmetry in the nuclear medium [43].

Several experiments have pursued the detection of deeply bound pionic states in different laboratories, by using some of the above suggestions: TRIUMF [44]– [47], Jülich [48], Indiana Cyclotron [49], LAMPF [50], RCNP [51] and GSI [42], [52]– [55].

The reaction we propose for the gamma-ray beam line at ALBA is [56]

$$\gamma + {}^AZ \rightarrow \pi^+ ({}^AZ\pi^-_b)$$

Since the reaction is two-body $\rightarrow$ two body, the π^+ energy is fixed for a certain scattering angle in the laboratory system and the creation of the π^- bound state will be identified as a peak in $d\sigma/d\Omega dE(\pi^+)$ over a background of inclusive (γ,π^+) cross section. The energy resolution should be of the order of 0.5 MeV, since one is talking about pionic states with $\Gamma \approx 0.35$ MeV and separation between levels of around 1-1.7 MeV, for the most bound states of heavy nuclei in the Pb region. The reaction is driven by the $\gamma N\Delta\pi^-$ Kroll-Ruderman term, which is sizeable since it is independent of the π^- (bound) momentum. On the other hand, the γ energy can be tuned to place the Δ on shell, thus magnifying the signal. We have found that γ-ray energies around 450 MeV are best. The unique feature of the proposed beam line at ALBA is that we can achieve the necessary resolution using the Nd:YAG laser in the 3rd harmonic (417 MeV) with collimation. Given its high interest, we propose to perform this challenging measurement.

1.1.7 Calibration of gamma-ray instruments for Nuclear Astrophysics

Nuclear astrophysics relies on gamma-ray line astronomy, mainly in the MeV range, to test its predictions. Some examples of gamma-ray lines already detected are the 511 keV line, tracing electron-positron annihilation in the interstellar medium and in the proximity of very compact objects such as black holes or neutron stars, the 1.809 MeV line, showing the galactic sites of the radioactive decay of the ^{26}Al isotope, or the 1.157 MeV line, coming from ^{44}Ti decay in young supernova remnants. However, some other gamma-ray lines still remain elusive, as for instance those emitted during supernova and nova explosions (i.e., ^{56}Co lines at 847 keV and 1.238 MeV, ^{7}Be line at 478 keV or ^{22}Na line at 1.275 MeV). Their detection is the only way to trace the nucleosynthesis of radioactive isotopes during these explosions, and thus to understand their explosion mechanism. Since supernovae are the major sources of the elements in the Universe, the knowledge of their nucleosynthetic activity is a really relevant topic for astrophysics.

The reason for the very rare detections of cosmic gamma-ray lines is that the MeV range faces important challenges from the instrumental point of view. The present generation of gamma-ray instruments makes use of geometrical optics - shadowcasting in modulating aperture systems - or quantum optics - Compton scattering. This kind of instruments is faced with the problem that *bigger does not necessarily mean better*. The reason for this apparent contradiction is that the collection area in traditional gamma-ray telescopes should be roughly equal to the detection area. Therefore, the larger the collection area, the larger the detection volume and thus the higher the instrumental background. This means that significant improvements in sensitivity need huge instruments, too expensive for space missions. An innovative concept for detecting gamma-rays in the MeV range, which overcomes this problem and allows for unprecedented sensitivities consists of focusing the gamma-rays from a large collection area onto a small detector volume [57]-[59].

The way to do this consists of taking advantage of the phase information of the photons. Gamma-rays can interact coherently inside a crystal lattice provided that angles of incidence are very small. Diffraction lenses have demonstrated their potential in laboratory measurements up to several hundred keV, as well as in stratospheric balloon flights, in the framework of the project CLAIRE. This project, developed at *Centre d'Etude Spatiale des Rayonnements* (CESR), was born to prove the principle of a Laue diffraction lens for nuclear astrophysics. The natural continuation is a project for a space mission named MAX (for Max von Laue). This mission concept proposes a space-borne crystal diffraction telescope, featuring a Laue lens able to focus in two energy bands, relevant for nuclear astrophysics (450-540 keV and 800-920 keV).

Last but not least: there is an increasing interest in the high-energy astrophysics community in the use of polarimetry in the MeV range as an important diagnostic tool for the nature of the cosmic sources of gamma-rays. Recent measurements with the RHESSI satellite have detected polarization in a gamma-ray burst [60].

The gamma ray beam line proposed at ALBA would be very well suited for the calibration of gamma-ray instruments for astrophysical observations, particularly the γ-ray lens. It would allow for the characterization of the crystals to be used to build the lens, a necessary step to make the whole project feasible. The experimental setup planned will be based on that used at

lower energies in the APS at Argonne National Laboratory some years ago [61] (see Appendix F for details). There is not at present any other European facility offering this unique opportunity for getting an intense, highly collimated and polarized beam in the MeV energy range

1.2 Applications in Industry and Medicine

Apart from the interest of the proposed beam line for basic research in nuclear physics and astrophysics, the availability of intense collimated γ-ray beams of several MeV represents a unique opportunity for a number of different applications in industry and medicine. These applications include industrial radiography and tomography, element identification, defect analysis, radiation damage testing, dosimetry and cancer therapy.

At present, these applications are based mainly on broad energy range bremsstrahlung beams or radioactive sources. The applied bremsstrahlung beams range from the low energy conventional X-ray tubes to the tenths of MeV end point energies reached with linear electron accelerators. The intensity provided by this sources diminishes inversely proportional to the γ-ray energy and the use of filters provides only a limited amount of monochromatization. Gamma ray radioactive sources can provide monochromatic beams but the highest energy available, 1.17 and 1.33 MeV from ^{60}Co, is rather modest.

Using a high power (1 kW) CO_2 laser at the proposed beam line an intense ($> 10^9 s^{-1}$) naturally collimated (few millimeters) beam with an end point energy of 16 MeV can be obtained. The variation of intensity with γ-ray energy is at most a factor of two, and using suitable collimators one can select low energy portions or high energy portions of the γ-ray spectrum, including a quasi monochromatic (200 keV FWHM) 16 MeV beam with a spatial extend of less than one millimeter.

1.2.1 Industrial applications

The use of γ-rays for non destructive inspection and analysis of manufactures and materials is rather extended nowadays. The unique characteristics of the beam generated at the proposed beam line would provide enhanced performances and would allow the use of new techniques.

Radiographic imaging: Transmission gamma-ray radiography and computed tomography (CT) has the advantage over the X-ray equivalent techniques, of the stronger penetration allowing the examination of larger pieces of material. Monochromatic sources are preferred since they provide higher image definition, so that ^{137}Cs and ^{60}Co radioactive sources are commonly used. However, it has been demonstrated [62, 63] the superiority of laser backscattering γ-ray beams with energies in the range 10-20 MeV to examine large metallic pieces and composites with resolutions of the order of less than one millimeter. This is related to the fact that the attenuation coefficient of photons in matter has a minimum around that energy. The quasi monochromatic 16 MeV beam at ALBA will be very useful to inspect bulky metallic industrial pieces (as motors) or composites (as concrete blocks). The usefulness of other imaging techniques as the Compton backscattering tomography [64] will need to be explored. An interesting possibility

to consider would be the use of positron emission tomography [65], but instead of using radioactive tracers utilizing the fact that for γ-rays of several MeV the production of e^-e^+ pairs becomes increasingly important. The subsequent annihilation of the positron in two 511 keV photons can be registered to reconstruct its position. Alternatively only one of the photons can be detected with an arrangement similar to those used in Compton backscattering tomography [66]. This would have the advantage of the higher energy and monochromaticity of the annihilation photon which provides better image definition. Additionally one expects better contrast also since the pair production process depends on Z^2 while the Compton process depends on Z.

Elemental analysis: Gamma ray sources are also the basis for non destructive analytical techniques to investigate the elemental composition of bulky pieces of material. Photon induced X-ray fluorescence with several MeV bremsstrahlung beams has been utilized [67] to detect traces (200 ppm) of heavy elements in materials. With the use of the continuous beam provided by the proposed beam line, detection limits of one part per million can be reached. Nuclear resonant fluorescence, absorption from a continuum and emission of nucleus specific gamma-rays from bound states, can be also employed to study the composition of materials. The high intensity, nearly flat spectrum and the energy range of the proposed beam is ideally suited for this kind of measurements. Better signal to background ratios, that is higher sensitivity, can be achieved through the population of isomeric states after the photon absorption [68] which allows activation measurements. For γ-rays above the particle emission threshold (5-10 MeV) a new possibility opens through the creation of unstable nuclei which emit characteristic radiation. It has been shown [67] that this allows the detection of some important elements with activation measurements not accessible otherwise. All these analysis techniques are of interest in a variety of fields like mining industry, geology, edafology and environmental sciences, art and archeometry, etc.

Defect analysis: We mentioned above the fact that γ-rays of several MeV generate positrons through the pair creation process. This opens the possibility to employ positron annihilation spectroscopy to study defects in crystals, metals, alloys and polymers [67]. The conventional technique employs radioactive positron sources which have a limited range in matter, an therefore is restricted to very thin materials or surface studies. The internal production of positrons with high energy γ-rays allows to study materials of considerable thickness. The measurement of the Doppler broadening of the 511 keV annihilation radiation gives information on the momentum distribution of the electrons in the sample which is related to the amount of point defects, voids or dislocations.

1.2.2 Medical applications

Cancer therapy: Gamma ray beams are used for the treatment of deep-seated tumors which are inoperable in many cases. Currently the treatments are based on bremsstrahlung beams of tenths of MeV end point energy. The use of a monochromatic beam with an energy in the range of the bremsstrahlung end point energies would have advantages from a clinical point

of view: for a similar therapy efficiency, they will deposit at the entrance (skin) of the patient lower doses reducing the morbidity of the treatments. On the other hand, the small size of laser backscattering beams makes them particularly interesting to perform radiosurgery in regions of difficult access such as the brain. It has been theoretically shown [69] that a monochromatic laser backscattering beam, as the one we can obtain at the proposed beam line, would provide a great improvement on this type of therapy, with a performance similar to treatments with 200 MeV protons. We propose to undertake a detailed study of related issues at ALBA.

Novel ideas for therapy treatments based on high energy quasi monochromatic gamma rays have been also advanced. For example [70] the use of high Z metallic implants, for example made of gold, close to the tumor will enhance the local dose through the production of electron-positron pairs. Additionally through (γ,n) reactions radioactive nuclei can be formed with suitable characteristics (as will be the case for gold producing ^{196}Au with $T_{1/2} \sim 6$ d and $E_\gamma \sim 350$ keV) to become *de facto* brachyterapy sources. Another idea [71] is to exploit the emmited neutrons as local sources for boron capture neutron therapy. These and similar issues can be explored as well at the proposed beam line.

Dosimetry: Dose measurements during or after photon therapy with good spatial resolution would be desirable from the clinical point of view but are currently not feasible. One possibility to accomplish this goal would be the photo-activation of positron emitters during treatment, associated with high spatial resolution Positron Emission Tomography (PET) [72]. Candidate isotopes for this technique could be: a) the long lived ^{26}Al which has a short lived isomeric state decaying by positron emission, which can be populated indirectly after photon absorption, b) the relatively long lived ^{48}Cr which can be excited by photons into a proton emitting resonance populating the short-lived β^+-unstable ^{47}V, and c) the relatively short lived ^{114}Te which in a similar manner populates the long-lived β^+-unstable ^{113}Sn. The first two can be used for time-differential on-line monitoring and the latter for post treatment integral dose measurements. The feasibility of this method can be investigated at the proposed γ-ray beam line.

Bibliography

[1] N. Pietralla *et al.*, Phys. Rev. Lett. **88** (2002) 012502.

[2] M. V. Andrés and J. Gómez-Camacho, Phys. Rev. Lett. **82** (1999) 1387-1390.

[3] M. Arnould and S. Goriely, Phys. Repts. **384**, 1 (2003).

[4] G. Wallerstein, *et al.*, Rev. Mod. Phys. **69**, 995 (1997).

[5] H. Utsunomiya, P. Mohr, A. Zilges, and M. Rayet, Nucl. Phys. A (2004), in press.

[6] Handbook on photonuclear data for applications, IAEA-TECDOC-1178 (2000).

[7] B.S.Ishkhanov *et al.*, Proceedings of the 10th International Seminar "Electromagnetic Interactions of Nuclei at Low and Medium Energies" (Moscow, April 16 - 18, 2003). Institute for Nuclear Research of the Russian Academy of Sciences. Moscow, Russia, ISBN 5-944274-012-7 (2004) 5.

[8] http://www.nea.fr/html/science/docs/2004/nsc-doc2004-10.pdf

[9] M. Göppert-Mayer, Phys. Rev. 74 (1948) 235

[10] K.-H. Schmidt et al., Nucl. Phys. A 665 (2000) 221

[11] S. Ilievski et al., Phys. Rev. Lett. 92 (2004) 112502-1

[12] H.A. Kramers, Physika VII 4 (1940) 284

[13] A. Gavron et al. Phys. Rev. Lett. 57 (1981) 1255

[14] B. Jurado et al., Phys. Rev. Lett. 93 (2004) 072501

[15] S. Boffi, C. Giusti, F.D. Pacati and M. Radici, *Electromagnetic Response of Atomic Nuclei* Clarendon Press, 1996.

[16] G. Orladini, Nucl. Phys. A 737 (2004) 210.

[17] `http://www.kph.uni-mainz.de/B1/`

[18] `http://www.legs.bnl.gov/`

[19] http://higs.tunl.duke.edu/

[20] http://www.cerncourier.com/main/article/39/6/14

[21] http://www.rcnp.osaka-u.ac.jp/Divisions/np1-b/

[22] A.M. Sandorfi. *Polarized Photon Facilities - Windows to New Physics* in Baryons'95: Proceedings of the 7^{th} International Conference on the Structure of Baryons, Santa Fe, USA (1995). Editors: W. Weise, B.F. Gibson, P.D. Barnes and J.B. McClelland (World Scientific, 1996).

[23] J. Yokokawa *et al*., J. Phys. Soc. Jpn 57 (1988) 695.

[24] S.R. Mokhtar, G. Co' and A.M. Lallena, Phys. Rev. C 62 (2000) 067304; G. Co' and A.M. Lallena, Ann. Phys. (N.Y.) 287 (2001) 101; S.R. Mokhtar, M. Anguiano, G. Co' and A.M. Lallena, Ann. Phys. (N.Y.) 292 (2001) 67; M. Anguiano, G. Co' and A.M. Lallena, J. Phys. G: Nucl. Part. Phys. 29 (2003) 1; M. Anguiano, G. Co', A.M. Lallena and S.R. Mokhtar, Ann. Phys. (N.Y.) 296 (2002) 235; M. Anguiano, G. Co' and A.M. Lallena, Nucl. Phys. A 744 (2004) 168.

[25] T.A.C. Maiolo, *Fotoni polarizati nello studio della struttura del nucleo atomico*. Tesi di Laurea. Universita' di Lecce. 2004.

[26] M. Benmerrouche, R.M. Davidson, and N.C. Mukhopadhyay, Phys. Rev. **C 39**, 2339 (1989). R.M. Davidson and N.C. Mukhopadhyay, Phys. Rev. **D 42**, 20 (1990).

[27] R.L. Walker, Phys. Rev. **182**, 1729 (1969). M.G. Olsson and E.T. Osypowski, Phys. Rev **D 17**, 174 (1978). S. Nozawa, B. Blankleider, and T.-S.H. Lee, Nucl. Phys. **A 513**, 459 (1990). R.M. Davidson, N.C. Mukhopadhyay, and R.S. Wittman, Phys. Rev. **D 43**, 71 (1991). H. Garcilazo and E. Moya de Guerra, Nucl. Phys. **A 562**, 521 (1993). M. Vanderhaeghen, K. Heyde, J. Ryckebusch, and M. Waroquier, Nucl. Phys. **A 595**, 219 (1995). T. Feuster and U. Mosel, Nucl. Phys. **A 612**, 375 (1997). D. Drechsel, O. Hanstein, S.S. Kamalov, and L. Tiator, Nucl. Phys. **A 645**, 145 (1999).

[28] C. Fernández-Ramírez, E. Moya de Guerra, and J.M. Udías, *Pion Electro- and Photoproduction on Nuclei in a Lagrangian Approach*. 6^{th} Workshop on Electromagnetically Induced Two-Hadron Emission, Pavia, Italy (2003). C. Fernández-Ramírez, E. Moya de Guerra, and J.M. Udías, in preparation.

[29] R.A. Arndt, R.L. Workman, Z. Li, and L.D. Roper, Phys. Rev. **C 42**, 1853 (1990), Phys. Rev. **C 42**, 1864 (1990). R.A. Arndt, I.I. Strakovsky, and R.L. Workman, Phys. Rev. **C 53**, 430 (1996). R.A. Arndt, W.J. Briscoe, R.L. Workman, and I.I. Strakovsky, SAID database, **http://gwdac.phys.gwu.edu**

[30] K. Ukai and T. Nakamura. *Data Compilation of Single Pion Photoproduction below 2 GeV. INS-T-550* (1997). **http://ccwww.kek.jp/databank/index_e.html**

[31] G. Blanpied *et al.*, Phys. Rev. **C 64**, 025203 (2001).

[32] R. Beck *et al.*, Phys. Rev. Lett. **78**, 606 (1997).

[33] H. Garcilazo and E. Moya de Guerra, Phys. Rev. **C 49**, R601 (1994). H. Garcilazo and E. Moya de Guerra, Phys. Rev. **C 52**, 49 (1995).

[34] A. Kievsky, M. Viviani, and S. Rosati, Nucl. Phys. **A 551**, 241 (1993), Nucl. Phys. **A 577**, 551 (1994). W. Glöckle, H. Witala, D. Hüber, H. Kamada, and J. Golack, Phys. Rept. **274**, 107 (1996). E. Garrido, D.V. Fedorov, and A.S. Jensen, Phys. Rev. **C 55**, 1327 (1997). E. Nielsen, D.V. Fedorov, A.S. Jensen, and E. Garrido, Phys. Rept. **347**, 373 (2001).

[35] V. Pascalutsa and D.R. Phillips, Phys. Rev. **C 67**, 055202 (2003).

[36] V. Bellini *et al.*, Nucl. Phys. **A 646**, 55 (1999).

[37] J.E.F.T. Ribeiro, Z. Phys. **C 5**, 27 (1980).

[38] F. J. Llanes-Estrada, eConf **C0309101**, FRWP011 (2003). **arXiv:hep-ph/0311235**

[39] A. Gómez Nicola and J.R. Peláez, Phys. Rev. **D 65** 054009 (2002). **arXiv:hep-ph/0109056**

[40] H. Garcilazo and A. Valcarce, Phys. Rev. **C 68**, 035207 (2003). J. Vijande, P. González, H. Garcilazo, and A. Valcarce, Phys. Rev. **D 69**, 074019 (2004).

[41] J. Nieves and E. Oset, Phys. Lett. **B282** (1992) 24.

[42] H. Gilg et al., Phys. Rev. **C62** (2000) 025201.

[43] E.E. Kolomeitsev, N. Kaiser and W. Weise, Phys. Rev. Lett. **90** (2003) 092501.

[44] M. Iwasaki et al., Phys. Rev. **C43** (1991) 1099.

[45] T. Yamazaki, Phys. Scrip. **48** (1993) 169.

[46] A. Trudel et al., TRIUMF E628 experiment, TRIUMF progress report, 1991 (unpublished); T. Yamazaki, Nucl. Phys. **A553** (1993) 221c.

[47] K.J. Raywood et al., Phys. Rev. **C55** (1997) 2492.

[48] H. Machner, talk at Topical Conf. on Particle production near threshold (Indiana 1990), Eds. H. Nann and E.J. Stephenson, AIP Conf. Proc. no. 221, p.232.

[49] G.T. Emery, talk at Topical Conf. on Particle production near threshold (Indiana 1990), Eds. H. Nann and E.J. Stephenson, AIP Conf. Proc. no. 221, p.192.; G.T. Emery IUCF Cooler experiment No. 02.

[50] K.K. Seth et al., Research Proposal at LAMPF, June 1992 (unpublished).

[51] N. Matsuoka et al., Phys. Lett. **B359** (1995) 39.

[52] T. Yamazaki, R.S. Hayano, H. Toki and P. Kienle, Nucl. Instrum. Methods **A292** (1990) 619.

[53] T. Yamazaki et al., Z. Phys. **A355** (1996) 219.

[54] H. Geissel et al., Phys. Rev. Lett. **88** (2002) 122301.

[55] K. Suzuki et al., Phys. Rev. Lett. **92** (2004) 072302.

[56] J. Nieves and E. Oset, Phys. Lett. **B244** (1990) 368.

[57] P. von Ballmoos *et al.* SPIE Proc. 5168 (2004) 482

[58] P. von Ballmoos *et al.* New Astron. Rev. 48 (2004) 243

[59] H. Halloin *et al.* SPIE Proc. 5168 (2004) 471

[60] W. Coburn and S. Boggs Nature 423 (2003) 415

[61] A. Köhnle *et al.* Nucl. Instr. Meth. A 416 (1998) 493

[62] H. Toyokawa *et al.*, Rev. Sci. Instr. 73 (2002) 3358

[63] H. Toyokawa *et al.*, Proc. 2003 Particle Accelerator Conference, Portland 2003

[64] P. Zhu *et al.*, Meas. Sci. Technol. 7 (1996) 281

[65] D.J. Parker *et al.*, Nucl. Inst. Meth. Phys. Res. A 348 (1994) 583

[66] G. Harding *et al.*, Nucl. Inst. Meth. Phys. Res. A 398 (1997) 409

[67] F.A. Selim *et al.*, Nucl. Inst. Meth. Phys. Res. A 495 (2002) 154

[68] A.P. Tonchev *et al.*, Nucl. Inst. Meth. Phys. Res. A 422 (1999) 510

[69] B. Girolami *et al.*, Phys. Med. Biol. 41 (1996) 1581

[70] K.J. Weeks, Nucl. Inst. Meth. Phys. Res. A 393 (1997) 544

[71] P.G. O'Shea *et al.*, Nucl. Inst. Meth. Phys. Res. A 375 (1996) 530

[72] J. Lopez Herraiz *et al.*, IEEE Medical Imaging Conference, Rome, 2004, IEEE Trans. Nucl. Sci., in press.

Chapter 2

Description of the gamma-ray source

The Compton scattering process of starlight on highly energetic electrons was proposed in 1948 [1] in order to explain the existence of highly energetic cosmic gamma-rays. Few years later, in 1963, it was pointed out ([2], [3]) the possibility to produce an energetic and highly polarized gamma-ray beam through Compton scattering of polarized laser light with the electrons accelerated in a high energy machine. The first installation for experiments in nuclear physics was build at Frascati [4]. At present several such facilities exist worldwide (see Section 2.2)

2.1 Gamma-ray beam characteristics

The characteristics of the γ-ray beam (energy, energy resolution, intensity, ...) will depend on the characteristics of the electron beam. These are fixed by the parameters of the ALBA ring lattice. These parameters are currently being optimized [5] but at present all indicates that it will be the so called DBA lattice [6] (except for minor final adjustments). The values given in this section are based on those parameters. The γ-ray beam parameters will also depend on the properties of the laser beam. Several laser sources will be employed in order to optimize the γ-ray beam characteristics. All the details of the calculations of the γ-ray beam parameters can be found in Appendix G.

In the Compton collision process between the laser photons and the ring electrons the maximum achievable gamma ray energy is a function solely of the laser photon energy and the electron energy. For a given laser photon wavelength the spectrum of energies extends from zero to this maximum. The intensity distribution with gamma-ray energy has a saddle shape being twice at the energy extremes than in the middle. For (linear or circular) polarized laser photons, the gamma rays are also polarized being the polarization transfer maximum at the top of the energy range. Most of the gamma-rays are emitted in a very narrow cone, providing a naturally collimated beam. The total gamma-ray intensity depends on the overlap of laser and electron density distributions and the Compton cross-section, that is on the storage ring intensity, the laser power and the beam size variations along the collision path. The selection of a gamma-ray energy from the continuum can be achieved in to ways: using collimation at zero degrees, which requires a laser source with variable wavelength in order to have a varying gamma-ray energy, or the tagging technique, which requires the determination of the scattered

electron energy in coincidence. The momentum of the scattered electron can be obtained from its deviation from the central trajectory after the next bending magnet.The ability to discern close momenta is related to the optics of the synchrotron ring. There is a minimum deviation which can be measured without disturbing the beam. Below the equivalent gamma-ray energy only the collimation technique can be employed. In both cases the achievable energy resolution depends on the position and momentum distributions of the colliding beams. On the other hand, the maximum obtainable intensity is limited by a series of factors: 1) electron beam depletion rate, 2) maximum laser power, and 3) counting rate limitation of the coincidence tagging technique

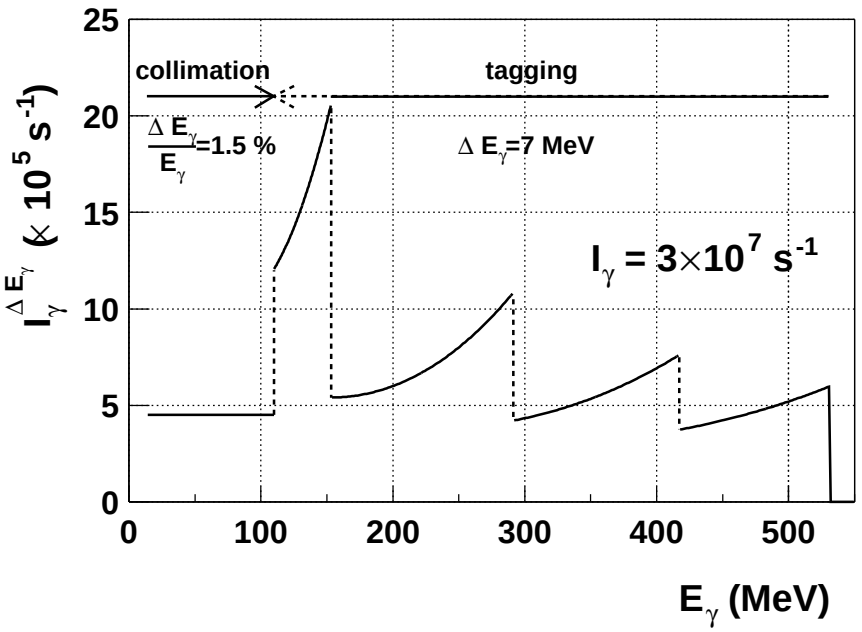

Figure 2.1: Gamma-ray beam intensity within the energy resolution bin size in the range 16 – 530 MeV, for a total intensity fixed to $3 \times 10^7 s^{-1}$

Using detailed Monte Carlo simulations the gamma-ray beam characteristics have been studied and optimized. In Fig. 2.1, Fig. 2.2 and Table 2.1 we present a summary of the gamma-ray beam properties which can be obtained at the proposed installation for ALBA. The gamma-ray energy range up to 16 MeV will be covered using a 1 kW CO_2 laser with which we expect to reach integrated intensities of $10^9 s^{-1}$. No energy determination is foreseen except for the maximum energy with collimation. The collimation technique will be used in the range of 16 – 110 MeV with a 10 W OPO source (see Appendix H), pumped with a Nd:YAG laser, with which we expect to reach integrated intensities of $5 \times 10^7 s^{-1}$ limited essentially by the laser power. The range from the limit for the tagging technique (120 – 160 MeV) to 530 MeV will be

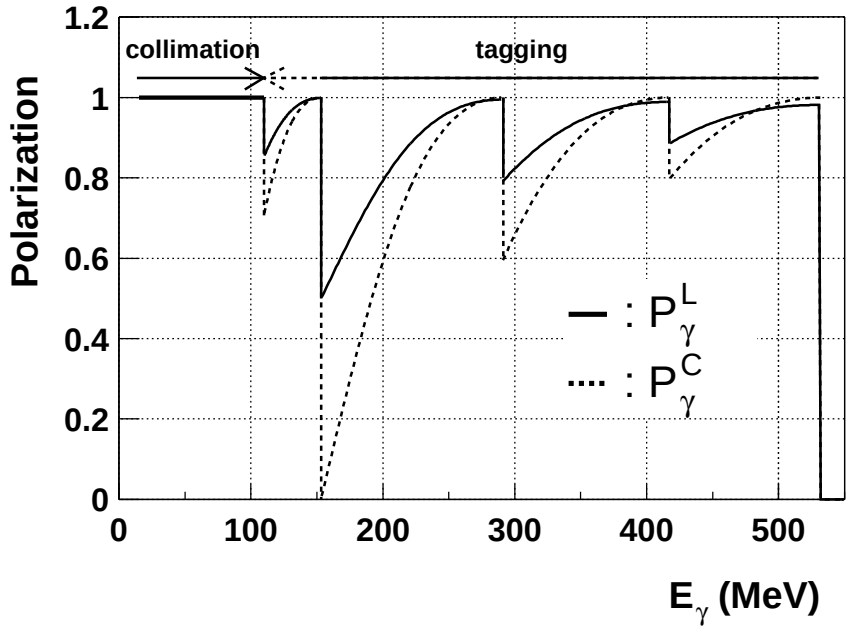

Figure 2.2: Gamma-ray polarization in the range 16 – 530 MeV.

Energy (MeV)	Laser Source	Energy Determination	Energy Resolution	Intensity ($s^{-1}MeV^{-1}$)	Polarization (%)
0.5 – 16	CO_2 (10.6 μm)	-	-	3×10^8	L: 0-100 C: 0-100
16 – 110	OPO (1.5 – 12 μm)	collimation	$\frac{\Delta E_\gamma}{E_\gamma} = 1.5$ %	$4 \times 10^6 - 4 \times 10^5$	L: 100 C: 100
$\sim$ 110 – 153	Nd:YAG (1.06 μm)	tagging	$\Delta E_\gamma = 7$ MeV	2×10^5	L: 85-100 C: 75-100
153 – 290	Nd:YAG (0.530 μm)			1×10^5	L: 50-100 C: 0-100
290 – 417	Nd:YAG (0.353 μm)			7×10^4	L: 80-99 C: 60-100
417 – 531	Nd:YAG (0.265 μm)			5×10^4	L: 90-98 C: 80-100

Table 2.1: Parameters of the gamma-ray beams at ALBA.

covered with a 100 W Nd:YAG laser working up to the fourth harmonic. Integrated intensities of $3 \times 10^7 s^{-1}$ will be reached, in this case limited by the electron beam depletion rate rather than by the tagging technique itself.

2.2 Comparison with other facilities

The sources of γ-rays presently available worldwide in the energy range of few MeV to 500 MeV are of two kinds: bremsstrahlung sources and laser backscattering sources. The latter are in general associated to synchrotron light sources and not dedicated machines. There are a number of differences between the beams produced at both types of facilities. Laser backscattering sources produce a nearly flat energy spectrum while bremsstrahlung sources have a $1/E$ spectrum shape, which in general is a disadvantage of the latter. Energy definition can be achieved at both types of facilities through tagging, while at laser backscattering installations also collimation can be used. The energy resolution with tagging is given by the electron spectrometer and it is conditioned at laser backscattering facilities by the electron storage ring optics. As a consequence worser resolutions are achieved at the latter. On the other hand with collimation comparable resolutions can be reached. The γ-ray beam intensity is limited by the tagging technique in both types of installations, so differences between both types of installations are rather due to differences in the implementation of the technique. Additionally, in the laser backscattering installations, both with collimation or tagging, the intensity is limited by the available laser power or the electron beam lifetime. Production of polarized γ-ray beams, either linear or circular, is simpler at laser backscattering sources, and in general a larger degree of polarization can be achieved.

The first laser backscattering source for nuclear physics experiments was built at Frascati [4] in the late 70's but has discontinued operation few years ago. The present existing sources are collected in Table 2.2 together with their main characteristics. To our knowledge, there are also ideas to build similar installations at two other places: the Advanced Photon Source at Argonne [7] and the Pohang Accelerator Laboratory in Korea [8].

The source proposed at Barcelona combines the energy ranges of HIGS and LEGS at USA, and would be complementary to the GRAAL facility in Europe. At low energies intensities and energy resolutions comparable to HIGS can be obtained, although it is expected to reach much higher intensities at HIGS after the upgrade. On the other hand we expect to reach higher intensities than LEGS.

A list of bremsstrahlung facilities functioning at present is given in Table 2.3. Not included are the low energy facilities without energy definition at Stuttgart [16], Darmstadt [17] and Rossendorf [18] (under construction).

In the range from 15-110 MeV it can be compared to the upgraded MAX-Lab, which would have comparable energy resolution and intensities, but lower degree of polarization. In the range 150-530 MeV it can be compared to MAMI, which has better energy resolution, comparable intensities and again lower polarization degree.

Name	Ref.	Energy (MeV)	Intensity ($s^{-1}MeV^{-1}$)	Resolution FWHM	Method	Polarization
ETL-LCS Tsukuba	[9]	1-40	$10^6 - 10^4$	2.5-7 %	collimation	L: 1
NewSUBARU Himeiji	[10]	1-40	10^4	-	collimation	L: 1
HIGS Durham	[11] (upgr.)	1-20 (1-220)	5×10^7 (10^7)	1 %	collimation	L: 1
LEGS Brookhaven	[12]	110-330	2×10^4	6 MeV	tagging	L: 0.7-1
ROKK Novosibirsk	[13]	100-1600	10^3	1-3 %	tagging	L: < 1
GRAAL Grenoble	[14]	400-1500	1.5×10^3	16 MeV	tagging	L: 0.2-0.96
LEPS Harima	[15]	1500-3500	2.5×10^3	35 MeV	tagging	L: 0.5-0.95

Table 2.2: Laser backscattering γ-ray sources.

Name	Ref. (MeV)	Energy ($s^{-1}MeV^{-1}$)	Intensity FWHM	Resolution	Polarization
MAX-Lab Lund	[19]	20-225	$< 10^6$	0.1-0.5 MeV	L: 0.4-0.6
MAMI Mainz	[20]	50-800	$8 \times 10^5 - 4 \times 10^4$	2 MeV	L: 0.4-0.7 C: 0.5-0.75
ELSA Bonn	[21]	340-3100	$4 \times 10^4 - 5 \times 10^3$	0.2-0.6 %	C: ~ 0.6
HallB-JLAB Newport News	[22]	1200-5700	$5 \times 10^3 - 1 \times 10^3$	0.1 %	no

Table 2.3: Bremsstrahlung γ-ray sources.

2.3 Installation

The γ-ray beam line should be installed employing one of the straight sections of the storage ring. According to the present specifications of the parameters of the DBA lattice this should be one of the four long straight sections (see Appendix G). Alternatively it could be situated in the short straight sections existing between the bending magnets of a DBA cell (where normally no insertion devices are placed).

A schematic layout of the beam line installation can be seen in Fig. 2.3. The dimensions in the figure are approximate but realistic. The aspects related with the radiation shielding are discussed in Appendix J.

In order to extract the gamma-rays a high vacuum tube should be coupled to the synchrotron vacuum pipe. For safety purposes a remote controlled (interlocked) beam shutter could be installed in the tube at the inner side of the accelerator shielding wall. The transport of the gamma-ray beam under vacuum minimizes the background for the measurements and reduces the dispersed radiation to non hazardous levels. The same tube will be used for the injection of the laser beam through an optical window located outside the shielding wall. A controlled mirror installed inside the vacuum pipe will provide the necessary alignment of the beam. The laser sources will be installed in the so called laser hutch on optical benches with the necessary optical elements to provide the adequate focusing position (at the center of the interaction region) and waist. The mirror will be a source of scattered radiation and appropriate shielding has to be provided locally and/or to the laser hutch.

The next element in the beam line would be the collimator (made of lead and other materials) which will be employed in part of the measurements. Since it will have to stop a large fraction of the beam (> 90 %) it will become a strong source of radiation, in particular neutrons. Concrete shielding will be required. In order to facilitate the manipulation (positioning, alignment, aperture) of the collimator, a small shielded room is required rather than embedding the collimator in the shielding. After the collimator a cleaning magnet will be placed in order to deviate the charged particles created in the collimator itself and in previous elements (mirror, windows, ...). In this room it will be also placed the monochromator crystal required for some of the astrophysics instrumentation studies. The vacuum tube could be interrupted before the collimator when it is in use or alternatively an in-vacuum collimator could be used, but in any case it will continue afterward up to the measuring station.

The sample under study and the different detection systems will be located in the measuring hutch. For some of the measurements, the sample will be in air and the beam tube will end shortly before. For some other measurements, sample and detectors might be located under vacuum. Some of the measuring detectors using the time of flight technique will need to be located relatively far away from the sample. The sample and the vacuum windows are a source of radiation and appropriate shielding has to be provided to the measuring hutch.

The last item in the beam line will be the beam dump situated immediately after the measuring hutch. The beam dump consists in a metallic beam stopper (iron, lead) surrounded by a thick concrete shielding.

The installation of the tagging system will require a modification of the storage ring vacuum

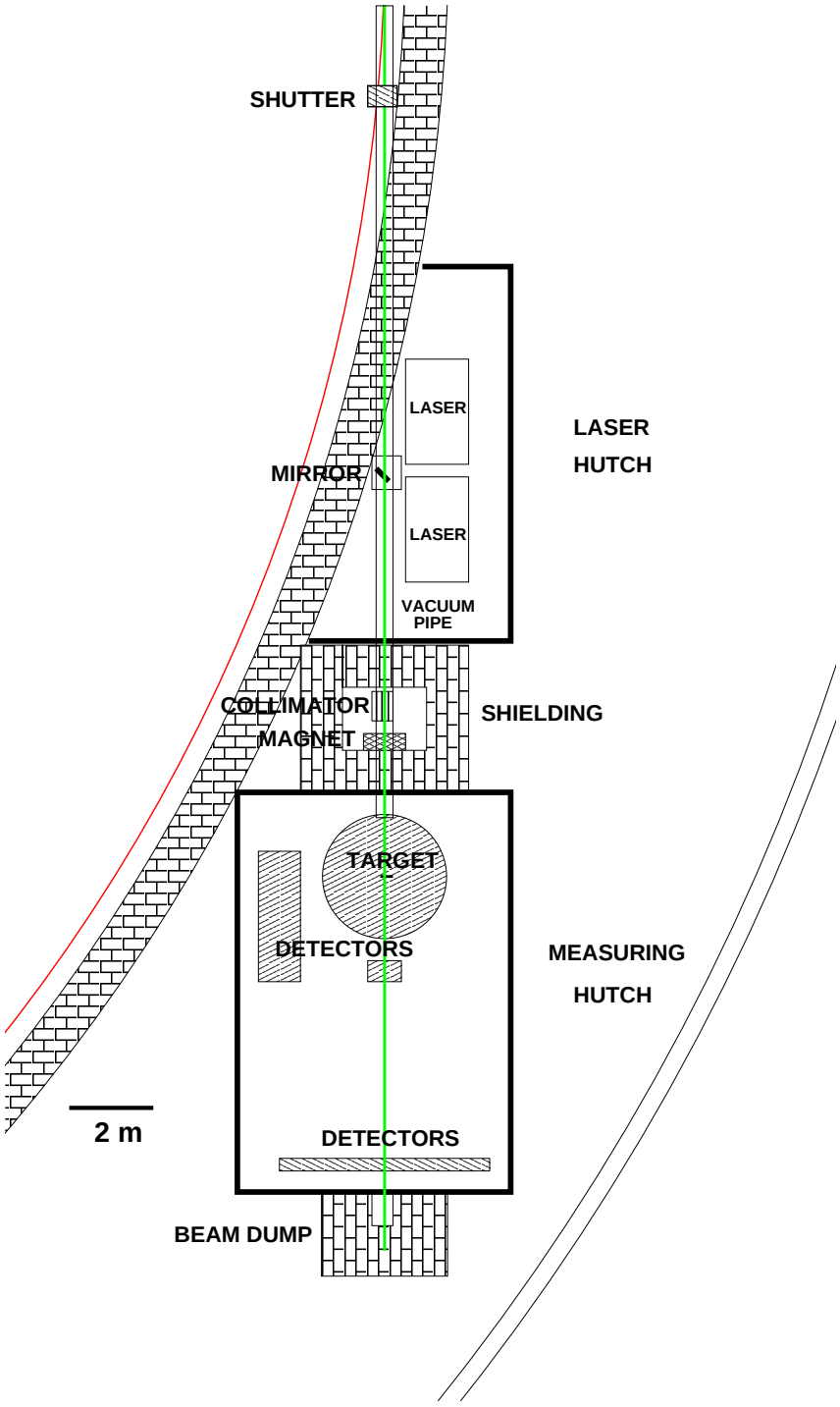

Figure 2.3: Schematic lay-out of the gamma-ray line installation, showing the laser hutch, the shielded collimator area, the measuring hutch and the beam dump

pipe at a suitable location after the next bending magnet following the straight section, in order to install the tagging detector. If the long straight section in the DBA lattice is chosen, it could be located between the first sextupole and the second quadrupole. The tagging detector, consisting in a Si micro-strip detector, a set of plastic scintillators and the associated electronics, should be installed in a retractable arm in order to remove the system into an isolated and radiation shielded vacuum chamber for servicing and protection from direct irradiation with the electron beam during synchrotron adjustments. Eventually an horizontal enlargement of the vacuum pipe preceding the tagging detector will be needed in order to accommodate the lower energy electrons.

2.4 Instrumentation

The gamma-ray beam line has to be equipped with a series of instruments, some of which are common to all or most of the experiments, while others are experiment specific. Common to all the measurements are:

Laser source: A key element of the gamma-ray beam line is the associated laser source. We plan to use several sources in order to optimize the properties of the beam produced. Two commercial laser devices are required: a high power (1 kW) CO_2 laser which will be used to generate an intense beam up to 16 MeV, and a high power (100 W) Nd:YAG laser which will be used both to cover the range $120-530$ MeV employing up to its fourth harmonic, and as pumping system of the OPO device. The OPO device will allow to cover the range $16-110$ MeV. The OPO itself will be developed at the Institut de Ciències Fotòniques (ICFO) in Barcelona (see Appendix H).

Tagger: The experiments with beam energies higher than about 120 MeV will require the use of the tagging technique in general. The position sensitive detector of the tagging system will consist in a Si micro-strip detector (see Appendix I) of about 1 cm height, 5 cm length and 300 μm thickness, with a strip pitch of about 100 μm. The use of a pair of such detectors will provide the redundancy required to minimize the effect of malfunctioning channels. The Si detector will be backed by a set of $10-20$ fast thin (5 mm) plastic scintillator pads with photomultiplier readout, for triggering purposes. Highly radiation resistant Si wafers can be built at the Centro Nacional de Microelectrónica (CNM) in Barcelona. The development of the dedicated electronics required to handle the large number of channels and the assembly of the detector will be done at the Instituto de Física Corpuscular (IFIC) in Valencia.

Beam monitors: The monitoring system will provide the necessary information on beam energy, intensity and polarization. The changes in beam intensity will be controlled by a stack of few thin plastic scintillators placed directly on the beam after the collimator and before the sample, with a very thin metallic converter in-between. A second unit could be placed just before the beam dump. The absolute values of the intensity will be obtained by comparison with the counts registered in a high efficiency detector placed directly on the beam at the measuring sta-

tion during normalization runs. Two such detectors are required: a Ge detector surrounded by a segmented BGO scintillation detector serving as Compton Suppression Shield or alternatively as Pair Spectrometer for the lower energies, and a large volume $\sim$ 50cm $\times$ 50cm NaI(Tl) scintillation detector for the higher energies. These detectors will serve also to monitor the energy distribution of the beam. The beam profile can be determined using a thin sheet of inorganic scintillator viewed by a CCD camera. The polarization of the beam will be controlled my measuring the laser beam polarization with a suitable optical polarimeter.

Data acquisition system: The data acquisition system has to collect the information from the different detection and monitor systems, for the on-line supervision of the measurement and its recording in the permanent storage media for the off-line analysis. The different measurements and experiments might have very different requirements in terms of the number of parameters, transfer rate and dead time, but a general standard system for the smaller scale experiments (up to $\sim$ 50 parameters) with adequate flexibility should be installed. Such a system could be based on the availability of several commercial electronic modules (ADCs, TDCs, memory buffers, histogramming units, ...) based on the CAMAC standard enhanced with the FERA bus for fast data transfers. The system will be driven and controlled with software running on PC under the Linux operating system, similar to the one developed at the Instituto de Física Corpuscular (IFIC) in Valencia.

The dedicated instrumentation required for the experiments, depends on the type of measurements, but still it is possible to identify several items which can be utilized for different experiments. The list of detectors will include large volume NaI(Tl) detectors, high efficiency Ge detectors, position sensitive Si detectors, moderation type neutron detectors, liquid and plastic scintillators for time of flight measurements, position sensitive ionization chambers, fission detectors, etc.

Bibliography

[1] E. Feenberg and H. Primakoff, “Interaction of Cosmic-Ray Primaries with Sunlight and Starlight”, Phys. Rev. 73, 449 (1948).

[2] R.H. Milburn, “Electron Scattering by an Intense Polarized Photon Field”, Phys. Rev. Lett. 10, 75 (1963).

[3] F.R. Arutyunian and V.A. Tumanian, “The Compton Effect on Relativistic Electrons and the Possibility of Obtaining High Energy Beams”, Phys. Lett. 4, 176 (1963).

[4] I. Federici, *et al.*, “Backward Compton Scattering of Laser Light against High-Energy Electrons: the LADON Photon Beam at Frascati”, Nuovo Cim. 59B, 247 (1980).

[5] J. Bordas, *et al.*, “A Concept for the Spanish Light Source CELLS”, Proceedings of the 9th European Particle Accelerator Conference, Lucerne, July 5-9, 2004.

[6] M. Muñoz, *et al.*, “The Lattice for CELLS”, Proceedings of the 9th European Particle Accelerator Conference, Lucerne, July 5-9, 2004, and private communication

[7] Y. Li, *et al.*, “Generation of Bright, Tunable, Polarized γ-Ray Sources by Scattering Laser Pulses from APS Electron Beams”, http://aps.anl.gov/asd/physics/people/ylli/ls303.pdf, Workshop on New Aspects of Quark Nuclear Physics with Polarized Photons, Argonne, 2003

[8] J.K. Ahn and E.S. Kim, “Design Study of the Compton backscattering photon beam facility at the Pohang light source”, Nucl. Instr. and Meth. A528, 600 (2004).

[9] H. Ohgaki, *et al.*, “Polarized gamma-rays with laser-Compton backscattering”, Nucl. Instr. and Meth. A375, 602 (1996).

[10] K. Aoki, *et al.*, “High-energy photon beam production with laser-Compton backscattering”, Nucl. Instr. and Meth. A516, 228 (2004).

[11] T. Scott Carman, *et al.*, “The TUNL-FELL inverse Compton γ-ray source as a nuclear physics facility”, Nucl. Instr. and Meth. A378, 1 (1996).

[12] A.M. Sandorfi, *et al.*, “High Energy Gamma Ray Beams from Compton Backscattered Laser Light”, IEEE Trans. Nucl. Sci. NS-30, 3083 (1983).

[13] G.Ya. Kezerashvili, *et al.*, “A Compton source of high energy polarized tagged γ-ray beams. The ROKK-1M facility.”, Nucl. Instr. and Meth. B145, 40 (1998).

[14] C. Schaerf, *et al.*, “The Graal Project: a polarized and tagged gamma-ray beam”, Nucl. Phys. News 2, 7 (1992).

[15] T. Nakano, *et al.*, “Multi-GeV laser-electron photon project at SPring-8”, Nucl. Phys. A684, 71c (2001).

[16] D. Belic, *et al.*, “The new photoactivation facility at the 4.3 MV Stuttgart DINAMITRON: setup, performance, and first applications”, Nucl. Instr. and Meth. A463, 26 (2001).

[17] P. Mohr, *et al.*, “Real photon scattering up to 10 MeV: the improved facility at the Darmstadt electron accelerator S-DALINAC”, Nucl. Instr. and Meth. A423, 480 (1999).

[18] F. Gabriel, *et al.*, “The Rossendorf radiation source ELBE and its FEL projects”, Nucl. Instr. and Meth. B161-163, 1143 (2000).

[19] http://www.maxlab.lu.se/kfoto/.

[20] S.J. Hall, *et al.*, “A focal plane system for the 855 MeV tagged photon spectrometer at MAMI-B”, Nucl. Instr. and Meth. A368, 698 (1996).

[21] J. Naumann, *et al.*, “A photon tagging system for the GDH-Experiment at ELSA”, Nucl. Instr. and Meth. A498, 211 (2003).

[22] D.I. Sober, *et al.*, “The bremsstrahlung tagged photon beam in Hall B at JLab”, Nucl. Instr. and Meth. A440, 263 (2000).

Appendix A

Low energy photo-disintegration experiments

The experiments proposed in this section require the use of monochromatic γ-ray beams in the range 5-15 MeV, which are not feasible within the present design of the γ-ray beam line. To cover this energy range the extension of the OPO source into the wavelength region of 12 - 30 μm will be required, or alternatively, the development of a new type of light source with variable wavelengths in this range and with enough laser power. The proposed measurements together with other interesting applications in this energy range should provide motivation for such development.

A.1 Physical motivation

The study of the interaction of monochromatic γ-rays with different nuclei has many applications in the study of nuclear structure, nuclear reactions and astrophysics. In particular, the study of the charged particles (mainly protons and α-particles), emitted by nuclei as a result of the absorption of gamma rays, has important implications related to the current research of different Spanish groups. We shall focus here on two specific applications: the investigation of the low energy continuum of weakly bound nuclei, and the investigation of reaction rates which are relevant to the astrophysical *p*-process.

In the last decade, an important fraction of the research in nuclear physics has been directed to the study of exotic nuclei. These nuclei have an excess of protons or neutrons, and therefore are unstable. The binding energies of the exotic nuclei are considerably smaller than that of the stable nuclei. This makes that the continuum of break-up states plays a very important role in the structure and in the reactions induced by exotic nuclei. In particular, the knowledge of the structure of the low-energy continuum (scattering states which are up to a few MeV above the break-up threshold) is essential to understand the properties of exotic nuclei [1]. The investigation of the break-up states in exotic nuclei is done through nuclear reactions, in which the observed cross sections are related to the continuum structure through intricate reaction mechanisms where coulomb and nuclear forces play important roles.

The experimental study of reactions such as (γ, p) and (γ, α) give direct information on the structure of the continuum. These experiments are relatively clean, in the sense that they depend only on the electro-magnetic interactions, and thus they are not sensitive to the nuclear forces. Presently, it is not possible in a facility such as ALBA to perform photo-absorption experiments on exotic nuclei. However, there is a variety of stable nuclei, which are weakly bound, such as the deuteron, ^{6,7}Li, ^{9}Be, etc. The investigation of their low-energy continuum through (γ, p) and (γ, α) reactions, complemented with their reaction cross sections, can be used to reduce the uncertainties in the theoretical models used to investigate the properties of exotic nuclei.

The study of proton-rich nuclei heavier than iron (p-nuclei) has a special relevance for the astrophysical p-process [2]. This process is responsible for the synthesis of neutron-deficient nuclei that are blocked from formation by either the r or s processes [3]. The p-process is essentially a sequence of (γ, n), (γ, p) or (γ, α) photo-disintegrations reactions, possibly complemented by captures of neutrons, protons or α-particles at energies typically far below 1 MeV of the Coulomb barrier in the case of charged particles.

Recent experiments have provided direct measurements of some (γ, n) reactions at the low energies of interest for the p-process, i.e close to the photo-disintegration threshold. One of the techniques is based on the construction of a quasi-thermal photon spectrum from a superposition of Bremsstrahlung spectra with different endpoint energies [4]. As an alternative, a Laser Inverse Compton (LIC) γ-ray source uses a real photon beam in the MeV region produced by head-on collisions of laser photons on relativistic electrons and produces quasi-monochromatic γ-rays in the energy range 1 to 40 MeV [4]. An important advantage of the LIC γ-rays over the Bremsstrahlung approach is their more intense peaking in the energy window of astrophysical interest in addition to their better quasi-monochromaticity. The Bremsstrahlung and LIC techniques have been used so far to measure the rates of a few (γ, n) reactions. In particular, the latter experimental approach has provided cross sections to the ground and isomeric state for the ^{181}Ta$(\gamma, n)^{180}$Ta reaction, which is of special interest in p-process models. These measurements have to be complimented by the determination of the ^{180}Ta$^{m}(\gamma, n)^{179}$Ta reaction rate. Another prime interest in p-process studies is the synthesis of the rare odd-odd p-nuclide ^{138}La. This requires the measurements of the ^{139}La$(\gamma, n)^{138}$La and ^{138}La$(\gamma, n)^{137}$La rates.

Direct determinations of reaction rates for the p-process suffer from two major limitations. The first is the fact that the p-process involves thousands of photo-reactions (not to speak of the secondary β^{+}, electron captures, and (n, γ) reactions) and that most of the involved nuclei are unstable, which means that only a tiny fraction of those reactions can be measured in the laboratory. The second limitation is that in a gas at high temperature, excited levels of the target nuclei are populated according to the Boltzmann statistics, so that photo-reactions on excited levels must be taken into account. This thermalization effect is specially important here because of the high temperatures involved in the p-process and because photo-disintegrations are specially sensitive to threshold effects. If the direct determination of astrophysical rates at work in the p-process is clearly out of reach, experimental studies of photo-disintegration cross sections in the relevant energy range and for nuclei as close as possible to the neutron deficient side of the valley of stability are of crucial importance to test the nuclear reaction models used to calculate the rates. Valuable pieces of information are also obtained, more traditionally, by the measurement of cross sections in the reverse, radiative capture channel. They can indeed be

used to constrain the calculation of the rates in the photo-reaction channel via the reciprocity theorem. One must keep in mind, however, that such measurements are but a fragment of the information needed for the calculation of the reverse rate. To be correct, such a calculation requires the knowledge of all non-negligible cross sections from any excited state of the target nucleus to any state of the residual one.

Direct measurements of photo-disintegration cross sections constitute therefore an independent set of data and the most straightforward way to constrain the calculation of the corresponding astrophysical rate. Improving the theoretical predictions for photo-disintegration rates will put *p*-process nucleosynthesis calculations on a firmer ground. As mentioned before the *p*-process takes place at very high temperatures but the nuclei involved are in a region of the nuclear chart where basic quantities like masses or β-decay rates are either known or rather reliably estimated. Experimental data on photo-reaction cross sections, even scarce, are therefore a very precious ingredient to test the validity of Hauser-Feshbach cross section calculations in the nuclear region of interest. Measurements of (γ, n) reactions on many more nuclei are certainly necessary (see Appendix B), but the investigation of (γ, α) and (γ, p) reactions in the energy range of interest is still a challenging prospect. In addition, the E1 and M1 γ strength functions below particle thresholds should be addressed in direct relation to photo-reactions on nuclear excited states under stellar conditions.

A.2 Experimental setup

A simple setup to measure (γ, p) and (γ, α) reactions consists in having an array of silicon based telescopes surrounding the target, in order to detect and identify any charged particle (specially protons and α-particles), that are produced due to the absorption of γ-rays. For a beam of polarized photons, the production of charged particles would be maximum along the direction of the electric field, which will be perpendicular to the beam direction. So, a simple setup, shown in Figure A.1, consists in two Double Sided Silicon Strip Detectors (DSSSD), which would be placed perpendicular to the beam, and a target that would be tilted 45 degrees. These DSSSD detectors are available from the Spanish groups which form the DINEX collaboration (CSIC-Madrid, Huelva and Sevilla). The size of this detector setup should not exceed a cube of $20 \times 20 \times 20$ cm^3.

A more adequate setup for the γ-ray line at ALBA would consist in the use of specially designed ionization chambers. These have the advantage that they are insensitive to the γ-rays. The design of the chamber can be optimized to differentiate protons and α-particles, and to give the total energy of the particles, considering that protons of up to 10 MeV can be produced. One design would consist in having eight individual ionization chambers, as the one shown in Figure A.2, placed in a cubic geometry in a scattering chamber that contains the target. Another possible design consists in a wired ionization chamber, containing the target, which would give information of the energy, the direction and the charge of the particles produced in the target.

It would be interesting to design a detector array that combines the detection of charged particles, envisaged here, with the detection of neutrons and gamma particles produced as a result of the interaction with the target.

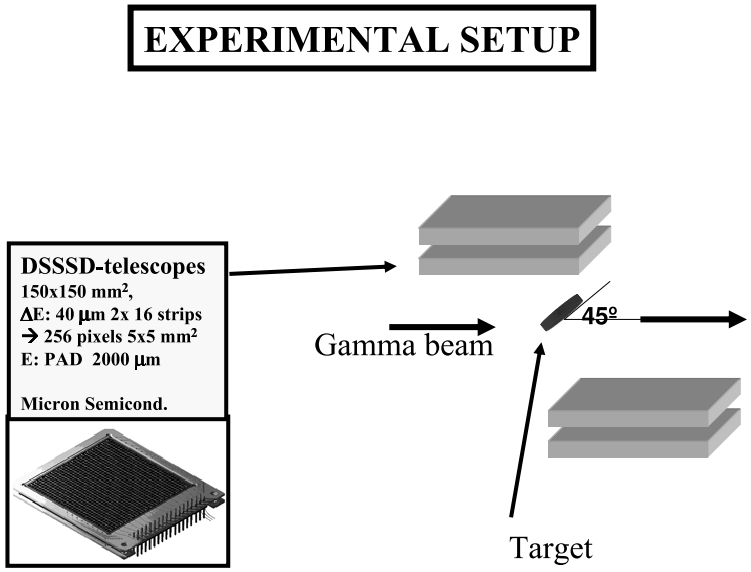

Figure A.1: Detector array based on available DSSSD detectors

A.3 Beam requirements and time estimate

The most important beam requirement to perform the (γ, p) and (γ, α) measurements is that the γ should have the adequate energy to extract a proton or an α-particle, that has a low energy, but sufficient to escape from the target and produce a signal in the detector array. This would require a range of energy between 8 and 15 MeV for the γ-ray. The energy resolution of the beam should be sufficient to allow for particle identification. Probably, 1 MeV could be enough. Considering the electron energy at ALBA, to produce γ-rays in this range of energies by photon backscattering, one will require lasers with wavelength between 10 and 20 nm.

To estimate the number of events, we will assume that the photon source, after collimation, produces 10^7 photons/s, in the adequate energy range. As an order of magnitude estimate, we take that the (γ, p) and (γ, α) cross sections will be of the order of 10 mb. The target thickness will be about 10 mg/cm^2. This thickness (about 10-20 μm), should not stop the charged particles coming out, and for a material with $A \simeq 100$, correspond to about 6×10^{19} particles per cm^2 in the target. This estimate will give about 6 charged particle events per second. The efficiency of the detector may be between 50% and 10%, depending on the polarization of the beam and the energy of the outgoing particles. That gives a reasonable counting rate, which should allow to perform experiments in the time scale of a few days.

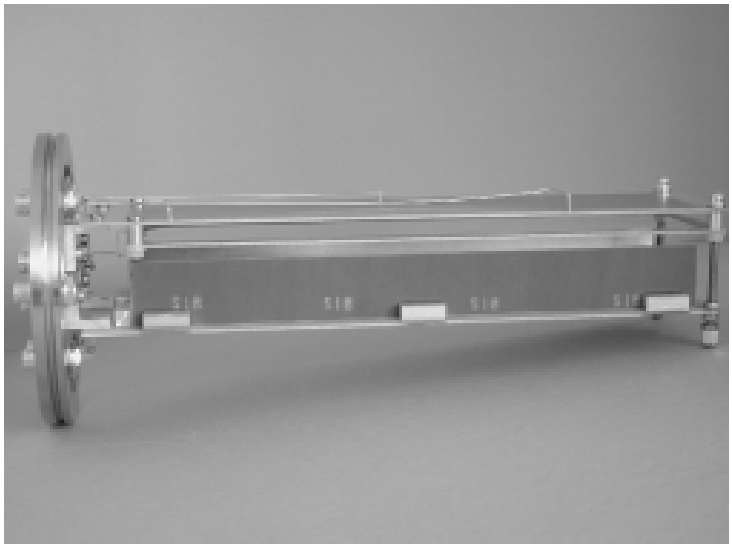

Figure A.2: A single ionization chamber recently design and built by the group of Sevilla in collaboration with the ETH-Zurich

Bibliography

[1] M. V. Andrés and J. Gómez-Camacho, Phys. Rev. Lett. **82** (1999) 1387-1390.

[2] M. Arnould and S. Goriely, Phys. Repts. **384**, 1 (2003).

[3] G. Wallerstein, *et al.*, Rev. Mod. Phys. **69**, 995 (1997).

[4] H. Utsunomiya, P. Mohr, A. Zilges, and M. Rayet, Nucl. Phys. A (2004), in press.

Appendix B

Photo-neutron cross section measurements

B.1 Introduction

Photonuclear reaction data are very important for understanding the structure and dynamics of the atomic nucleus and the nuclear reaction mechanisms. Moreover, photo-induced reaction cross sections are also of importance for a variety of current or emerging applications [1]. Among them are:

- Radiation shielding design and radiation transport analysis. Of particular concern are photoneutrons produced by photons with energies above the neutron separation energy - typically above 8 MeV.
- Calculations of the dose absorbed in the human body during radiotherapy.
- Physics and technology of fission reactors (influence of photo-reactions on the neutron balance) and fusion reactors (plasma diagnostics and shielding).
- Activation analysis, safeguards and inspection technologies for identification of materials through radiation induced by photonuclear reactions using portable bremsstrahlung devices.
- Nuclear waste transmutation.
- Astrophysical nucleosynthesis.

The most important incident γ-ray energy range is up to 25 MeV, the upper energy of most electron/photon accelerators, which also corresponds to the energy range of photo-absorption primarily via the giant dipole resonance. Photonuclear data up to energies of approximately 50 MeV are useful for some medical accelerator technologies under development that utilize higher energy photons. Additionally, it is also desirable to have photonuclear data up to incident energy of approximately 150 MeV due to their use in emerging accelerator-driven transmutation technologies, to complement the neutron and proton high-energy libraries that are being implemented in fully-coupled neutron, photon, charged particle radiation transport simulations [2].

The IAEA has proposed a priority list of materials (43 elements) for which photonuclear data are needed. The list is summarized below and starts with structural materials, shielding and bremsstrahlung target materials, followed by biological and fissionable materials.

1. Structural, shielding and bremsstrahlung materials: Be, Al, Si, Ti, V, Cr, Fe, Co, Ni, Cu, Zn, Zr, Mo, Sn, Ta, W, Pb
2. Biological materials: C, N, O, Na, S, P, Cl, Ca
3. Fissionable materials: Th, U, Np, Pu
4. Other materials: H, K, Ge, Sr, Nb, Pd, Ag, Cd, Sb, Te, I, Cs, Sm, Tb

The scarceness of available photonuclear data is best illustrated by an example: ^{56}Fe is a standard part in the composition of structural materials (steel alloys) and shielding for charged particles and high energy neutrons, among others. Thus, it would be more than reasonable to assume that the photonuclear cross section of ^{56}Fe has been measured in detail, which is far away from the real situation.

Fig. B.1 shows the evaluated cross sections from the JENDL photonuclear data file [3] as found in the *Handbook on photonuclear data for applications* [1] and the available experimental data on which the evaluation is based. The largest data set corresponds to the (γ,1xn) channel and covers only the Giant Dipole Resonance (GDR) energy range between 12 MeV and 24 MeV. No data are available above and, in addition, the experimental values deviate systematically from the evaluated cross section above 21 MeV. The (γ,abs) channel has been evaluated in absence of experimental information above 10 MeV, and there is no data neither for the (γ,xn) nor for the (γ,2nx) channels.

Such a situation is not an exception but the common rule for the availability of photonuclear data. The Laser Compton-backscattering facility at ALBA would represent a clear step forward in the right direction.

It is not only the scarceness of the experimental data but also its accuracy which is under discussion. Most of the data available have been measured at Bremsstrahlung γ-ray sources (BR) and also at Quasi Monochromatic Annihilation (QMA) facilities.

At a BR facility, the γ-ray energy spectrum is a continuum and therefore no reaction cross section but the reaction yield folded with the photon energy distribution is measured. The reaction cross section is obtained after solving the inverse problem defined by the relation between the yield $Y(E)$, the γ-ray energy distribution $D(E,k)$ and the photonuclear cross section $\sigma(k)$ shown in Eq.B.1

$$Y(E) = \int D(E,k)\sigma(k)dk \tag{B.1}$$

Alternatively, the γ-ray energy spectrum at a QMA facility is assumed to be more monochromatic, thus making the analysis less complicated a priori. As shown in Eq.B.2, at a QMA

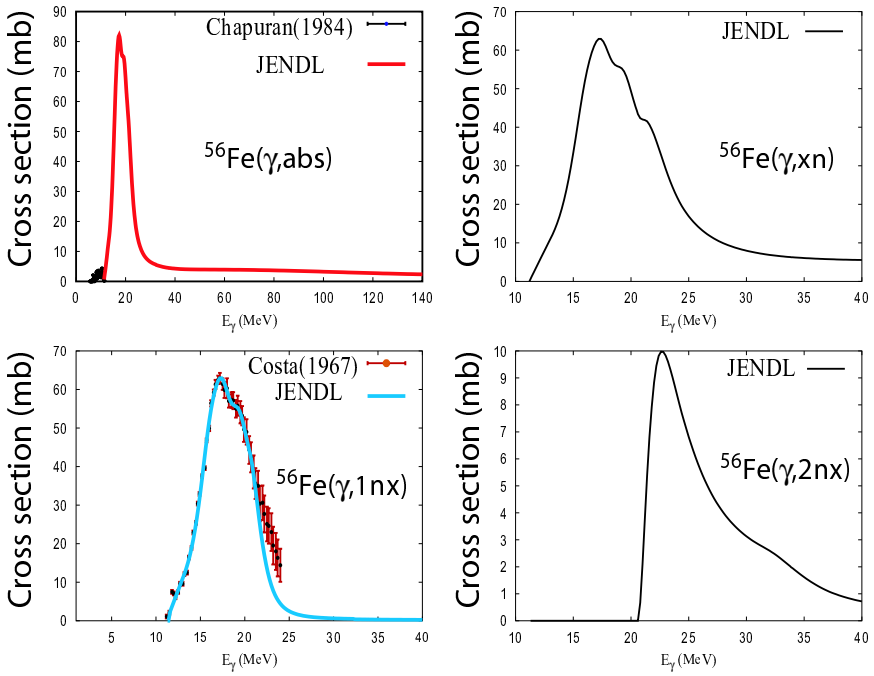

Figure B.1: Evaluated photonuclear cross section for ^{56}Fe and experimental data used for the evaluation [1].

γ-source the cross section is obtained by subtracting the contribution of the positron bremsstrahlung spectrum, always present in the annihilation spectrum $Y_{e^+}(E)$ of the positron beam, by an independent measurement of the pure bremsstrahlung background $Y_{e^-}(E)$ done with an electron beam and by assuming that it is identical to the one due to the positron beam.

$$\sigma(E) \approx Y(E) = Y_{e^+}(E) - Y_{e^-}(E) \tag{B.2}$$

A recent work [4] has shown that there exists a systematic difference between photonuclear data measured at BR and QMA facilities. The differences are both in the integral cross sections, which can be as large as 30% on average between data sets, and in the resolution. As shown in Fig. B.2 for the case of ^{16}O , the resolution achieved in the (γ,xn) cross section after analyzing the bremsstrahlung data [5] is surprisingly better than for the QMA data from two different experiments [6, 7].

Such differences are attributed to the non monochromaticity of the QMA γ-ray beams and the necessary bremsstrahlung background subtraction performed during the data analysis. Data from Laser Compton-backscattering facilities like the one proposed at ALBA present clearly lower systematic uncertainties associated to the analysis techniques, thanks to the better monochromaticity of the γ-ray beam. Indeed, the correctness of the BR data is assessed in [4] by comparison to a third data set from a monochromatic γ-ray source [8].

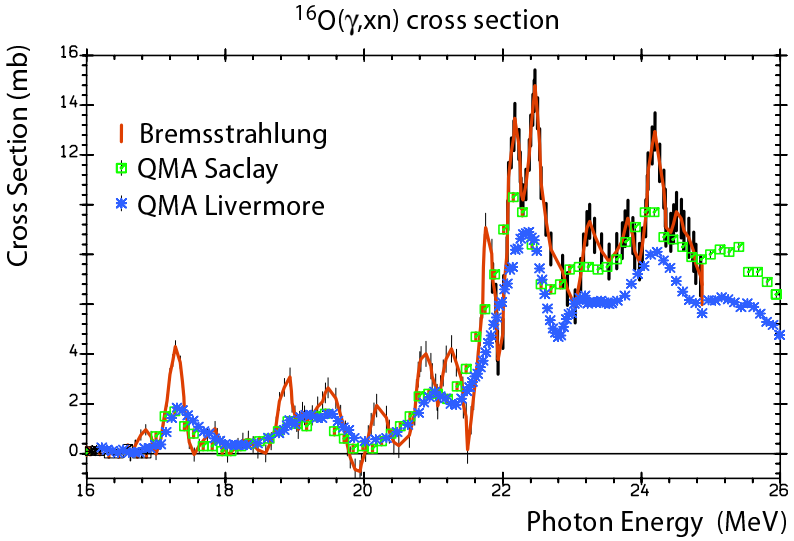

Figure B.2: Comparison of the ^{16}O (γ,xn) cross sections measured at a Bremsstrahlung facility [5] and at two different Quasi Monochromatic Annihilation installations [6, 7].

B.2 The experimental setup

The characteristics of the γ-ray beam line proposed at ALBA define the photonuclear cross section measurements that can be performed. With its initial design, it will be possible to measure the photonuclear cross section in the range between 15 MeV and the largest γ-ray energy of $\sim$ 500 MeV. Such a range covers the Giant Dipole Resonance (GDR) region for the lighter nuclei (below Cu).

- For γ-ray energies 15 MeV $< E_\gamma <$ 110 MeV, monochromatic beams will be available with collimation. Thus, point wise cross section measurements will be performed by tuning the laser (OPO device) wavelength.

- For γ-ray energies $E_\gamma >$ 150 MeV the scattered electron escaping from the synchrotron will be detected and used as a tagging for determining the incident E_γ. The cross sections will be measured with a white γ-ray spectrum.

It should be kept in mind as well that in 5 years from now, a more advanced OPO device could be available and extend the range of the monochromatic beams to lower energies, thus allowing to cover the GDR for heavier nuclei. At a longer term, the development of a compact Free Electron Laser (FEL) with the appropriate wavelength range would be also a very interesting possibility.

The general layout of the experimental setup at ALBA is shown in Fig. B.3. The γ-ray beam intensity will be monitored before and after the photonuclear detection setup with a low interaction monitor (such as a thin ionization chamber) and a high efficiency monitor (such as

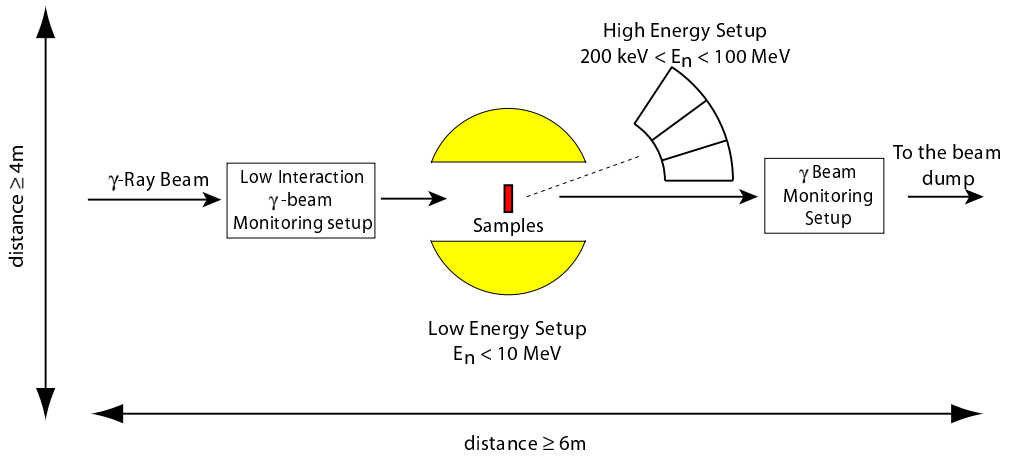

Figure B.3: A generic setup for photonuclear cross section measurements at ALBA.

plastic or an inorganic scintillator), respectively. The neutron detectors will be placed between the monitors. As indicated in Fig. B.3, a 6m long $\times$ 4m wide counting room would be large enough for the setup, although a larger longitudinal dimension (i.e. larger distance between detectors and monitors) will be always preferred.

For the 15 MeV $< E_\gamma <$ 110 energy range, a detector similar to the Berlin Neutron Ball [9] could be used. It consists of a large tank of Gd doped liquid scintillator, with an inner radius of 20 cm and a thickness of 50 cm, viewed by several photomultiplier tubes. Neutrons are moderated in the scintillator and finally captured in Gd producing a γ-ray cascade which is detected. Efficiencies range from 70 % below 10 MeV to 10 % at 100 MeV. A similar but smaller detector, GARANDO [10], has been used at the ETL Laser Compton-backscattered facility [11], to measure neutrons in the low energy range. A different design is defined by the use of a massive moderator blocks surrounding the samples. Inside the moderator, a series of position sensitive proportional counters loaded with neutron converters (like ^{3}He, BF_3) is inserted at different distances from the sample, thus allowing to measure the neutron multiplicities and the neutron energies after taking into account the distance of the detector firing to the samples. Such detection systems have some clear advantages over the liquid scintillators: they are less sensitive to the γ-ray background (an interesting feature at a γ-ray facility), and relatively high intrinsic efficiencies can be achieved up to high neutron energies (tens of MeV). An example of a detector of the characteristics mentioned is NERO[12] at MSU.

For measurements at high energies a complementary array of plastic and liquid (NE213) scintillators placed at a convenient distance $\geq$ 1 m from the samples can be used for detecting neutrons by means of its Time Of Flight (TOF). TOF systems are considered to be the best for neutron spectrometry and differential and total cross section measurements. However, the typical detection efficiencies are lower than for the moderation based systems due to the smaller solid angle coverage and can only be applied if the time of γ-ray causing the reaction is known with good precision. At ALBA this will be possible for $E_\gamma >$ 150 MeV, where the tagging technique is available. Alternatively, the detection of γ-rays emitted in the final nucleus could

provide the start signal as well as providing improved neutron energy resolution [13].

The moderation based detectors may require also the use of a time start signal in order to reduce the intrinsic background level. This can be achieved at ALBA in a working mode where the electron ring is partially filled and a pulsed laser is used. For example, one fourth of the synchrotron circumference occupied would produce $\sim$ 250 ns γ-ray pulses.

B.3 Beam time estimate

In the first phase we want to use moderation based systems. The mean moderation time of a neutron is of the order of $10-100\mu s$. Thus, a reaction rate of $\leq 10^3$ reactions/s is acceptable since it allows to resolve events spaced in time by 1 *ms* on average. Assuming the case of ^{27}Al, this would imply to deal with samples with the unrealistic thickness $n = 10$ at/b ≈ 1.7 m of ^{27}Al as shown in Equation B.3

$$n_{^{27}Al} = \frac{w}{\sigma I_\gamma} = \frac{10^3 \text{ s}^{-1}}{10^5 \gamma \text{s}^{-1}\ 10^{-3} \text{ b}} = 10 \text{ at/b} \tag{B.3}$$

where $I_\gamma = 10^5 \gamma \text{s}^{-1}$ is the expected collimated γ-ray beam intensity and a typical photonuclear cross section of $\sigma = 10^{-3}$ b outside the GDR resonance region has been adopted. So one should not expect pileup problems for this type of detectors

According to these estimates, a typical measurement with an average 20% efficiency moderation based detector and a $n = 0.1$ at/b sample would require 1 hour to measure one energy point with 1 % statistical accuracy (10^4 counts) and a few days would be required to measure the full energy range up to 100 MeV with a reasonable binning.

Bibliography

[1] Handbook on photonuclear data for applications, IAEA-TECDOC-1178 (2000).

[2] M.B. Chadwick *et al.,* "Cross-section evaluations to 150 MeV for accelerator-driven systems and implementation in MCNPX", Nucl. Sci. Eng. 131 (1999) 293.

[3] JENDL Photonuclear Data File (2004), http://wwwndc.tokai.jaeri.go.jp/jendl/jendl.html

[4] B.S. Ishkhanov *et al.*, Proceedings of the 10th International Seminar "Electromagnetic Interactions of Nuclei at Low and Medium Energies" (Moscow, April 16 - 18, 2003). Institute for Nuclear Research of the Russian Academy of Sciences. Moscow, Russia, ISBN 5-944274-012-7 (2004) 5.

[5] B.S. Ishkhanov *et al.*, Yadernaya Fizika 12 (1970) 892.

[6] A. Veyssiere *et al.*, Nucl. Phys. A 227 (1974) 513.

[7] R.L. Bramblett *et al.*, Phys. Rev. 133 (1964) B869

[8] L.M. Youg, "Photoneutron Cross Sections and Spectra from Monoenergetic Photons on Yttrium, Praseodimium and Lead in the Giant Dipole Resonance", Ph.D. Thesis, Univ. of Illinois - USA (1972)

[9] U. Jahnke *et al.*, Nucl. Instr. and Meth. A 508 (2003) 295.

[10] H. Toyokawa *et al.*, Nucl. Instr. and Meth. A 422 (1999) 95.

[11] T. Yamazaki *et al.*, IEEE Trans. Nucl. Sci. NS-32 (1985) 3406.

[12] H. Schatz *et al.* http://www.nscl.msu.edu/ hosmer/nerouser.html

[13] J.R.M. Annand *et al.*, Nucl. Instr. and Meth. A 400 (1997) 344.

Appendix C

Photo-fission experiments

C.1 Introduction

Fission constitutes the most clear example of a large-scale collective motion in nuclear matter where both, the nuclear structure and the dynamics of the atomic nucleus manifest. This is the reason why fission is considered as a unique laboratory to investigate the atomic nucleus. However, the probes used to characterize the structure and the dynamics of the nucleus through fission are very often influenced by the reaction mechanism used to induce fission. In this sense, photons represent the cleanest approach since the excitation energy produced in the reaction corresponds to the initial energy of the photon, only a very small amount of angular momentum is induced and the composition of the target nucleus is not modified. However, the use of photon induced fission has been limited by the lack of dedicated facilities.

The possibility to produce quasi-monoenergetic γ-rays in a Compton backscattering facility opens new opportunities to investigate fission under very clean and well defined conditions. In addition, the large energy range that can be covered using lasers with different wavelengths, offer the possibility to investigate phenomena that manifest at different energy domains. For example it is well known that pairing and shell effects disappear with the excitation energy of the nucleus. However, multi-phonon excitations as well as the role of nuclear viscosity are expected to manifest mainly at higher excitation energies.

Here we present a physics program to investigate different aspects of photo-fission that can be addressed with the present design of the γ-ray beam line for ALBA. In addition, we will also propose some future possibilities concerning photo-fission investigations below 16 MeV.

C.2 Temperature dependence of shell effects

C.2.1 Physics case

The different components appearing in the yields and in the kinetic-energy distributions of the fragments produced in low-energy fission are attributed to shell effects [1]. At low energies, all nuclei with mass numbers from 230 to about 256 predominantly split into a heavier and a lighter

fragment while symmetric splits are strongly suppressed. Over this whole range, the gross behaviour of the fission process is governed by the constant position of the heavy component around mass number 138 [2]. Three different fission components have been identified to explain the measured yields and kinetic-energy distributions, two asymmetric ones, the Standard I and the Standard II and one symmetric, the Superlong. The Standard I mode is characterized by a spherical heavy fragment around mass number 134 and a deformed light fragment. Standard II is characterized by a deformed heavy fragment near mass number 145 and a slightly deformed or spherical light fragment. Finally, in the Superlong component both fragments are strongly deformed. This latter component becomes more important in fission at higher excitation energies.

Important progress was obtained few years ago from an experiment where the charge distributions and kinetic-energy distributions of fission fragments produced in the electromagnetic induced fission of more than 70 different fissile secondary beams were investigated [3]. However, very few experiments provide information on the excitation energy dependence of the different fission modes associated to shell effects. Once more, the gamma ray facility at ALBA could be used for a detailed investigation of the washing out of shell effects with excitation energy by measuring the mass or charge distributions of fission residues at different gamma energies. Since Shell effects are expected to disappear around 50 MeV, the present design of the backscattering γ-ray line of ALBA will allow to cover the range between 16 and 60 MeV.

From an experimental point of view this experiment requires the isotopic identification of the fission residues produced in these reactions. However, this requirement represents nowadays a real challenge. Another possibility is to restrict ourselves to the mass distribution of the fission residues.

C.2.2 Experimental setup

We propose to determine the mass of the fission residues using time-of-flight techniques. A possible setup would consist on a two-arm time-of-flight spectrometer to detect both fission residues. The start detector could be a micro-channel plate while we can use micro-strip silicon detectors for the stop. The simplest configuration would be to use 5x5 cm^2 DSSSD placed at 1 m from the target. The small solid angle covered by this setup could be overcome by longer beam times.

C.2.3 Beam time estimation

At the present moment is very difficult to have a realistic estimate of the beam time. Some of the parameters that difficult this estimation are the final design of the experimental setup and the number of fissile species that can be investigated at ALBA. With respect to this later point one should remember that nature provides us only with five stable fissile nuclides. The possibility to use radioactive samples at ALBA would increase our experimental possibilities.

A very preliminary estimate would be some two weeks beam per target plus some four weeks to setup and test the experiment. A full experimental program including the measurement of 4 targets would require 3 months beam time.

C.3 Multi-phonon excitations

C.3.1 Physics case

In heavy nuclei, giant resonances decay by neutron emission since charged particle emission is suppressed by the Coulomb barrier. In the case of fissile nuclei, fission decay competes with (multiple) neutron emission according to the corresponding partial decay widths, Γ_f and Γ_{xn}. Since fission probabilities increase with excitation energy, multi-phonon giant resonances should appear "enhanced" in the fission channel in comparison to single-phonon states. This effect makes multi-phonon studies in electromagnetic fission particularly attractive.

Evidences for multi-phonon giant resonances in electromagnetic fission of ^{238}U have only been presented recently [4]. In this case, electromagnetic dissociation of nuclei in peripheral heavy ion collisions at relativistic energies through single- and multi-phonon excitations has been used. Although this technique allows to investigate secondary radioactive beams, the main experimental limitation arises in reconstructing the primary excitation energy of the fissioning nucleus. Since the fission fragments are highly excited and emit a multiplicity of particles and γ rays, a complete and precise calorimetry would be required. In the cited work the problem is overcome by exploiting the known linear relationship between primary excitation energy and the prompt neutron multiplicity accompanying the fission process.

The experiments proposed at ALBA can be considered as an ideal case since the primary excitation energy of the fissioning nucleus can be established with an accuracy better than 10%. In addition the high intensity of γ rays allow to reach very low cross section processes. Here the limitation comes from the fact that only stable nuclei can be investigated, namely ^{238}U.

From an experimental point of view such an investigation just requires the measurement of the total fission cross section as a function of the incident energy of the γ rays in an energy range between 15 MeV and some 60 or 70 MeV.

C.3.2 Experimental setup

Total fission cross sections can be measured using parallel plate chambers (PPAC) placed around the target. A similar setup has been used successfully at the n_ToF facility. Additional information could be obtained by measuring in coincidence the multiplicity of emitted neutrons. In this later case, we could use the neutron detector proposed for other experiments at the ALBA γ-ray line. From a technical point of view parallel plate chambers are based on a well known and relatively cheap technology. In addition we are talking about a very reduced number of electronic channels.

The only specific requirement for this setup is a gas system. Then the design of the infrastructures around the γ-ray line facility at ALBA should include a gas handling system.

C.3.3 Beam time estimate

In this case we are considering only the photo-fission of ^{238}U. Consequently, the beam time should not exceed some two to three weeks. However some additional beam time would be

required to test the experimental setup. In total we could consider some two months beam time program.

C.4 Nuclear dissipation in fission

C.4.1 Physics case

The success of the statistical model of Bohr and Wheeler [5] to describe the fission process was questioned by Kramers [6] soon after. According to this later work, fission should be considered as a diffusion process above the nuclear energy-potential in the deformation coordinate. Such a process can be described by the corresponding Fokker-Planck or Langevin equation where the diffusion process is not only governed by the nuclear potential but also by a dissipation coefficient. This coefficient represents the coupling between the intrinsic and collective degrees of freedom populated in fission.

In the pioneering work of Kramers, only the stationary solution of the Fokker-Planck equation describing fission dynamics was proposed. The complete time-dependent solution of the Fokker-Planck equation was not introduced till the eighties by Grangé and collaborators [7]. In this new work, the authors have shown that the fission flux across the barrier needs time to reach its asymptotic value defined by the stationary solution of the Fokker-Planck equation proposed by Kramers. The main consequence of this work is that the hindrance of the statistical fission width is not only due to stationary but also to transient effects. In fact, during this transient time until the stationary regime of the fission width is reached, other de-excitation channels are favored. Consequently the nuclear system cools down reducing again the fission probability with respect to these other channels.

The work of Grangé and collaborators was triggered by the experimental observation of anomalous enhanced pre-scission neutron multiplicities in fission induced in heavy-ion collisions [8]. The large pre-scission neutron multiplicities were interpreted as a signature of the delay of fission at high excitation energies. Meanwhile, other evidences for the hindrance of fission induced by dissipation and transient effects were obtained from the analysis of gamma-rays emitted during the de-excitation of the GDR [9] or directly measuring the fission time using crystal blocking techniques [10].

Recently a novel technique based on the use of fission induced in peripheral heavy-ion reactions at relativistic energies has been proposed [11, 12]. The advantage of this reaction mechanism is that the excited fissioning nucleus is produced with well defined initial conditions that can be easily described using the Serber model [13]. In addition, these reactions lead to almost undeformed nuclei covering a large range in excitation energy. In these works, the fission cross sections, the charge distribution [12] or the isotopic distribution [11] of fission residues have been used as signatures of the fission dynamics.

The γ-ray line at ALBA offers the possibility to investigate photo-fission at high energies. The advantage of this reaction mechanism is the low amount of angular momentum induced in the collision, simplifying the description of the initial conditions of the fissioning nucleus.

Different observables can be used to investigate this process. The simplest would be the

evolution of the total fission cross section with the energy of the incoming γ ray. A more complete detection set up would require the measurement of the charge of the final fission fragments and the possibility to detect neutrons.

C.4.2 Experimental setup

This experiment could benefit from the two experimental setups proposed in the previous experiments. A real challenge would be to develop a new ionization chamber with dedicated digital electronics providing both the mass and charge of the fission products.

C.4.3 Beam time estimate

When going up in energy the fission cross sections goes down and the beam times will become longer. If we consider to investigate the fission of ^{238}U at energies between 50 and 530 MeV a rough estimate for a beam time would be some four weeks.

C.5 Future possibilities

If in the future a method is successfully developed to extend the range of monochromatic γ-rays to lower energies there is a number of additional interesting aspects which could be investigated. Some examples are mentioned below.

C.5.1 Pair breaking and even-odd structure in fission fragment yields

The enhanced production of even elements and the appearance of asymmetric splittings are typical examples of structural effects in low-energy fission. The observed even-odd structure in the final fission residues is related to the survival probability against pair breaking from the superfluid configuration at saddle down to the scission point. These measurements are relevant to characterize the viscosity of cold nuclear matter and then the coupling between collective motion and intrinsic single-particle degrees of freedom [14].

The first systematic overview on even-odd structure in a continuous region of fissioning nuclei was obtained only a few years ago by studying electromagnetic-induced fission from excitation energies around 11 MeV, using secondary beams [3]. This experiment showed that even-Z fissioning systems lead to an enhanced production of even fission residues with an increase of the local even-odd effect for asymmetric charge splits. At the same time, odd-Z fissioning systems lead to a positive even-odd effect for the light fission residue and a negative even-odd effect for the heavy fission partners. These results could be interpreted with theoretical considerations based on the statistical model. The local even-odd effect of the odd-Z fissioning systems and an essential part of the variation of the even-odd effect of the even-Z fissioning nuclei have been attributed to the larger single-particle phase space available for the unpaired nucleons in the heavier fragment. Once this effect was considered, the enhanced production of fission fragments with even neutron or even proton number was quantitatively explained by the

number of excited states with a completely paired configuration of the proton or the neutron subsystem at the scission point [15]. I was shown that the subsystem of one kind of nucleons (e.g. protons) may remain in the ground-state configuration with a certain probability, while the energy is stored in quasi-particle excitations of the other kind of nucleons (e.g. neutrons), even if the excitation energy exceeds the pairing gap.

However, very little is known about the excitation-energy dependence of proton even-odd effects in fission-fragment yields. Some results were obtained few years ago using fission induced by bremsstrahlung radiation and reconstructing the fission yields with gamma-spectroscopic methods [16]. Theoretical predictions and some measurements indicate that the transition from a superfluid phase to a Fermi liquid takes place at excitation energies around 10 MeV [17].

The gamma facility at ALBA offers the possibility to carefully investigate the evolution of the even-odd structure in the final yields of fission residues as a function of the excitation energy. Such an experiment would require at least the full charge identification of the fission residues. This is a real challenge since such a measurement has only been done at Lohengrin at ILL [18] combining magnetic and energy loss analysis. Other possibilities are based on the full digitization of the signals induced by both fission fragments in an ionization chamber. The final alternative is the use of gamma-spectroscopic techniques.

C.5.2 Basic nuclear data

Photo-fission is considered as an optimum non-destructive probe for the survey of fissile material through the detection of beta-delayed neutrons emitted by the fission fragments. This technique is valid to detect small quantities of any fissile nuclei in any kind of container since both gammas and neutrons are deeply penetrating radiations. This method can be applied to determine the amount of radioactive material in the containers used for nuclear waste disposal or to control the proliferation of nuclear material by installing detection systems based on this principle in ports or airports terminals.

To detect the fissile material one just need to detect the delayed-neutron emission. However, the identification of that material requires a precise knowledge of all fission residues produced in photo-fission reactions and to characterized the delayed-neutron emission. Nowadays, very few data on photo-fission can be found in the data bases. A detailed experimental program should be performed to obtained all the data required for these applications. Once more the γ ray facility at ALBA with an extended energy range offers unique possibilities for these applied investigations.

C.6 Conclusion

Fission induced by quasi-monoenergetic γ rays offers several possibilities for experiments in which the excitation energy dependence of structural effects that manifest in fission like pairing or shell effects can be investigated. However, the most promising experiments are related to the search of evidences for multi-phonon excitations or to the characterization of the fission dynamics at high excitation energy. In addition, basic nuclear data that could be used in some

applications related to the detection of fissile material could be accurately measured. The experimental techniques used in most of these experiments are well known and only the precise determination of the mass and charge of the fission fragments seems to be a real challenge.

Bibliography

[1] M. Göppert-Mayer, Phys. Rev. 74 (1948) 235

[2] K.F. Flynn et al., Phys. Rev. C 5 (1972) 1725

[3] K.-H. Schmidt et al., Nucl. Phys. A 665 (2000) 221

[4] S. Ilievski et al., Phys. Rev. Lett. 92 (2004) 112502-1

[5] N. Bohr and J.A. Wheeler, Phys. Rev. 56 (1939) 426

[6] H.A. Kramers, Physika VII 4 (1940) 284

[7] P. Grangé, L. Jun-Qing and H.A. Weidenmüller, Phys. Rev. C27 (1983) 2063

[8] A. Gavron et al. Phys. Rev. Lett. 57 (1981) 1255

[9] P. Paul and M. Thonnensen, Ann. Rev. Nucl. Part. Sci. 44 (1994) 65

[10] D. Hilsher and H. Rossner, Ann. Phys. Fr. 17 (1992) 471

[11] J. Benlliure, et al., Nucl. Phys. A 700 (2002) 469

[12] B. Jurado et al., Phys. Rev. Lett. 93 (2004) 072501

[13] R. Serber, Phys. Rev. 72 (1947) 1114

[14] F. Gönnenwein, Mass, charge and kinetic energy of fission fragments, in: C. Wagemans (Ed.), The Nuclear Fission Process, CRC Press, London, 1991, p. 409

[15] F. Rejmund et al., Nucl. Phys. A 678 (2000) 215

[16] K. Persyn et al., Nucl. Phys. A 620 (1997) 171

[17] A.V. Ignatyuk et al., Sov. J. Nucl. Phys. 36 (1982) 32

[18] H.G. Clerc et al., Nucl. Phys. A 247 (1975) 74

Appendix D

Proton emission with polarized photons

D.1 Introduction

In the last years, nucleon emission induced by electromagnetic probes, both photons and electrons, has been used as a tool to investigate the effects of different physical processes involving atomic nuclei. Among them one can mention here those due to short-range nucleon-nucleon correlations (SRC), meson-exchange currents (MEC) or final state interactions (FSI) [1].

SRC refer to those contributions which are related to the strong repulsion between two nucleons occurring when they are separated by a short distance. This effect is very well known in free nucleon-nucleon scattering and to a certain degree survives in atomic nuclei, beyond the nuclear mean field. Deviations from calculations performed in the mean field approach will inform about the role played in the nuclei by these correlations due to the nucleon-nucleon interaction.

This interaction is usually described in terms of the exchange of particles (mesons) between the nucleons. Electromagnetic probes interact with the nuclear charge and current, whose main terms are due to protons and neutrons. However, these probes can also interact with the charges and currents generated by the exchanged mesons. These are known as MEC. In light nuclei their effect is very well known. However in heavier nuclei it is obscured by the uncertainties associated to the nuclear wave function description.

FSI describe the interactions between the emitted nucleons in a given process and the residual nucleus. They are very important in many situations and in some of them they are the dominant mechanism.

The proposal of building a line of backscattered laser photons for nuclear physics and applications at the synchrotron ALBA under construction in Barcelona, opens the possibility to perform new photon-nucleus experiments.

From the experimental point of view, one of the main problems with the photon facilities is to achieve a compromise between good energy resolution, high degree of polarization and high photon flux. This difficulty has hampered the development of the experimental programs. However, laser backscattering technique allows one to gather simultaneously these three designing goals [2].

The proposed line is expected to provide photons up to 500 MeV. Up to about 110 MeV the

energy selection is made by direct collimation in the backward direction. In this case a 1.5% of relative energy resolution is expected. For more energetic photons, the energy selection is done by electron tagging, and the resolution is expected to be of about 7 MeV.

An analysis of the available low energy experimental data, below the pion production threshold, shows that they are old, incomplete and not accurate enough to disentangle interesting effects predicted by the theory [3]. This indicates the need of new experiments as well as theoretical efforts to implement modern realistic forces in calculations for nuclei with $A > 4$. In this appendix we discuss the opportunities offered by experiments with both polarized and unpolarized photons up to 110 MeV, in light-medium nuclei, to investigate the effects of MEC, SRC and FSI.

D.2 Experimental status

One method to produce photons for nuclear physics experiments is to use *bremsstrahlung*, as it is done at MAMI (MAinz MIcrotron) in Mainz [4]. Another established technique is the laser backscattering, as it has been proposed for the line at ALBA. The latter technique is much more suitable for polarization measurements. In the world, there is a number of facilities of this type, for example LEGS (Laser Electron Gamma-ray Source) [5], which produces photons up to 470 MeV, and HIGS (High Intensity Gamma Source) [6], with photon energies between 2 and 200 MeV. Higher energies can be achieved in GRAAL (GRenoble Anneau Accelerateur Laser) [7], where resonances beyond the $\Delta(1232)$ region, and meson production, can be studied within the operation range between 550 and 1500 MeV. The LEPS facility (Laser Electron Photon Experiment at SPring-8) [8] has even a larger high energy limit (2400 MeV).

Almost all the experimental work relative to one-nucleon photo-emission in light-medium nuclei, has been done with unpolarized photons [1]. As far as we know, the $(\vec{\gamma}, p)$ reaction has been studied only by Yokokawa *et al.* in 1988 on the ^{12}C target at excitation energies between 40 and 70 MeV [9].

D.3 Proposed measurements

In this section we propose a set of experiments to be done on ^{12}C, and ^{16}O nuclei. Their nuclear structure requires a simple description and permits a good control of the theoretical uncertainties.

Calculations have been performed in the framework of a model which permits to take into account, in addition to the one-body (OB) contributions, the SRC and MEC in electromagnetic processes involving nuclei with $A > 4$, in such a way that different processes, like inclusive electron scattering, one- and two-nucleon emission induced by electron scattering and real photon scattering, can be described by using the same methodology. The idea was to have a consistent view of the different processes. The model has been applied to processes involving electron [10] and photon [11, 12] scattering.

Here our interest is focused on one-nucleon emission experiments induced by polarized photons. In particular we are interested in the proton emission process. As previously stated,

the measurements of this kind are scarce [9]. This situation opens interesting possibilities for the nuclear physics photon line at ALBA.

For linearly polarized photons, the cross section is given by

$$\frac{d\sigma}{d\Omega} = \sigma_0 \left(1 + \Sigma \cos 2\phi\right) ,$$

where σ_0 is the unpolarized cross section, ϕ is the angle between the photon polarization and the reaction plane and Σ is the asymmetry. This quantity is defined as

$$\Sigma = \frac{W_{\rm TT}}{W_{\rm T}} = \frac{\sigma_{\parallel} - \sigma_{\perp}}{\sigma_{\parallel} + \sigma_{\perp}}$$

where $W_{\rm T}$ and $W_{\rm TT}$ are the transverse and transverse-transverse responses and $\sigma_{\parallel}$ and $\sigma_{\perp}$ are the cross sections measured with the linear photon polarization parallel and perpendicular to the reaction plane, respectively.

In Fig. D.1, the results obtained for the asymmetry calculated for the processes ^{12}C($\vec{\gamma}$,p)^{11}B(g.s.) (left panels) and ^{16}O($\vec{\gamma}$,p)^{15}N(g.s.) (right panels) are shown for various values of the photon energy ω. The OB (dashed lines), OB+SRC (dotted lines) and OB+MEC (dashed-dotted lines) results and those including all the effects (full lines) are plotted (see [13, 14] for details concerning the SRC function and the MEC operators considered).

In the figure the importance of MEC effects is evident at angles above 90$^{\rm o}$. The effect is non-negligible even at low energies for the two nuclei studied and grows with the photon energy in ^{12}C. In this nucleus the modification of Σ is considerably larger than for ^{16}O for a given photon energy.

In addition, we have found [13, 14] that if one uses different correlation functions, the interference between the SRC and the MEC behaves differently, provoking important modifications of the asymmetry obtained when only the MEC are taken into account. This can be seen in Fig. D.2 where the previous result (left panels), obtained with the S3 correlation function, is compared to the so-called gaussian (G) correlation function (right panels). The latter gives rise, first, to a non-negligible effect with respect to the bare OB calculation (dashed curve wit respect to the dotted curve) and, second, to an appreciable interference with the MEC effects (full versus dashed-dotted curves).

To determine the experimental details necessary to perform this kind of experiments, the cross sections are needed. These are shown in Fig. D.3 for the ^{12}C($\vec{\gamma}$,p)^{11}B(g.s.) (full curves) and ^{16}O(γ,p)^{15}N(g.s.) (dotted curves) processes. The calculations have been done by including OB currents, SRC and MEC. The left, central and right panels show σ_0 [11], $\sigma_{\parallel}$ and $\sigma_{\perp}$, respectively. Three photon energies ω have been considered.

In general, ^{12}C shows larger cross sections than ^{16}O what makes it a better candidate for these experiments. On the other hand we have found [11] that the cross sections obtained with OB currents only have a sharp decrease for large values of the nucleon emission angle. In this region, SRC produce cross sections which are one order of magnitude larger. However, this effect cannot be disentangled because in these cross sections the MEC play an important role, more important than that of the SRC. Therefore the effect of SRC is overwhelmed by that of the MEC.

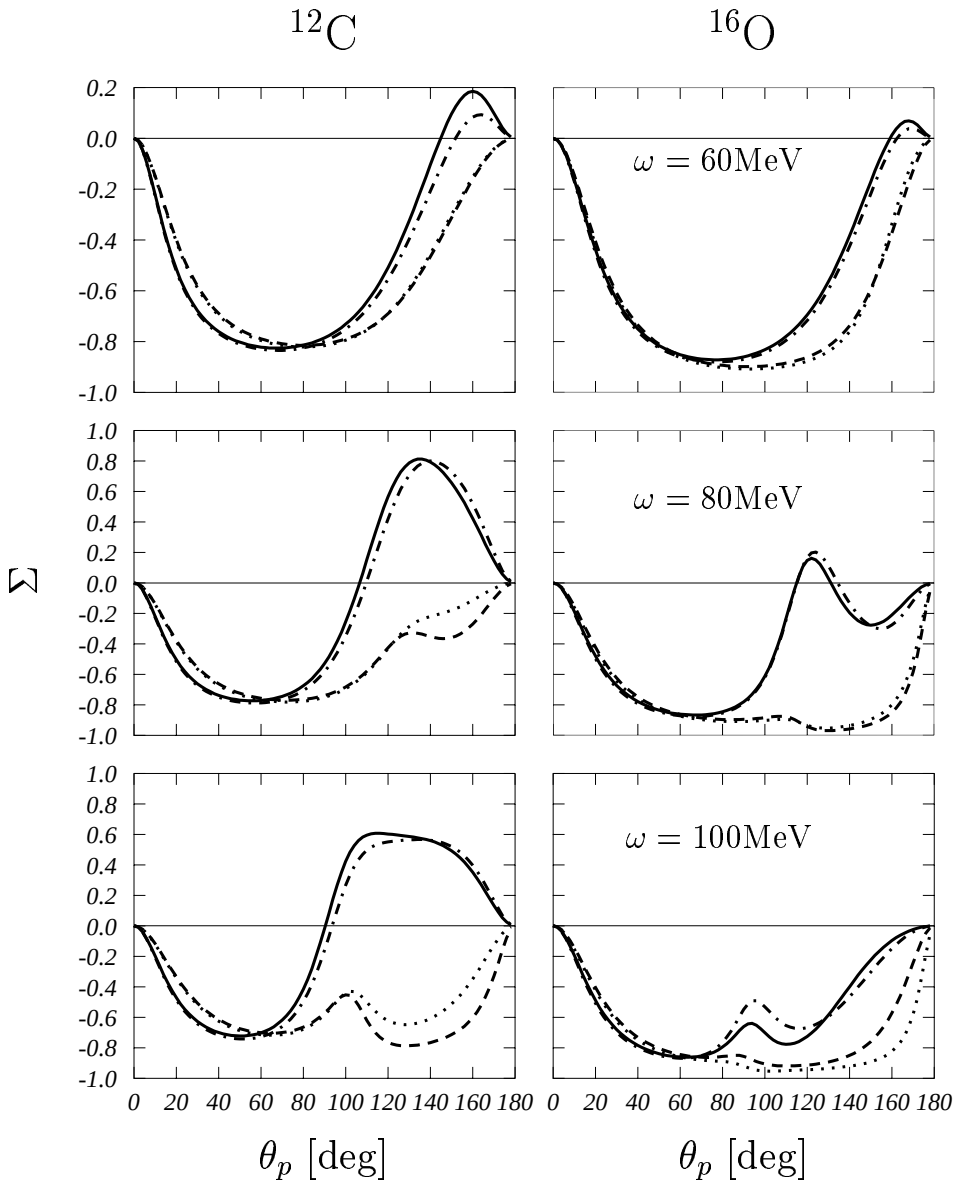

Figure D.1: Angular distributions of the ^{12}C($\vec{\gamma}$,p)^{11}B(g.s.) (left panels) and ^{16}O($\vec{\gamma}$,p)^{15}N(g.s.) (right panels) asymmetries. The dashed lines have been calculated in the independent particle model by using OB currents only. The dotted lines include the effects of the SRC, the dashed-dotted lines the MEC and the full lines all the effects (see [13, 14] for details).

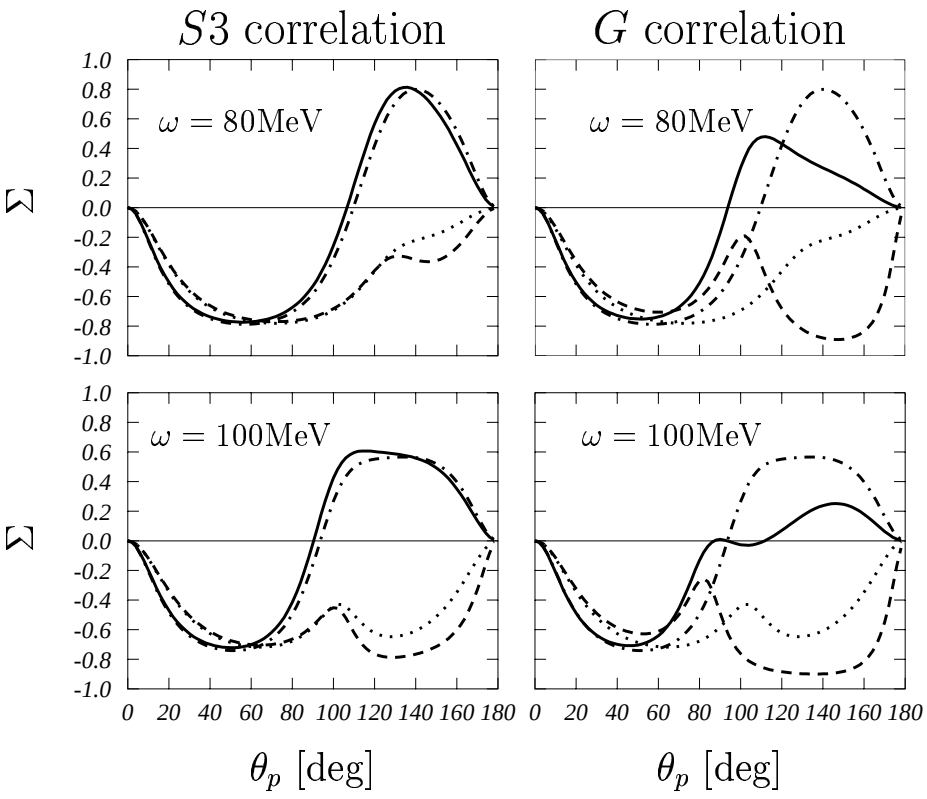

Figure D.2: Angular distributions of the ^{12}C($\vec{\gamma}$,p)^{11}B(g.s.) asymmetries for the *S*3 (left panels) and *G* (right panels) correlation functions and for two photon energies (see [13, 14] for details). The curves have the same meaning as in Fig. D.1.

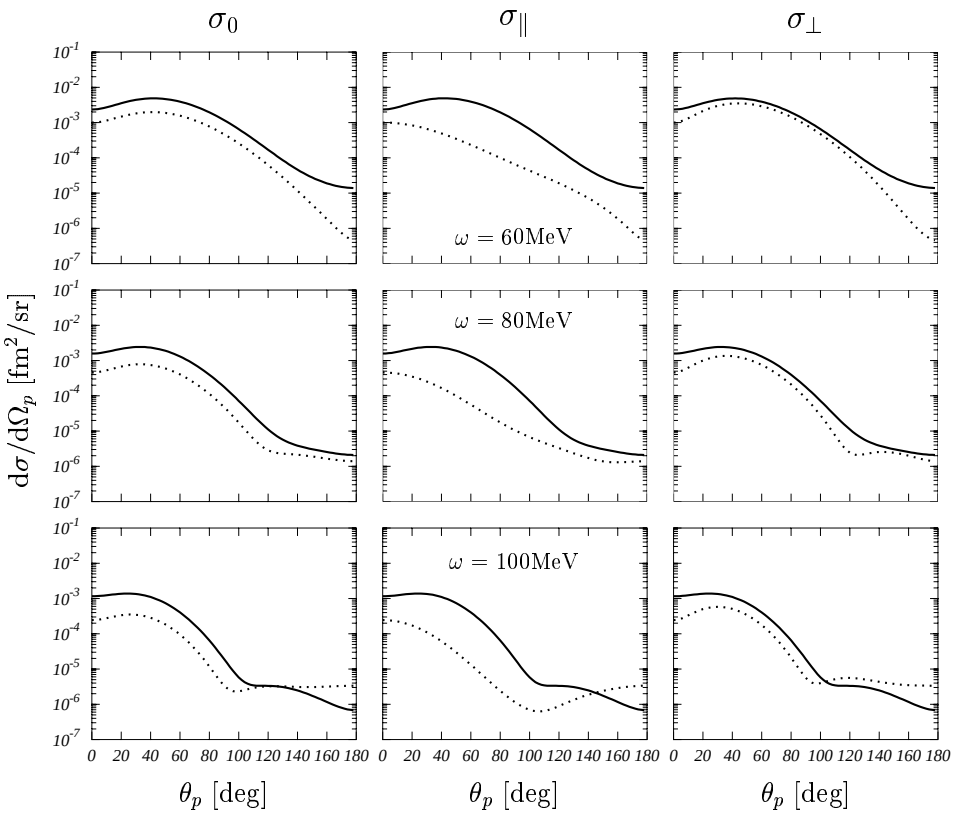

Figure D.3: Angular distributions of the ^{12}C($\vec{\gamma}$,p)^{11}B(g.s.) (full curves) and ^{16}O($\vec{\gamma}$,p)^{15}N(g.s.) (dotted curves) cross sections for different photon energies. Left panels represent the unpolarized cross section σ_0, while central and right panels correspond to the $\sigma_\parallel$ and $\sigma_\perp$, respectively. The calculation have been done by considering OB and MEC contributions as well as the SRC (see [13, 14] for details).

D.4 Experimental details

We need to determine the asymmetry of the proton emission, in the directions parallel and perpendicular to the γ-ray polarization plane, as a function of azimuthal angle for some selected gamma ray energies. Experimentally the challenge is to achieve enough energy resolution to separate the ground state and the excited states in the final nucleus, and achieve enough statistics to determine the asymmetries with enough precision. The energy resolution is severely compromised by the energy lost by the proton before leaving the sample, which limits the useful target thickness and thus the statistics.

We propose to perform experiments in two phases. In the first phase thin samples ($\sim$ 100 mg/cm^2) will be used and a set of four proton detectors will be placed symmetrically around 60° and 120° (where the sensitivity to the searched effects is maximum). The detectors are of the ΔE-E type, to allow for proton identification, consisting in a thin (2 mm) plastic scintillator and a $4 \times 4 \times 4$ cm^3 CsI(Tl) scintillator with photodiode read-out which can reach resolutions of 1 % [15], sufficient for our purposes. Each detector subtends a solid angle of 100 msr when placed at 10 cm from the sample. Assuming a collimated intensity of 4×10^5 s^{-1} for a beam energy of 80 MeV with a 1.5 % resolution, it would require 2 days of measuring time to determine an asymmetry of $\Sigma = 0.5$ at 120° with a precision of 10 % in a ^{12}C sample, according to the cross section estimates. For the ^{16}O sample 2 weeks measuring time would be necessary.

A more ambitious setup can be used in a second phase, to measure even lower cross sections. To overcome the sample thickness limitation one could use the method employed in Ref. [16]. Taking advantage of the good collimation of the γ-ray beam an elongated (wire-type) thin sample could be employed. To reconstruct the angle of proton emission, position sensitive detectors should be employed. This could be achieved with two DSSSD (Double Sided Si Strip Detectors) per telescope acting as ΔE detectors, similar to those developed by the Huelva-Sevilla-Madrid collaboration (see Appendix A). It could also be achieved with a single DSSSD and a position sensitive E-detector, which could be a CsI(Tl) crystal read out with an array of APDs (Avalanche Photo Diodes), or even a Double Sided Strip Ge Detector as the one which is being considered by the Madrid-Valencia collaboration for the future FAIR-Darmstadt facility. The real challenge will be the development of a 4π array which could allow the measurement of correlations in two-proton emission with polarized γ-rays.

D.5 Future developments

In the previous sections we have discussed those experiments which can be done in a rather straightforward way. Nevertheless, there is a number of experiments which can be proposed at a later stage and which would complete the experimental program in this area of interest.

One-neutron emission experiments are the obvious complement to the (γ,p) experiments described above. In this sense it is important to note that there is much controversy concerning the discrepancy between theory and experiment in the cross sections of the (γ,n) experiments in comparison with those of the one-proton emission process. In addition there are very few data

for both kind of experiments [17].

In this case the problem would be the neutron detection and the determination of its energy. One possibility is to use a detector based on the proton recoil after the collision with the detected neutron. A better alternative is the use of time-of-flight techniques. Due to the time structure of the electron beam and the way of generating the photon beam, the trigger for the process cannot be based on time signals provided by the synchrotron or the laser. However one can use the detection in coincidence of photons coming from the decay of the excited residual nucleus. This procedure would be also valid for proton emission.

One-nucleon emission processes can be investigated in deep by considering other polarization degrees of freedom apart from the polarization of the incident photons. For example, it is possible to consider nuclear targets with non-zero angular momentum and to polarize them. In this case, additional nuclear responses are accessible and new information can be obtained. The complex apparatus involves a refrigerator (low temperature), pumping system (vacuum), magnets and other complementary systems such as, for example, nuclear magnetic resonance to measure the polarization value. Though more complicated, there is already considerable experience at different experimental facilities [18].

Measuring the polarization of the outgoing nucleon permits to access to new information about the nuclear structure. The polarization of the emitted proton can be measured by using a polarimeter based on elastic proton-proton-scattering [19]. For neutrons more sophisticated polarimeters are needed [20].

Finally, two-nucleon emission can also be considered as a possibility for future developments. In recent years, two-nucleon emission have been investigated with unpolarized photons [21]. ^{9}Be, ^{12}C and ^{16}O have been used as targets and photon energies above 100 MeV have been considered. Experiments performed with polarized photons [22] have dealt with both $(\vec{\gamma}, pp)$ and $(\vec{\gamma}, pn)$ for energies ranging between 160 and 350 MeV in ^{12}C and ^{16}O.

In a recent calculation [13] we have found that the (γ,pp) cross sections are sensitive to the MEC parametrization chosen and this puts further interest in this kind of processes. The experiment should require a 4π detector setup with enough resolution and charged particle identification capability. This would allow to measure two-proton or neutron-proton emission, as well as proton knockout with pion production. These kind of detectors have been employed at MAMI [23].

D.6 Conclusions

Polarized photons with energies up to 110 MeV appear to be a useful tool to make high precision nuclear physics. By choosing the kinematics, the contributions of the different physical mechanisms can be enhanced or reduced and this permits to investigate subtle effects such as those produced by the SRC and the MEC. In this respect, the proposed nuclear physics line at the ALBA synchrotron is a very interesting facility because of the estimated high energy resolution and the possibility to obtain photons with almost 100% polarization. The wide spectrum of experimental work to be developed with this facility would cover an almost completely unexplored area since nucleon emission data obtained with polarized photons are very scarce.

Bibliography

[1] S. Boffi, C. Giusti, F.D. Pacati and M. Radici, *Electromagnetic Response of Atomic Nuclei* Clarendon Press, 1996.

[2] A.M. Sandorfi. *Polarized Photon Facilities - Windows to New Physics* in Baryons'95: Proceedings of the 7^{th} International Conference on the Structure of Baryons, Santa Fe, USA (1995). Editors: W. Weise, B.F. Gibson, P.D. Barnes and J.B. McClelland (World Scientific, 1996).

[3] G. Orladini, Nucl. Phys. A**737** (2004) 210.

[4] `http://www.kph.uni-mainz.de/B1/`

[5] `http://www.legs.bnl.gov/`

[6] `http://higs.tunl.duke.edu/`

[7] `http://www.cerncourier.com/main/article/39/6/14`

[8] `http://www.rcnp.osaka-u.ac.jp/Divisions/np1-b/`

[9] J. Yokokawa *et al*., J. Phys. Soc. Jpn **57** (1988) 695.

[10] S.R. Mokhtar, G. Co' and A.M. Lallena, Phys. Rev. C **62** (2000) 067304; G. Co' and A. M. Lallena, Ann. Phys. (N.Y.) **287** (2001) 101; S. R. Mokhtar, M. Anguiano, G. Co' and A. M. Lallena, Ann. Phys. (N.Y.) **292** (2001) 67; M. Anguiano, G. Co' and A. M. Lallena, J. Phys. G: Nucl. Part. Phys. **29** (2003) 1.

[11] M. Anguiano, G. Co', A. M. Lallena and S.R. Mokhtar, Ann. Phys. (N.Y.) **296** (2002) 235.

[12] M. Anguiano, G. Co' and A. M. Lallena, Nucl. Phys. A **744** (2004) 168.

[13] T.A.C. Maiolo, *Fotoni polarizati nello studio della struttura del nucleo atomico*. Tesi di Laurea. Universita' di Lecce. 2004.

[14] T.A.C. Maiolo, M. Anguiano, G. Co' and A.M. Lallena, *in preparation*.

[15] W.G. Gong *et al*., Nucl. Instrum. Meth. A268 (1988) 190.

[16] A.C. Shotter *et al*., Phys. Rev. C37 (1988) 1354.

[17] A. Meucci, C. Giusti, F. D. Pacati, Phys.Rev. C64 (2001) 064615.

[18] http://polt05.physik.uni-bonn.de/PTWorldWide.html

[19] http://kaa.desy.de/polarimeter/pol/node3.html

[20] http://www.physics.ohio-state.edu/ nucex/chargex/cooper_thesis/dan_thesis.html

[21] M. Kanazawa *et al*., Phys. Rev. C**35** (1987) 1828; E.D. Hackett *et al*., Phys. Rev. C**53** (1996) R1047; Th. Lamparter *et al*., Z. Phys. A**355** (1996) 1; I.J.D. MacGregor *et al*., Phys. Rev. Lett. **80** (1998) 245; P.D. Harty *et al*., Phys. Rev. C**57** (1998) 123; T.T-H. Yau *et al*., Eur. Phys. J. A**1** (1998) 241; D.P.Watts *et al*., Phys. Rev. C**62** (2000) 014616; K.R. Garrow *et al*., Phys. Rev. C**64** (2001) 064602.

[22] S. Franczuk *et al*., Phys. Lett. B**450** (1999) 332; C.J.Y. Powrie *et al*., Phys. Rev. C**64** (1999) 034602; R. Lindgren *et al*., http://www.legs.bnl.gov/pub/o16_uva/o16prl_bnl65187.ps

[23] G. Audit et al., Nucl. Instr. Meth. A301 (1991) 473.

Appendix E

Photon-nucleon experiments

E.1 Introduction

Appart from photonuclear experiments to study the structure of the atomic nucleus, it is possible to resolve the nucleon interior structure through the interaction with photons if the energy is above 150 MeV. These experiments belong to the realm of Intermediate Energy Physics (IEP), that is, the particle/nuclear physics area which studies the structure of the matter, nuclei and particles at scales of the order of 0.1 up to 2 GeV.

At present this is one of the richest fields in physics as it involves the production of the lightest mesons through the excitation of nucleon resonances, which constitutes the most important source of information on chiral effective Lagrangians and the behavior of QCD at low energies, fixing the parameters involved in the theoretical descriptions.

In this Appendix we propose experiments of production of mesons, excitation of nucleon resonances and Compton scattering of photons at intermediate energies. In figure E.1 the meson and baryon spectra that can be studied with photon-nucleon reactions at intermediate energies are displayed.

We will give more detail on the studies that can be achieved with the present design goal of 530 MeV maximum photon energy, but we should keep in mind that this limit represents just the state of the art of laser technology. This area of research is quickly evolving and we cannot close the issue of the actual maximum energy of the incident photons without taking into account the improvements that, for sure, laser technologies will experiment in the next years.

Among the different meson production experiments, research on baryon excitations through pion photoproduction is of great interest – from both theoretical [2, 3, 4] and experimental [5, 6] points of view – due to new available data, specially in the $\Delta(1232)$ region. The main difficulty is the isolation of each resonant contribution from the background due to other resonances and the non-resonant contributions (v.g. light meson exchange). The new generation of high precision experimental facilities are of great importance in this research area. Because of its energy range and relatively high intensity, the proposed beam line will be an excellent tool to study $\Delta(1232)$ and possibly the Roper N(1440) nucleon resonances by means of Compton scattering and pion photoproduction on free protons and light nuclei.

According to the design parameters (see Table 2.1 of Chapter 2), we can compare ALBA to

LEGS [7], that is the facility that most closely resembles it, and to MAMI-A2 [8], a bremsstrahlung γ-ray source at Mainz for a similar energy range. We can observe also that the energy range spanned by the proposed beam line is the region less well covered by backscattering facilities and this is the main reason why there are almost no measurements of the photon asymmetry in $(\vec{\gamma}, p)$, and just a few cross-sections are available in the literature for energies between 150 and 300 MeV (see for instance Fig. E.2). This γ-ray energy range is neither well covered by bremsstrahlung facilities. Among them, only MAMI-A2 and MAX-Lab (Lund) [9] facilities span a similar energy range with a photon intensity comparable to the proposed beam line, but a lower degree of photon polarization. Furthermore, compared to bremsstrahlung sources, laser-backscattering facilities like ALBA produce a photon beam that is virtually free from $e^+ - e^-$ background. This background has been found responsible for systematic error in the measurement of pion production cross-section at MAMI [10].

The Spanish intermediate energy physics community is very active and present in several universities and laboratories. At present there are no –and have never been– intermediate energy physics facilities in Spain, of any kind. To finish this introduction we would like to stress that the proposed gamma ray beam line represents the most cost-effective single measure that can have the highest impact in a field of physics in our country. Having the opportunity of performing experiments at such a facility is the dream of any intermediate energy physicist, and having it in Spain is undoubtedly the best opportunity that the IEP community of Spain has ever faced.

E.2 Experiments proposed

In the energy range from 150 to 500 MeV, we propose the measurement of Compton scattering $(\vec{\gamma}, \gamma)$ and pion photoproduction $(\vec{\gamma}, \pi)$ on free protons, deuteron, ^{3}He, and ^{4}He and more complex nuclei. One must notice that for free nucleons, with the same setup and in the same experiment one can measure Compton scattering and pion production. For nuclear targets additionally in the same experiment one would also measure single proton knockout.

In what follows we review the particularities of the observables and then we will describe the experimental equipment needed.

E.2.1 Compton scattering and pion photoproduction on free protons: $\mathbf{p}(\vec{\gamma}, \gamma)$, $\mathbf{p}(\vec{\gamma}, \pi^0)$ and $\mathbf{p}(\vec{\gamma}, \pi^+)$

This kind of experiments constitute a first step in the development of an experimental pion photoproduction programme. We suggest to repeat the experiments performed over the last years, specially at LEGS [10] and MAMI [11], and to complete the experimental analysis by increasing the database of multipoles and polarization observables in order to solve discrepancies among results of different laboratories. It has to be said that there are important discrepancies between the last analysis at Brookhaven and experimental data obtained at Mainz over the last decade[1]. Taking into account the larger intensity of ALBA, repeating the experiments with similar statistics as the one achieved at LEGS can be done in 3-4 months.

[1] A detailed comparison among different experimental data can be found in Ref. [10]

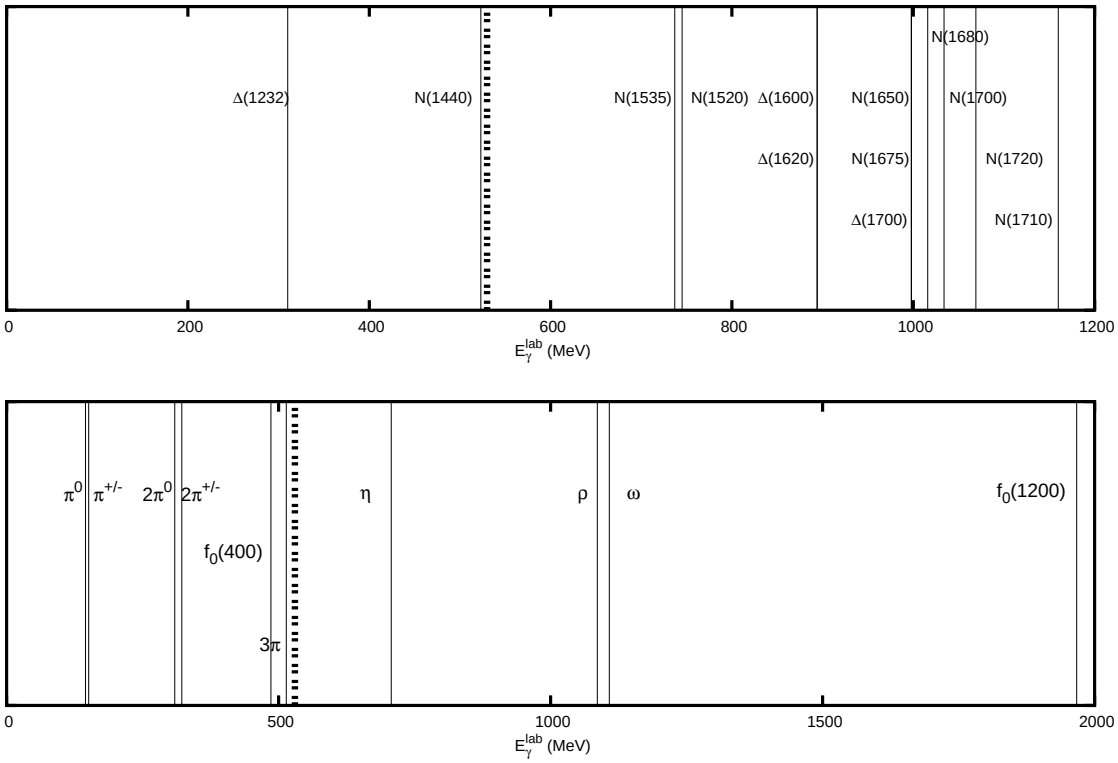

Figure E.1: Upper panel: Spectrum of nucleon resonances on free protons depending on the incident photon energy in laboratory frame. We show resonances with three and four stars in Ref. [1]. Resonance masses are taken from the pole position data of Ref. [1]. Lower panel: Spectrum of meson production on free protons depending on the incident photon energy in laboratory frame. Because of the large energy range for f_0 we show its value for both maximum and minimum masses. The dashed line stands for the preliminary maximum energy at ALBA.

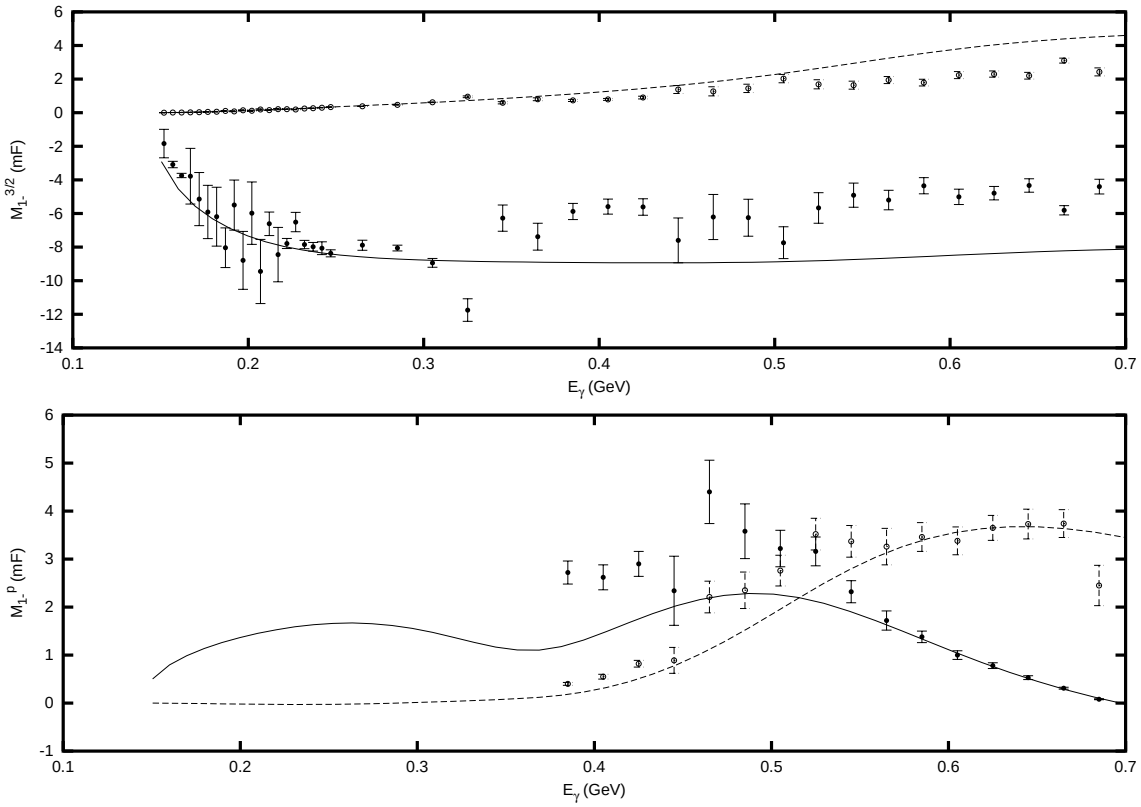

Figure E.2: Real (solid symbols) and imaginary (empty symbols) part of some of the multipoles determined from pion photon scattering on nucleons[5]. We can see that for the case of the multipole $M_{1-}^{3/2}$ there is an acceptable coverage of photon energies, while for the M_{1-}^{p} one there is a lack of data below 360 MeV. The fit have been taken from Ref. [4]

Detailed experimental study of multipoles is critical. The $E_{1+}^{3/2}$ multipole is dramatically affected by final state interactions between the outgoing pion and the proton. There are large uncertainties in this multipole and a lack of experimental knowledge between 300 and 400 MeV, that the last experiment at LEGS has started to fill in [10]. It would be of great interest to increase the experimental database for several multipoles in the low energy region (v.g. E_{0+}^{p}, E_{1+}^{p} and M_{1+}^{p} below 200 MeV, M_{2-}^{p} below 400 MeV and M_{1-}^{p} and $M_{2-}^{3/2}$ in the whole energy range of the synchrotron). New experimental techniques would be needed to achieve these measurements.

The latest theoretical analysis of Compton scattering [12] does not agree with those performed for pion photoproduction [3], specially with regards to the E2/M1 ratio (EMR) of $\Delta(1232)$ and helicity amplitudes. These observables are of importance because theoretical models predict values between -0.5% and -6% depending on the existence of a pion cloud around the nucleon. Experiments performed in the last years favor models with the pionic cloud, although the EMR is not quite well known, $EMR = -2.5 \pm 0.5\%$ in Ref. [1] and $EMR = -3.07 \pm 0.26(stat. + syst.) \pm 0.24(model)\%$ in Ref. [10]. The solution of the theoretical-experimental puzzle about the $\Delta(1232)$ is one of the aims of this proposal. If enough photon energy is available also the Roper resonance could be studied. The Roper resonance is of great interest for MEC descriptions and its structure and properties are not clear. The recent claims of a pentaquark antidecuplet would seem to require an $N(1650)$ to satisfy the Gell-Mann-Okubo rule with the known $\Sigma(1770)$ and the reported $\Theta(1540)$, $\Xi(1860)$. This resonance has been identified with the $N(1710)$ mixed with the $N(1440)$ and split by level repulsion. If ideal mixing is supposed, the lightest resonance (the Roper) has a significant pentaquark component with no hidden strangeness, that is, it can be viewed as largely a baryon with an additional light quark-antiquark pair. The $N(1710)$, carrying the hidden strangeness, would remain out of the reach of the proposed beam line.

E.2.2 Compton scattering and pion photoproduction on nuclei

The use of nuclear targets instead of free protons reduces the energy transferred to the recoiling system and thus increases the energy available to excite nucleon resonances (see for instance Fig. E.3. Furthermore, the Fermi motion of nucleons inside nuclei widens up even more the range of kinematically allowed processes, for a given photon energy. Additionally, targets as ^{3}He are easily polarized, what adds new observables to study. On the other hand, the recoiling system being complex, many different reaction channels can happen, but suitable coincidence techniques would help isolating the particular channel of interest.

Compton scattering and pion photoproduction on deuteron: $\mathbf{d}(\vec{\gamma},\gamma)$, $\mathbf{d}(\vec{\gamma},\pi^0)$, $\mathbf{d}(\vec{\gamma},\pi^+)$ and $\mathbf{d}(\vec{\gamma},\pi^-)$

The aim is to use deuteron as a first step to study pion photoproduction on light nuclei [13] and to establish the influence of $\Delta(1232)$ in its structure. Combination with previous analysis on protons allow to obtain information about the neutron. We need to measure differential and total cross sections as well as polarization observables. The amount of experimental information is

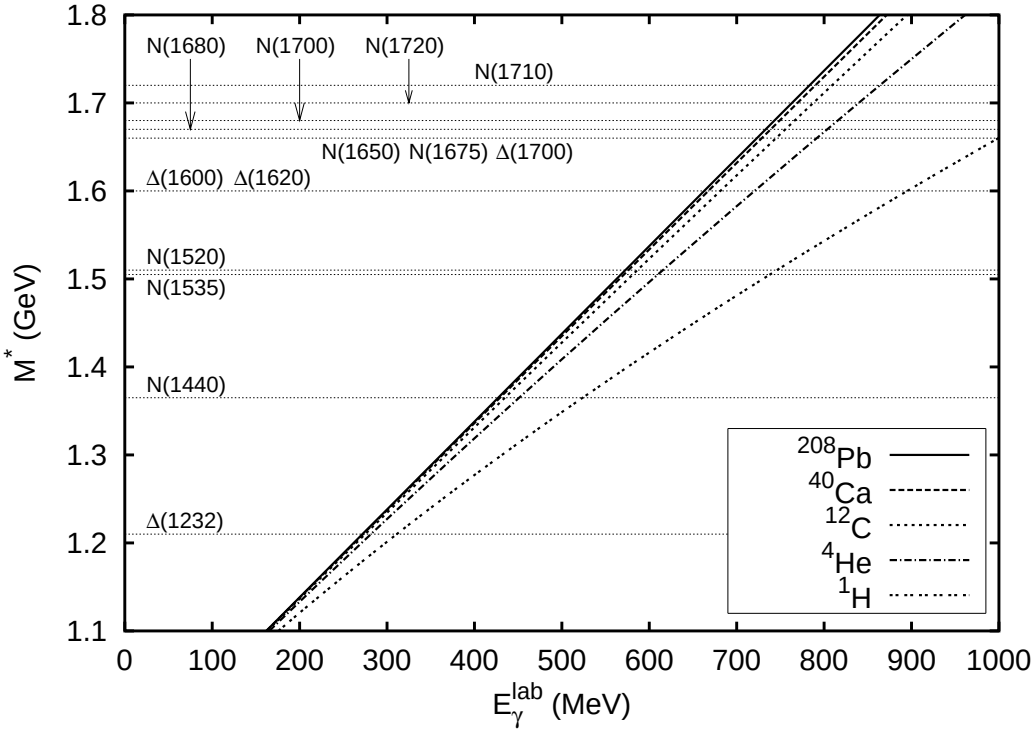

Figure E.3: Available energy for resonance excitations with different targets depending on the incident photon energy in the laboratory frame. Pole masses of nucleon resonances are marked in the figure as horizontal lines.

really small and the majority of the experiments were performed many years ago [6]. Thus, a large reduction of the error bar for the observables is expected. The role of other resonances, such as the Roper, is also of great interest.

Compton scattering and pion photoproduction on ^{3}He: $^3\mathbf{He}(\vec{\gamma},\gamma)$, $^3\mathbf{He}(\vec{\gamma},\pi^0)$, $^3\mathbf{He}(\vec{\gamma},\pi^+)$ and $^3\mathbf{He}(\vec{\gamma},\pi^-)$

As far as we know, there are no pion photoproduction experiments on ^{3}He with polarized photons in the energy range of the proposed beam line. Nevertheless, this process is of great interest at present thanks to realistic three-body models [14] developed in the last years and Compton [12] and pion photoproduction models [4] with consistent $\Delta(1232)$ description. In this way we would be able to perform an acceptable theoretical analysis of the influence of the $\Delta(1232)$ in systems like ^{3}He and few body systems. In addition, availability of polarized ^{3}He and polarized photon beams allow the determination of many helicity asymmetries which can provide information about models.

Compton scattering and pion photoproduction on ^{4}He: $^4\mathbf{He}(\vec{\gamma},\gamma)$, $^4\mathbf{He}(\vec{\gamma},\pi^0)$, $^4\mathbf{He}(\vec{\gamma},\pi^+)$ and $^4\mathbf{He}(\vec{\gamma},\pi^-)$

^{4}He is a high density and highly bound nucleus, compared to any other light nuclei. With only four nucleons, ^{4}He is strongly bounded and the role of the pion is emphasized. Thus, pion photoproduction appears as an excellent mechanism to study the pion in the nuclear medium. The role of the $\Delta(1232)$ and final state interactions may be also important, being of great interest for physicist who are developing few body models. Because of ^{4}He spin ($J = 0$), the contribution of photons with polarization parallel to the scattering plane is zero and the asymmetry $\Sigma = -1$ for any energy. There are experimental data in the energy range of 200 to 300 MeV [15] where no violation of $\Sigma = -1$ was found. High precision measurements of possible violations of this asymmetry in a broad energy range seems to be a suitable mechanism to search for internal structure effects in ^{4}He.

E.3 Experimental Setup

We will survey briefly the basic equipment required. It shares many common elements with other proposals. For instance, the recoil detector can be the same as described in the nucleon knockout proposal (see Appendix D), and the ToF spectrometer can be as the one described in the photon-neutron experiments (see Appendix B).

1. A relatively economical setup to detect particles, nucleons, pions and photons, would be a set of two large NaI(Tl) detectors (circa 48×48 cm) along with several 3-4 smaller ones (24×36 cm, 13×15, 24×25, 8×13) as employed at LEGS. Cooled CsI can be used with resolution advantages, as well as cooled pure NaI, but resolution here is not an important constrain. Also segmentation is not needed, but probably it would be less expensive to build the large scintillators from smaller blocks. Large segmented NaI(Tl) detectors with

associated veto are being employed to detect γ-rays of up to 800 MeV with an impressive 1 MeV resolution at MAMI-A2 and MAX-Lab.

2. Recoil detectors. These are to be placed near the target in order to detect and stop the relatively less energetic particles knocked out more or less transversely to the beam direction. A combination of plastic (veto) and inorganic scintillators and multiwire proportional chambers can be used, as in LEGS.

3. ToF spectrometers can be utilized to detect energetic particles more in the forward beam direction, recoiling protons and others. In its simplest form, it can be made out of 2 to 3 meter long 150×15 mm^2 cross-section plastic bars plus drift chambers and tracking detectors near the target (several small 100×100 mm^2 wire chambers). This can be also used as a part of a neutron ToF spectrometer with good efficiency. Note that a high efficiency neutron ToF detector plus calorimeter at intermediate energies is being built at JLAB for the e02013 experiment with involvement of an Spanish group [16]. Particle identification would be obtained with $\Delta E/E$ measurements in the tracking and ToF detector.

4. Cell of liquid H_2 (LH_2) for the proton target.

With a basic setup similar to the one just above described, many good experiments were performed at LEGS. The most difficult discrimination of Compton (γ,γ) and neutral pion production events would be achieved by comparing the γ-ray energy deposited in a large 'γ only vetoed' NaI detector near the target with the recoiling proton ToF to the bar array [10]. As an improvement of this setup, that would increase the counting rate, 4π configurations are suggested. They are available at several γ-ray facilities. DAPHNE, for instance, formerly at MAMI-A2 can achieve full 4π coverage with $3-4$ MeV resolution in the energy range of 100 to 800 MeV [17]. It has been replaced by the BNL Crystal Ball [18], with even better performance (1 MeV resolution). These detectors are relatively expensive but they can be shared among several facilities during their non overlapping experimental seasons.

A more modern setup would use high resolution thin silicon strips for tracking and ΔE layer of the telescope. There are several groups in Spain with experience in the use and production of such devices.

Alternatively, if a low density target is employed, like the gas jet of hydrogen proposed for the FAIR/EXL facility, tracking of the recoiling nuclear system would allow for a very precise kinematics determination. This would also be achieved with an active target system (gas chamber).

With around 10^7 photons per second, taking into account the modest values of the cross-section and that the targets will not be too thick, the demands on the electronics for counting rate are not too high. A few kHz of events are expected at most, for the most demanding measurements if a 4π recoil detector setup is chosen. The time resolution demands put at the coincidence and ToF setups would be moderate. Time resolutions of the order of 0.5 ns and less are today routinely achieved and should be enough for the experiments proposed in this chapter.

E.4 Beam time estimation

To have an idea of relative yield of different processes, cross-sections for photons in the 150 to 530 MeV range are approximately as follows:

1. Photoabsorption on single protons: a few hundreds of μbarns.
2. Pion photoproduction on single protons: a few tenths of μbarn/sr.
3. Compton scattering on protons: a few hundreds of nbarn/sr.
4. Single-nucleon knockout: 100 nbarn/sr (at 200 MeV).

With an usual 100 mg/cm^2 target thickness (liquid hydrogen target LH_2), beam time needed to achieve 10% statistical uncertainty for Compton scattering on protons, the less favoured case, with the expected intensity for the 150 to 530 MeV range would be just a few weeks. Note that during that same period and during the same experiment, data on all the other processes mentioned would also be taken simultaneously. If good tracking near the target can be obtained, vertex reconstruction techniques are possible and multiple thin targets can be used, increasing the counting rate by the number of layers of targets employed.

E.4.1 Further experiments

Further meson production: In the energy range expected for the proposed beam line the production of further mesons can be envisioned. By looking at figure E.1 we observe that the threshold for two-pion production is well below 500-600 MeV. This channel has been studied in the past, but precision studies would be possible at ALBA. An exotic channel is readily available through double-charged pion production $\gamma Z \to (Z-2)\pi^+\pi^+$. This isospin $I = 2$ channel cannot hold a molecular-type resonance as the strong interaction is repulsive [19], but at ALBA we could exclude the presence of any intrinsic narrow state (automatically a tetraquark) such as the much debated pentaquark in a flavor-exotic *KN* wave. Exotic spectroscopy is expected to come to the forefront of research in the upcoming years [20].

On the contrary, the production of $I = 0$ pion pairs is guaranteed to give a window into the established physics of the σ resonance [2] [$f_0(400-1200)$], a broad structure in $\pi\pi$ scattering and final states that is expected to have a large molecular-type tetraquark component [21]. The connection of this resonance to the Roper [22] can also be studied for example by the two-pion plus nucleon decay of the Roper.

Finally, study of higher resonances and production of heavier mesons cannot be discarded, as the improvements in laser technologies come fast these days. For instance, although photoproduction of $\eta(547)$ requires some 700 MeV on a hydrogen target, its threshold is lowered on heavier nuclei and can be within reach of ALBA depending on its final energy range. Again, precision studies of $SU(3)$ Lagrangian are now possible, and topics like hidden strangeness or $SU(3)$ breaking could potentially be addressed. The role of this meson inside nuclei could also

[2] Current estimates put it at 500 MeV

be studied from its characteristic two-photon decay. It also provides three-pion final states with very well defined energy.

Pentaquark: Since the first experimental traces of its existence [23], the pentaquark, $\Theta^{+}(1540)$ is undoubtedly one of the hottest topics in intermediate energy physics. Due to this interest of the scientific community it should be studied whether the ALBA facility gives any possibility to contribute to research on the non-three quark baryons and mesons states. A pentaquark production experiment on free nucleons requires an amount of energy that is far away from the ALBA facility, but there are other possibilities that should be considered. For the same reasons as in subsection E.2.2 the threshold energy of pentaquark production is reduced on nuclei. The energy reduction from the free case is considerable and it would be possible to excite a pentaquark with only 800 MeV on a ^{12}C target. If these kind of experiments could be carried out, ALBA would become one of the first facilities of the world to start an experimental programme on pentaquark excitation in nuclei, beginning the study of its properties and effects in nuclear medium.

Bibliography

[1] K. Hagiwara *et al.*, Phys. Rev. **D 66**, 010001 (2002).

[2] M. Benmerrouche, R.M. Davidson, and N.C. Mukhopadhyay, Phys. Rev. **C 39**, 2339 (1989). R.M. Davidson and N.C. Mukhopadhyay, Phys. Rev. **D 42**, 20 (1990).

[3] R.L. Walker, Phys. Rev. **182**, 1729 (1969). M.G. Olsson and E.T. Osypowski, Phys. Rev **D 17**, 174 (1978). S. Nozawa, B. Blankleider, and T.-S.H. Lee, Nucl. Phys. **A 513**, 459 (1990). R.M. Davidson, N.C. Mukhopadhyay, and R.S. Wittman, Phys. Rev. **D 43**, 71 (1991). H. Garcilazo and E. Moya de Guerra, Nucl. Phys. **A 562**, 521 (1993). M. Vanderhaeghen, K. Heyde, J. Ryckebusch, and M. Waroquier, Nucl. Phys. **A 595**, 219 (1995). T. Feuster and U. Mosel, Nucl. Phys. **A 612**, 375 (1997). D. Drechsel, O. Hanstein, S.S. Kamalov, and L. Tiator, Nucl. Phys. **A 645**, 145 (1999).

[4] C. Fernández-Ramírez, E. Moya de Guerra, and J.M. Udías, *Pion Electro- and Photoproduction on Nuclei in a Lagrangian Approach*. 6^{th} Workshop on Electromagnetically Induced Two-Hadron Emission, Pavia, Italy (2003). C. Fernández-Ramírez, E. Moya de Guerra, and J.M. Udías, in preparation.

[5] R.A. Arndt, R.L. Workman, Z. Li, and L.D. Roper, Phys. Rev. **C 42**, 1853 (1990), Phys. Rev. **C 42**, 1864 (1990). R.A. Arndt, I.I. Strakovsky, and R.L. Workman, Phys. Rev. **C 53**, 430 (1996). R.A. Arndt, W.J. Briscoe, R.L. Workman, and I.I. Strakovsky, SAID database, **http://gwdac.phys.gwu.edu**

[6] K. Ukai and T. Nakamura. *Data Compilation of Single Pion Photoproduction below 2 GeV. INS-T-550* (1997). **http://ccwww.kek.jp/databank/index_e.html**

[7] A.M. Sandorfi. *Polarized Photon Facilities – Windows to New Physics* in Baryons'95: Proceedings of the 7^{th} International Conference on the Structure of Baryons, Santa Fe, USA (1995). Editors: W. Weise, B.F. Gibson, P.D. Barnes, and J.B. McClelland (World Scientific, 1996).

[8] **http://wwwa2.kph.uni-mainz.de/A2/**

[9] **http://www.maxlab.lu.se/**

[10] G. Blanpied *et al.*, Phys. Rev. **C 64**, 025203 (2001).

[11] R. Beck *et al.*, Phys. Rev. Lett. **78**, 606 (1997).

[12] V. Pascalutsa and D.R. Phillips, Phys. Rev. **C 67**, 055202 (2003).

[13] H. Garcilazo and E. Moya de Guerra, Phys. Rev. **C 49**, R601 (1994). H. Garcilazo and E. Moya de Guerra, Phys. Rev. **C 52**, 49 (1995).

[14] A. Kievsky, M. Viviani, and S. Rosati, Nucl. Phys. **A 551**, 241 (1993), Nucl. Phys. **A 577**, 551 (1994). W. Glöckle, H. Witala, D. Hüber, H. Kamada, and J. Golack, Phys. Rept. **274**, 107 (1996). E. Garrido, D.V. Fedorov, and A.S. Jensen, Phys. Rev. **C 55**, 1327 (1997). E. Nielsen, D.V. Fedorov, A.S. Jensen, and E. Garrido, Phys. Rept. **347**, 373 (2001).

[15] V. Bellini *et al.*, Nucl. Phys. **A 646**, 55 (1999).

[16] **http://www.jlab.org/exp_prog/CEBAF_EXP/E02013.html**

[17] G. Audit *et al.*, Nucl. Instr. Meth. **A301** (1991) 473.

[18] **http://www.gwu.edu/ ndl/research5e.htm**

[19] J.E.F.T. Ribeiro, Z. Phys. **C 5**, 27 (1980).

[20] F. J. Llanes-Estrada, eConf **C0309101**, FRWP011 (2003). **arXiv:hep-ph/0311235**

[21] A. Gómez Nicola and J.R. Peláez, Phys. Rev. **D 65** 054009 (2002). **arXiv:hep-ph/0109056**

[22] H. Garcilazo and A. Valcarce, Phys. Rev. **C 68**, 035207 (2003). J. Vijande, P. González, H. Garcilazo, and A. Valcarce, Phys. Rev. **D 69**, 074019 (2004).

[23] T. Nakano *et al.*, Phys. Rev. Lett. **91**, 012002 (2003).

Appendix F

Calibration of gamma-ray instruments for Nuclear Astrophysics

F.1 Introduction

Nuclear astrophysics relies on gamma-ray line astronomy, mainly in the MeV range, to test its predictions. Some examples of gamma-ray lines already detected are the 511 keV line, tracing electron-positron annihilation in the interstellar medium and in the proximity of very compact objects such as black holes or neutron stars, the 1.809 MeV line, showing the galactic sites of the radioactive decay of the ^{26}Al isotope, or the 1.157 MeV line, coming from ^{44}Ti decay in young supernova remnants. However, some other gamma-ray lines still remain elusive, as for instance those emitted during supernova and nova explosions (i.e., ^{56}Co lines at 847 keV and 1.238 MeV, ^{7}Be line at 478 keV or ^{22}Na line at 1.275 MeV). Their detection is the only way to trace the nucleosynthesis of radioactive isotopes during these explosions, and thus to understand their explosion mechanism. Since supernovae are the major sources of the elements in the Universe, the knowledge of their nucleosynthetic activity is a really relevant topic for astrophysics. Other scientific objectives for MeV gamma-ray astronomy include the sun, galactic compact objects, active galactic nuclei, gamma-ray bursts, and cosmic gamma-ray background.

The reason for the very rare detections of cosmic gamma-ray lines is that the MeV range faces important challenges from the instrumental point of view. In addition to the general difficulties of gamma-ray detection (few signal photons have to be extracted from very intense backgrounds), the MeV range is specially difficult, since it corresponds to the energy range where Compton scattering (with small cross sections) is dominant, making it harder to handle than photoelectric absorption or pair formation, at lower and larger energies, respectively. Actually, the present generation of gamma-ray instruments makes use of geometrical optics - shadowcasting in modulating aperture systems - or quantum optics - Compton scattering. This kind of instruments is faced with the problem that *bigger does not necessarily mean better*. The reason for this apparent contradiction is that the collection area in traditional gamma-ray telescopes should be roughly equal to the detection area. Therefore, the larger the collection area, the larger the detection volume and thus the higher the instrumental background. This means that significant improvements in sensitivity need huge instruments, too expensive for space mis-

sions. An innovative concept for detecting gamma-rays in the MeV range, which overcomes this problem and allows for unprecedented sensitivities consists of focusing the gamma-rays from a large collection area onto a small detector.

Last but not least: there is an increasing interest in the high-energy astrophysics community in the use of polarimetry in the MeV range as an important diagnostic tool for the nature of the cosmic sources of gamma-rays. In a recent workshop held in Stanford (USA), a large number of studies related to this topic were presented (see [1]), showing the potential relevance of polarization measurements and some ways to make it technically feasible. In fact, recent measurements with the RHESSI satellite have shown that this is the case (see [2] for the detection of polarization in a gamma-ray burst).

A gamma-ray beam line at the future spanish synchrotron ALBA, based on the inverse Compton scattering of laser photons with highly-relativistic electrons from the synchrotron ring, would be extremely useful for the analysis of the performance of a gamma-ray lens and other planned instruments in the MeV domain. There is not at present any other european facility offering this unique opportunity for getting an intense, highly collimated and polarized beam in the MeV energy range.

F.2 Steps toward a gamma-ray lens for nuclear astrophysics

Gamma-rays can interact coherently inside a crystal lattice provided that the angles of incidence are very small. As a consequence of the small scatter-angles Bragg diffraction in the Laue geometry is more convenient: photons propagate through the entire crystal, using all the crystal thickness for diffraction.

In a crystal diffraction lens, crystals are arranged in concentric rings such that they will diffract the incident radiation of a particular energy onto a common focal spot where the detector is placed (Fig. F.1).

In order to be diffracted, an incoming gamma-ray must satisfy the Bragg-relation:

$$2\, d_{[hkl]}\, sin\theta \;=\; n\,\frac{hc}{E}\,, \tag{F.1}$$

where $d_{[}hkl]$ is the crystal plane spacing, θ the incident angle of the photon, n the reflection order, and E the γ-ray energy. The crystal plane spacing is given by the lattice constant of the material, a, and the Miller indexes, $[hkl]$, according to the expression:

$$d_{[hkl]} \;=\; \frac{a}{\sqrt{h^2+k^2+l^2}}\,. \tag{F.2}$$

A crystal at a distance r from the optical axis is oriented so that the angle between the incident beam and the crystalline plane is the Bragg angle θ. All crystals arranged in the same concentric ring use the same crystalline planes ($[hkl]$) to diffract the incoming gamma-ray.

Laue diffraction lenses have demonstrated their potential in laboratory measurements ([4], [5], [6], [7]).

The CLAIRE project, developed at CESR, was born to prove the principle of a Laue diffraction lens for nuclear astrophysics. Its natural continuation is a project for a space mission named MAX (for Max von Laue).

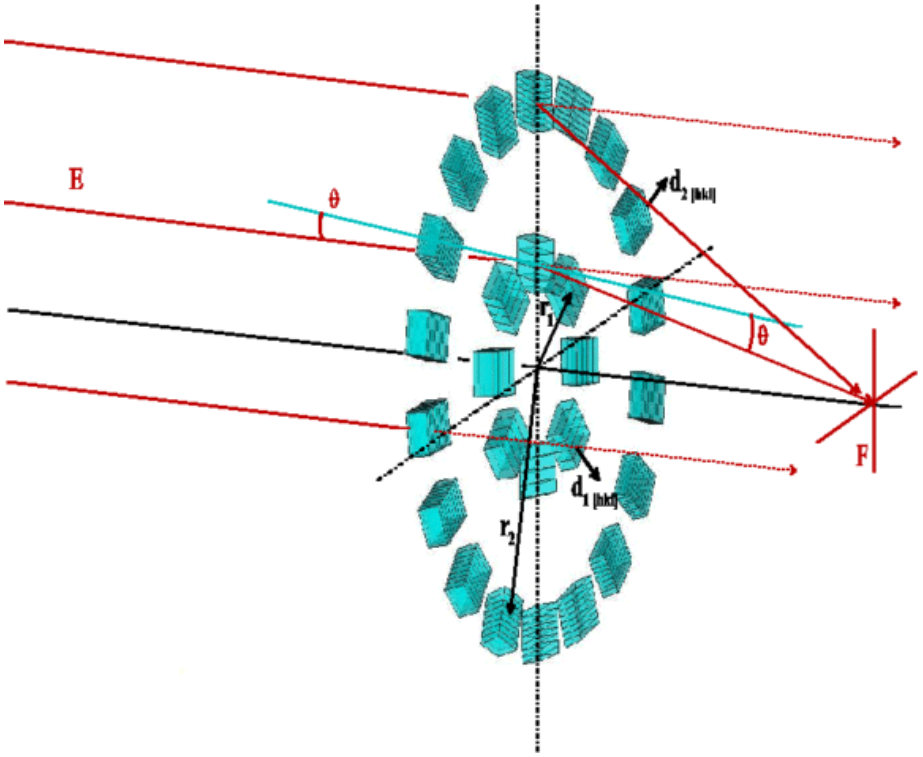

Figure F.1: The basic design of a crystal diffraction lens in Laue geometry. Crystals are disposed on concentric rings such that γ-rays are focused into a common focal spot by Bragg-reflection in Laue geometry

F.2.1 CLAIRE: a prototype

CLAIRE is a balloon-borne telescope dedicated to validating the concept of a crystal diffraction lens for nuclear astrophysics (see [3]). CLAIRE's lens consists of 556 Ge-Si mosaic crystals, focusing 170 keV γ-ray photons onto a 3x3 matrix of Ge detectors placed at its focus. In June 2001, the instrument was flown on a stratospheric balloon by the French Space Agency CNES (see [8]). CLAIRE was also tested on a long optical bench that was set up at an aerodrome near Figueres, Spain (see [9]). Both experiments successfully demonstrated the working principle of the γ-ray lens. For more information about CLAIRE, please refer to [10] and [11].

F.2.2 MAX: a space mission

The MAX mission concept proposes a space-borne crystal diffraction telescope [12, 13], featuring a Laue lens able to focus in two energy bands, relevant for nuclear astrophysics (450-540 keV and 800-920 keV). Two rings assemblies (an outer ring with Ge crystals and an inner one with Cu crystals) would focus the photons into a small detector placed in a spacecraft flying in formation with the lens spacecraft.

F.3 Experimental proposals for the Gamma-Ray Line beam

We propose three types of measurements: **diffraction efficiencies of mosaic crystals**, **whole lens tuning** (short term measurements) and **other calibrations** (long term measurements). We detail below just the first most immediate experimental proposal.

F.3.1 Measurement of diffraction efficiencies in mosaic crystals

The precise measurement of the diffraction efficiency of mosaic crystals is essential to determine the main properties of the gamma-ray lens telescope, i.e., effective area, field of view and energy bandpass.

Measurement status

The first measurements of diffraction efficiencies of Ge mosaic crystals (10 mm $\times$ 10 mm size) in the energy range from 200 to 500 keV were made at the Advanced Photon Source synchrotron (APS) at Argonne National Laboratory [14]. These measurements allowed to perform a detailed study about diffraction efficiency in the [111] and [220] crystalline planes. Second and third order diffraction efficiencies ([440] and [333] planes) were also measured, as well as the dependency of diffraction efficiency on *mosaic width* (as defined in the Darwin model of mosaic crystals). A Monte Carlo simulation ray-tracing program based on the Darwin model of the mosaic crystals was written in order to model these results. General agreement was found between the model and the experimental measurements; therefore, the first determination of γ-ray lens performance were possible.

The gamma-ray beam line (GRL) would allow to repeat the measurements performed at the Advanced Photon Source synchrotron in other energy ranges *(0.5 to 1 MeV)* and with other crystals *(Cu or Si)*. Both the measurements in other energy ranges and with other crystals are an essential step for the development of the future project MAX.

Experimental setup

The experimental setup, similar to the APS experiment [14], is shown in Fig. F.2. The experiment consists of a block (Cu,W,...) to absorb low-energy photons, a first crystal, a second crystal and an HPGe detector. The first and second crystals form a double-crystal monochromator. The distance between them will be long (around 500cm) due to the small Bragg angle at high energy. Table F.1 shows these angles for Ge(a=5.65$\dot{A}$). In the case of Cu(a=3.61$\dot{A}$), these angles will be larger since the *lattice constant* is smaller (see equations (F.1) & (F.2)).

Using the coordinate system shown in Fig. F.2, both the first and the second crystal should be able to be translated along the x- and y-axis. The HPGe detector should be translated in three directions using a translation stage. If we define θ as the rotation angle about the x-axis, ϕ as the rotation angle about the y-axis, and χ as the rotation angle about the z-axis, the first crystal should be able to rotate in ϕ, whereas the second crystal must rotate in ϕ, θ and χ. The ϕ rotation will be used to adjust the Bragg angle, whereas the χ and θ rotations are needed to align the

reflection plane (hkl)	Bragg angle (degree)	Energy (keV)
111	0.218	500
311	0.417	500
111	0.109	1000
311	0.208	1000

Table F.1: Bragg angles for Ge.

second crystal perpendicular to the beam direction. Therefore two stages able to rotate in ϕ, θ and χ angles are needed for the crystals.

A HPGe-detector at 10m from the first crystal will be used to measure the diffracted and transmitted flux of the crystals. The energy spectrum will be measured using the detector and a multichannel analyzer (MCA).

To measure the diffraction efficiency as a function of energy, the first crystal will be adjusted in the Bragg angle to select a narrow band of energies. After accumulating the MCA spectrum of the singly diffracted beam, the second crystal will be centered on the diffracted beam of the first crystal. A rocking curve (curve of the intensity versus angle) of the second crystal at the Bragg angle will be measured. Finally, an MCA spectrum of the doubly diffracted beam with the second crystal adjusted to the peak of the rocking curve will be accumulated. These measurements will be repeated at several energies from 200 to 1000 keV. The ratio of doubly diffracted to singly diffracted flux is then a measure of the diffraction efficiency.

Experimental devices and beam time

Crystals will be provided by research institutes belonging to the MAX-CLAIRE collaboration. The HPGe detector used in the CLAIRE project (and in the long distance test in Ordis) as well as the electronics and the data acquisition system could be used to make the measurements in the gamma ray beam line.

In order to make the measurements in the GRL it is essential to have a pointing system that allows to center the gamma-ray beam on the crystal. Also, we must have stable supports (optical bench or similar) in order to place the crystals and detectors. In addition, the crystals must be mounted on devices that allows to control their displacement and their rotation with high accuracy.

From the flux obtained with the CO_2 laser system [15], and the data from the APS measurements [14], we can estimate the beam time necessary for each measurement, i.e. the accumulation time of the MCA spectrum of a singly diffracted beam, necessary to measurement the diffraction efficiencies (see above). These times will be around a few minutes and could be smaller than a minute if the gamma-beam absorption is reduced. The characterization of a single crystal (measurement of the diffraction efficiencies for a given diffraction plane) would typically involve around 2800 of such exposures. In order to make this estimation we suppose that the energy steps in the range from 300keV to 1000keV is 10 keV; and also we admit that 40 exposures are enough to obtain the rocking curve of the second crystal. This rough estimation

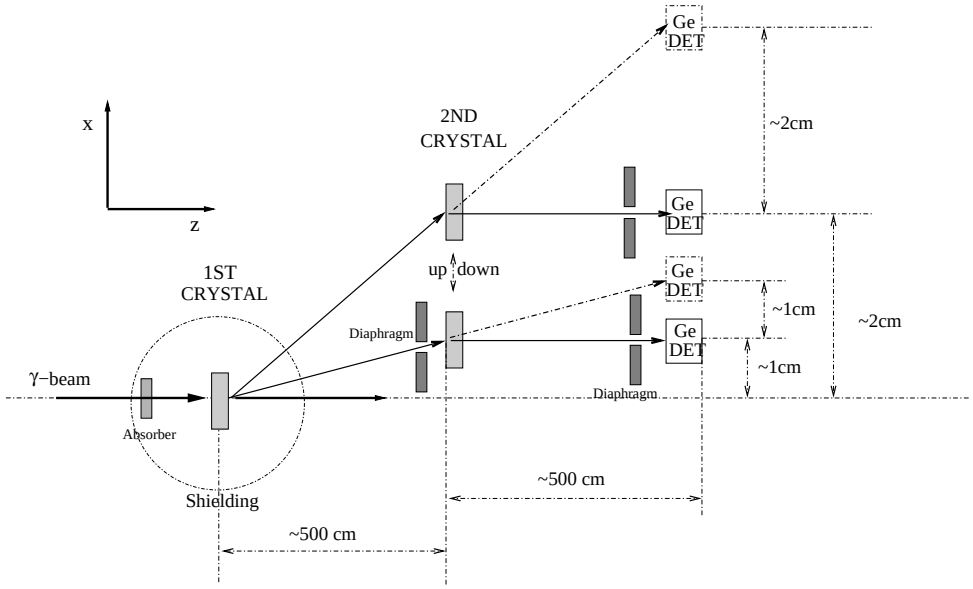

Figure F.2: The experimental setup of the GRL experiments. A block(Cu,W,...) to absorb low-energy photons, a first crystal, a second crystal and an HPGe detector. The distances between first and second crystal and the detector are shown. Also shown are the vertical displacement of the detector and the second crystal for the singly diffracted and doubly diffracted beam, both at 500KeV and at 1000keV.

of the number of exposures and the time per exposure allows us to consider that the total time necessary to make the measurements of diffraction efficiencies in the crystals relevant to MAX, is around one month.

F.3.2 Tuning the crystals of the Laue diffraction lens

Tuning the lens means than each crystal of the lens should be oriented so that the angle between the incident beam and the crystalline plane is the Bragg angle. This orientation of the crystals allows to define the lens focus and the corresponding focal distance, from the Bragg angle and the distance of each crystal to the *optical axis*. Therefore, the focal distance depends on the diffracted energy, because the Bragg diffraction angle depends on it (see Eq. (F.1)).

The focal distance of the CLAIRE lens is 279 cm for 170 KeV, whereas focal distances around 100 m are envisioned for MAX. It is clear that any type of lens able to focus gamma rays has extremely long focal distances, much larger than typical lab sizes. Incidentally, there is another type of gamma-ray lens under study at CESR, the Fresnel lens, which has typical focal distances of 10^6 km, thus needing distances around 500 m at least to perform the scaled tests needed to validate the functioning principle of the lens [16]. In the case of the Laue lens CLAIRE, the long distance test performed in Ordis and the CNES stratospheric balloon flight proved that the tuning of the lens can be performed at a distance shorter than the focal length provided that the energy of the photons is scaled accordingly (see above, section 2.1). An alternative way to reduce the focal length without reducing the diffracted energy would

be to use second and third diffraction orders. Despite the decreasing diffraction efficiency as reflection order increases, a large incoming flux as expected in the GRL would permit such type of measurements. This would allow for the tuning of the whole lens, a very important step indeed, to guarantee the performance of the lens.

F.3.3 Other calibrations

Another important application of the GRL would be the calibration of detectors. The GRL would provide an excellent photon source that would make possible to measure the capability to detect polarization, in addition to the standard sensitivity of the detector.

There is a previous experience of a GRL used to calibrate an instrument, based on the Compton scattering technique to detect gamma-rays in the MeV energy range. This was the Medium Energy Gamma-ray Astronomy (MEGA) instrument, in the 400 KeV - 50 MeV range, successfully calibrated at HIGS (High Intensity Gamma-ray Source), in Durham, USA [17].

F.4 Summary

The GRL would be very well suited for the calibration of gamma-ray instruments for astrophysical observations, particularly the γ-ray lens. It would allow for the characterization of the crystals to be used to build the lens, a necessary step to make the whole project feasible. In addition it would be a really timely facility, already in the commissioning phase, since it would be operating at the epoch when testing of the crystals for the space mission MAX should be performed.

Bibliography

[1] X-Ray Polarimetry Workshop, SLAC, Stanford, California 9-11 February 2004: http://heasarc.gsfc.nasa.gov/docs/heasarc/polar/ polar.html

[2] W. Coburn and S. Boggs, Polarization of the prompt gamma-ray emission from the gamma-ray burst of 6 December 2002, Nature 423 (2003), 415-417.

[3] P. Laporte *et al.*, CLAIRE - towards the first light for a gamma-ray lens, Nucl. Instr. Meth. A442 (2000) 438-442

[4] Smither, R.K. (1989), Smither, R.K. (1989), Variable focus crystal diffraction lens, Review of Scientific Instruments, vol. 60, 2044-2047

[5] von Ballmoos, P., Smither, R. K. (1994), A positron annihilation radiation telescope using Laue diffraction in a crystal lens, Astrophys. Jour. Suppl., vol. 92, 663-669

[6] Naya, J.E., et al (1996), Experimental results obtained with the positron-annihilation-radiation telescope of the Toulouse-Argonne collaboration, NIMA, vol. 373, 159-164

[7] Köhnle, A. et al. (1997), Recent progress in focusing gamma rays, Proc. SPIE, vol. 3114, 488-498

[8] P. von Ballmoos *et al.*, CLAIRE's first light, New Astronomy Reviews 48 (2004a), 243-249.

[9] web-TGD: Web of the Long Distance Test (Ordis 2003): http://www.ieec.fcr.es/hosted/claire/tgd.html

[10] H. Halloin it et al., CLAIRE γ-ray lens: flight and long distance test results, 2004, SPIE proc, Vol. 5168, 471-481

[11] H. Halloin, Premières lumières d'une lentille gamma, PhD, Univ. Paul Sabatier, Toulouse 2004.

[12] P. von Ballmoos *et al.*, MAX-a gamma-ray lens for nuclear astrophysics, 2004b, SPIE proc, Vol. 5168, 482-491

[13] web-MAX: Web of the mission concept MAX: http://www.cesr.fr/ pvb/MAX/index.html

[14] A. Köhnle *et al.*, Measurement of diffraction efficiencies relevant to crystal lens telescopes, Nucl. Instr. Meth. A416 (1998) 493-504

[15] J.L. Taín, A gamma-ray beam line for nuclear physics and applications at ALBA (http://ific.uv.es/gamma/aurora/aurora.htm)

[16] G. Skinner *et al.*, Fresnel Lenses for X-ray and Gamma-ray Astronomy Proc. SPIE Volume 5168 pp 459-470, 2003

[17] R. Andritschke *et al.*, The calibration setup of the MEGA prototype at the high intensity γ-ray source, NewAR 48 (2004) 281-285.

Appendix G

Calculation of beam parameters

The generation of energetic γ-rays at ALBA is possible through the process of Compton scattering of laser photons from the highly energetic electrons circulating in the synchrotron ring. It is an alternative method to the generation of γ-rays through the electron bremsstrahlung process and has specific advantages. The characteristics of the γ-ray beam (energy, intensity, etc.) depend on the parameters of the colliding electron and laser beams and will be explored in the next sections.

G.1 Relevant parameters of the ALBA synchrotron ring

The accelerator parameters from the original design [1] of the synchrotron at LLS are presently being reconsidered [2], with the aim to achieve improved performances. The exact characteristics of the γ-ray beam will depend on the parameters of the lattice finally chosen but at present all indicates that it will be the so called DBA lattice and its parameters (except for minor final adjustments) can be considered representative.

The accelerator complex includes a 100 MeV linac, the booster which brings the energy up to the nominal value of 3.0 GeV, and the ring itself. The booster and the ring will share the same shielding tunnel. The ring has a circumference length of about 266 m. In the normal operation mode the ring is filled with about 1.4×10^{12} electrons grouped in 20 ps long (r.m.s.) bunches separated by 2 ns. Electrons are refilled in a time interval of about 100 s in order to keep the intensity within 1 % of its nominal value (250 mA).

The basic DBA cell includes two units, each one consisting of a bending magnet plus a series of quadrupole and sextupole magnets (see Fig. G.1). Four cells are grouped into a symmetric unit (super period) which is repeated four times in order to complete the ring. Apart from the electron ring energy E_e and intensity I_e, relevant quantities for the calculation of the γ-ray beam parameters are the horizontal and vertical beam sizes and divergences along the straight sections between bending magnets, where the collision between laser photons and electrons can take place. The r.m.s. envelopes σ_X (horizontal) and σ_Y (vertical), and the r.m.s. slope envelopes $\sigma_{X'}$, $\sigma_{Y'}$ can be calculated from the beam emittances ε_X, ε_Y and the so called betatron functions β_X, β_Y and their derivatives (see for example [3]). The beam energy resolution contributes to

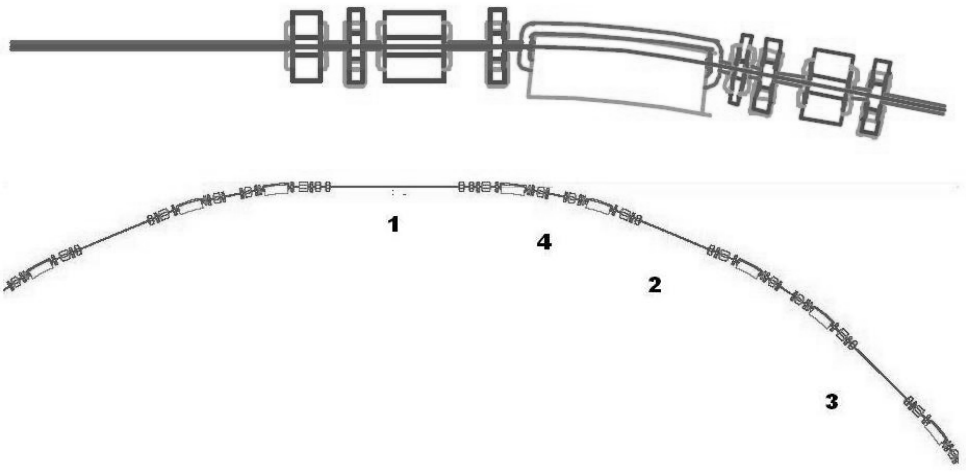

Figure G.1: DBA lattice unit and super cell.

the horizontal sizes and slopes through the horizontal momentum dispersion η_X and the angular momentum dispersion $\eta_{X'}$ functions, which also determine the trajectories of electrons away from the nominal ring energy. The dynamic aperture or momentum acceptance of the ring $\Delta p/p_0$ determine the maximum admissible deviation from the central trajectory.

The relevant parameters for the DBA cell are summarized in Table G.1.

Ring	
Intensity I_e	0.250 A
Energy E_e	3.0 GeV
Resolution σ_{E_e}/E_e	0.001
Horizontal emittance ε_x	3.6 nmrad
Vertical emittance ε_y	0.036 nmrad
Momentum acceptance $\Delta p/p_0$	0.03

Straight sections				
	1	2	3	4
Interaction length L_{int} (m)	13.2	8.6	8.6	3.9
Horizontal beam envelope σ_X (μm)	228	113	131	280
Vertical beam envelope σ_Y (μm)	14	6.5	6.5	17
Horizontal slope envelope $\sigma_{X'}$ (μrad)	21	66	41	20
Vertical slope envelope $\sigma_{Y'}$ (μrad)	2.6	5.5	5.5	2.1

Table G.1: Parameters of the DBA cell

Besides the three distinct long straight sections which will be considered usually for insertion devices (labelled 1, 2, 3 in Fig. G.1 and G.2) in the symmetric DBA super-cell, we also

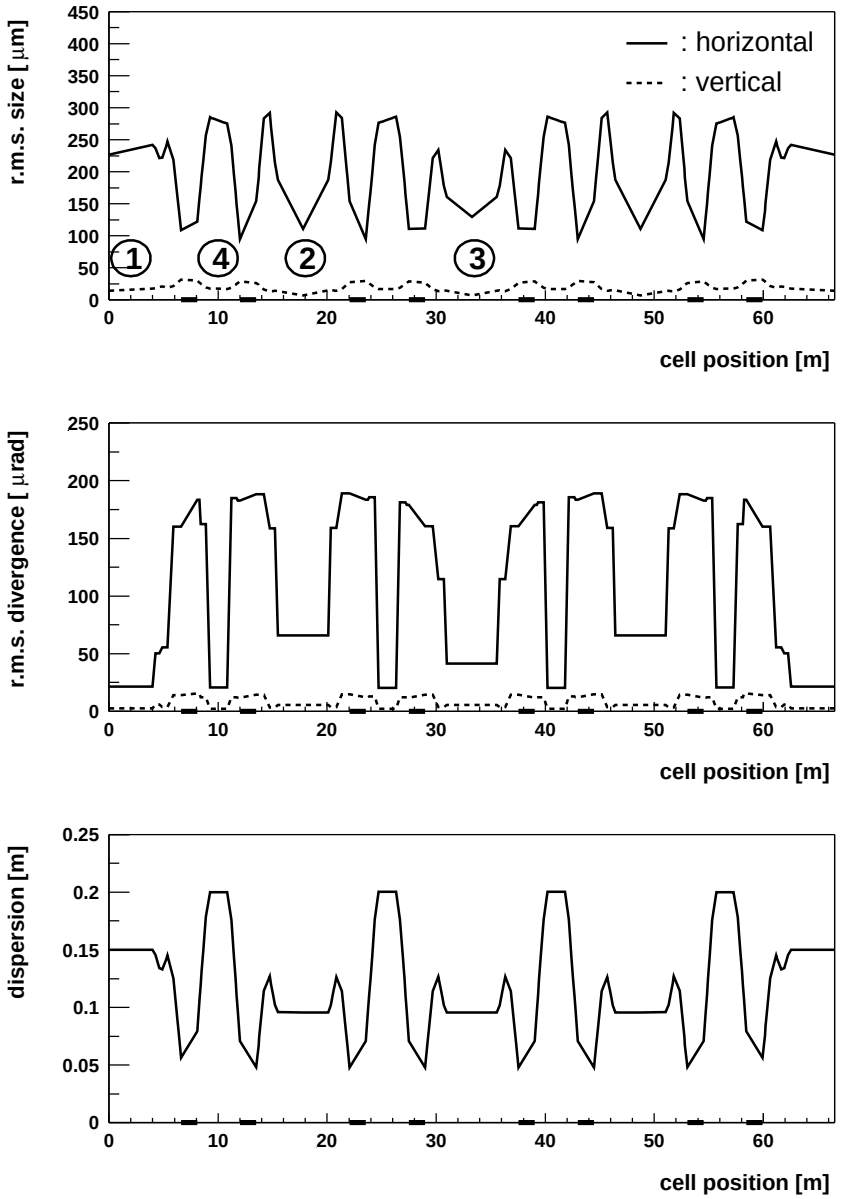

Figure G.2: Beam size, divergence and dispersion along the DBA cell (super period). Indicated in the horizontal axis are the positions of the bending magnets.

consider the straight section between the bending magnets of the DBA doublet (labelled 4) as candidate for the interaction with the laser beam. It should be noticed that the value of the interaction length L_{int} quoted in the table corresponds to the distance between bending magnets, where the interaction of laser and electron beam will take place. This is larger than the usually quoted value, which is the available space for insertion devices. In the table the values of the electron beam size and divergence are given at the middle of the straight sections. The evolution of the beam size and divergence and of the dispersion along the cell is shown in Fig. G.2. These electron beam parameters have been calculated from the DBA lattice optical functions [4].

G.2 Compton scattering on energetic electrons

Back in 1963, it was pointed out ([5], [6]) the possibility to produce an energetic and highly polarized γ-ray beam through Compton scattering of polarized laser light with the electrons accelerated in a high energy machine.

The kinematics of the collision is described by the modified Compton formula [7]:

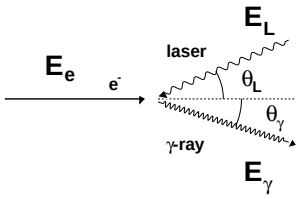

$$E_\gamma = \frac{(1+\beta_e cos\theta_L)E_L}{1-\beta_e cos\theta_\gamma + \frac{E_L}{E_e}\left[1+cos(\theta_\gamma+\theta_L)\right]} \tag{G.1}$$

Here E_e, E_L and E_γ, are respectively the electron, laser photon and γ-ray energies, β_e the electron velocity in units of c, and θ_γ (θ_L) the angle of the outgoing (incoming) photon with respect to the incident electron direction, not necessarily in the same plane. For fixed E_e and E_L, the maximum possible γ-ray energy is obtained for the backscattered photon ($\theta_\gamma = 0°$) in a head-on collision ($\theta_L = 0°$).

Laser	CO_2	Nd:YAG	Nd:YAG(SH)	Nd:YAG(TH)	Nd:YAG(FH)
E_L (eV)	0.117	1.17	2.34	3.51	4.68
E_γ^{max} (MeV)	16.0	153.1	291.3	416.7	531.0

Table G.2: Maximum γ-ray energies for several commercial lasers

In Fig. G.3 we represent the maximum γ-ray energy obtainable for $E_e = 3$ GeV (the nominal energy of ALBA) as a function of laser wave-length. Indicated in the figure and in Table G.2 are the maximum γ-ray energies which can be obtained with some of the commercially available high power lasers. All γ-ray energies are possible between the minimum ($\equiv E_L$) and the maximum. Due to the relativistic "boost" the scattered gamma rays are strongly forward focused,

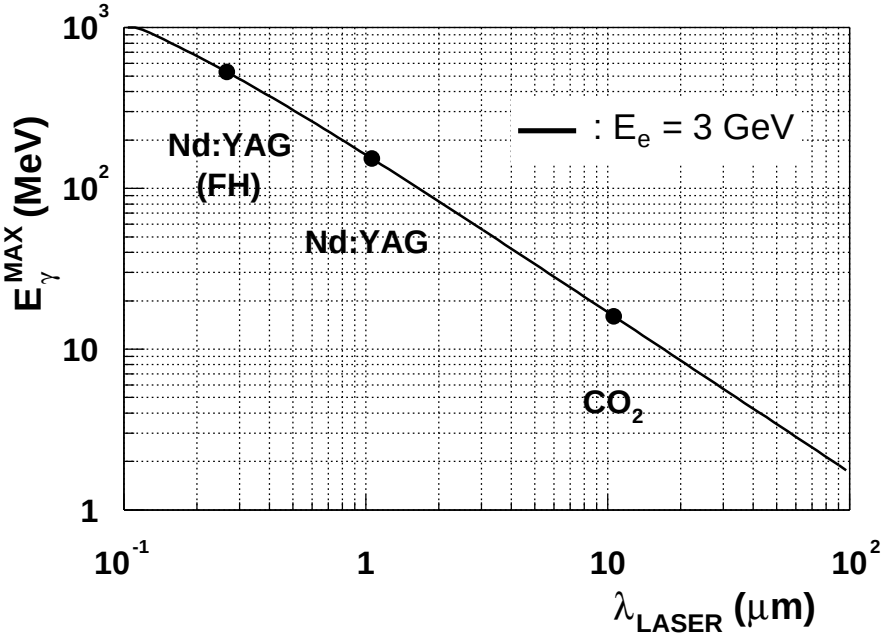

Figure G.3: Maximum γ-ray energy as a function of laser photon energy for $E_e = 3$ GeV.

thus forming a beam, as can be deduced from Fig. G.4, which shows the angle θ_γ as a function of $z = E_\gamma/E_\gamma^{\max}$, the energy of the γ-ray normalized to the maximum energy. We see that the top 90 % range of γ-ray energies is contained within a cone of angle 0.55 mrad. This figure and the following, has been calculated for $E_e = 3.0$ GeV and $E_L = 1.17$ eV (Nd:YAG laser in its fundamental mode), but will change little over the range of energies of practical high power lasers when the relative energy variable z is used.

The γ-ray energy spectrum can be obtained through the proper integration of the differential cross section angular distribution. The expression can be written as follows [8]:

$$\frac{d\sigma_C}{dz} = \frac{1}{2(1+x)} C_{00} = \frac{1}{2(1+x)} \left[1 - y + \frac{1}{1-y} - \frac{4y}{x(1-y)} + \frac{4y^2}{x^2(1-y)^2} \right] \qquad \text{(G.2)}$$

where $x = 4E_eE_L/m_e^2c^4$, $y = E_\gamma/E_e$. Again, $d\sigma_C/dz$ does not vary much with E_e and E_L, and we represent in Fig. G.5 the normalized (by σ_C) values. The distribution has a saddle shape, with the maxima at the energy extremes being twice than in the middle. The total cross section is a slowly varying function of electron and laser energies, and has a value of approximately $\sigma_C = 0.6$ b.

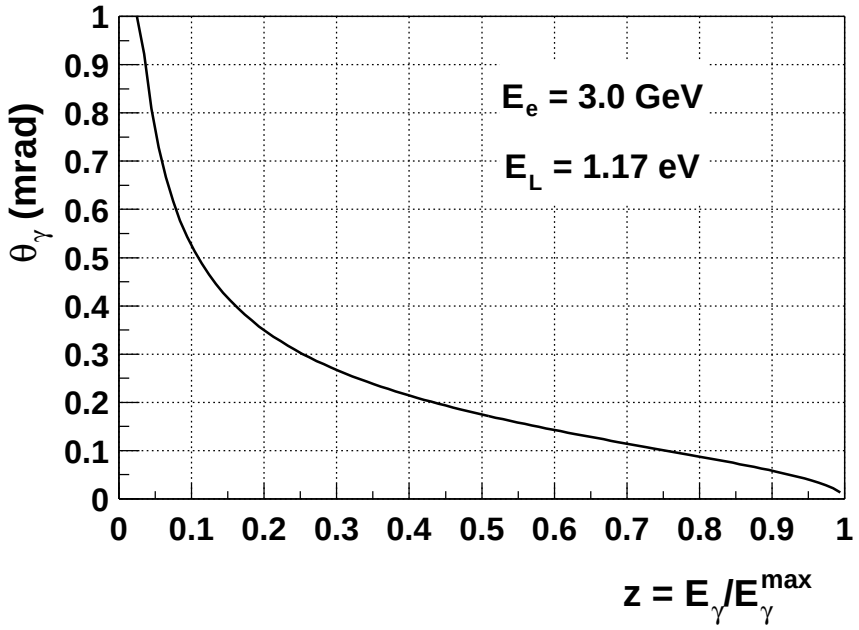

Figure G.4: γ-ray energy as a function of the scattering angle

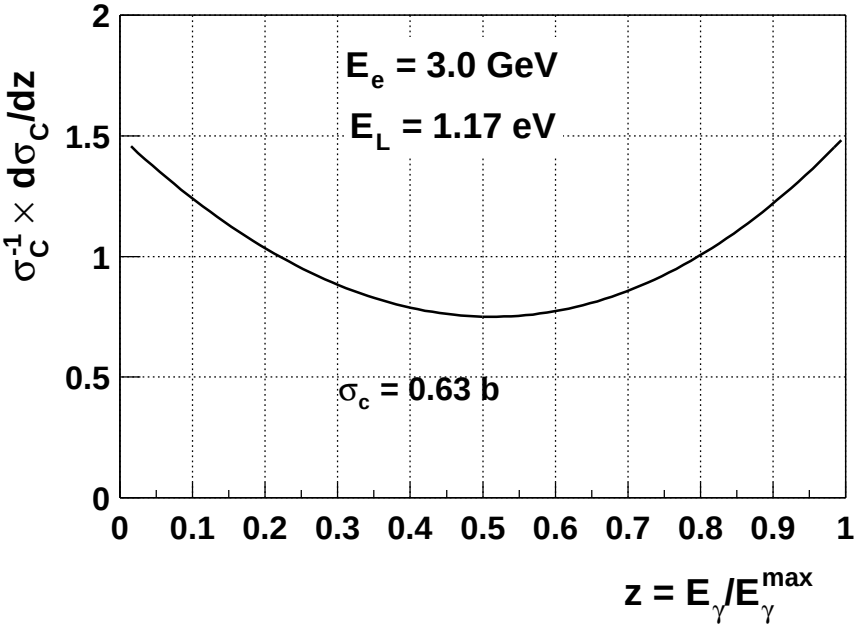

Figure G.5: γ-ray relative intensity as a function of energy

If the laser beam is polarized, either linearly or circularly, the polarization is transferred to the backward scattered gamma. For fully polarized laser photons the degree of linear P_γ^L or circular P_γ^C polarization of the scattered γ-ray is given by [8]:

$$P_\gamma^L = \frac{1}{C_{00}} \frac{2y^2}{x^2(1-y)^2} \quad \text{(G.3)} \qquad , \qquad P_\gamma^C = -\frac{1}{C_{00}} \left(\frac{2y}{x(1-y)} - 1 \right) \left(1 - y + \frac{1}{1-y} \right) \quad \text{(G.4)}$$

In Fig. G.6 we represent the degree of polarization of the γ-ray as a function of $z = E_\gamma / E_\gamma^{\max}$. We observe that the sign of the circular polarization is inverted for the backscattered photon. We also observe that the degree of polarization decreases with decreasing energy. Polarizations in excess of 80 % are obtained for the top 30 % energy range.

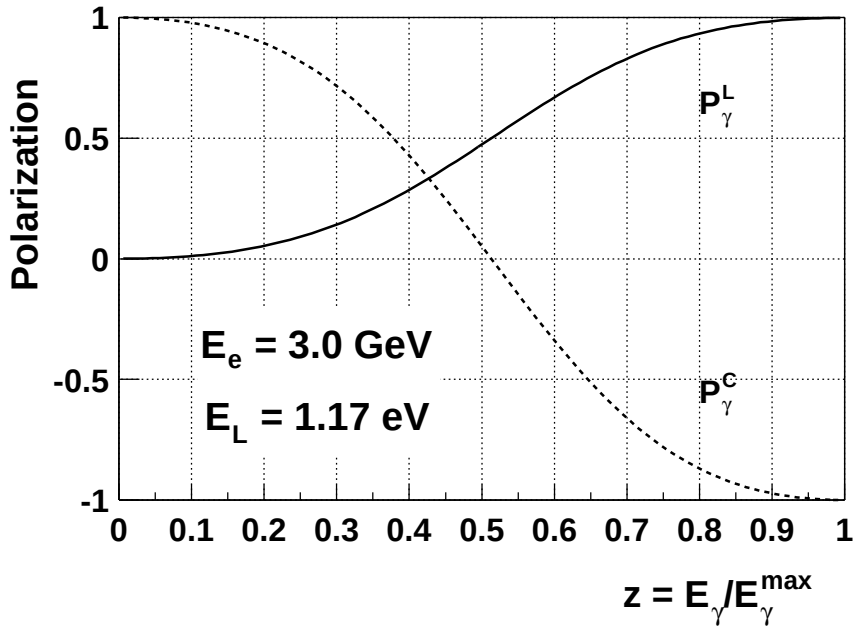

Figure G.6: γ-ray polarization as a function of energy

G.3 Gamma-ray beam intensity

The intensity of the γ-ray beam depends on the overlap of the colliding electron and laser photon densities and on the Compton scattering cross-section [8]:

$$I_\gamma = 2c\sigma_C \int n_e n_L dV \quad \text{(G.5)}$$

The electron density distribution can be adequately represented by gaussian distributions [3] of their position in both X (horizontal) and Y (vertical) transverse directions, and by a uniform distribution in the longitudinal direction Z (ignoring the beam spatial structure). The latter is justified since the temporal structure of the beam is smeared out by the transit time along the straight section ranging from 13 ns to 44 ns depending on its length. The parameters of the transverse gaussian distributions are the RMS spatial envelopes: σ_X and σ_Y. The electron velocity distribution can be adequately represented by gaussian distributions of the transverse (horizontal and vertical) slopes and by a gaussian distribution of the energy.The parameters of the transverse gaussian distributions are the RMS slope envelopes: $\sigma_{X'}$ and $\sigma_{Y'}$, while the energy distribution parameter is the RMS energy resolution σ_{E_e}:

$$n_e = \frac{1}{c}\frac{I_e}{e}\frac{1}{(2\pi)^{5/2}\sigma_X\sigma_Y\sigma_{X'}\sigma_{Y'}\sigma_{E_e}}\exp\left(-\frac{x^2}{2\sigma_X^2}-\frac{y^2}{2\sigma_Y^2}-\frac{x'^2}{2\sigma_{X'}^2}-\frac{y'^2}{2\sigma_{Y'}^2}-\frac{E_e^2}{2\sigma_{E_e}^2}\right) \tag{G.6}$$

The laser beam, with well defined wavelength, is assumed to have the focusing characteristics of the diffraction limited fundamental transverse mode TEM_{00}. The laser intensity distribution follows [9] a transverse circular gaussian distribution with a waist at the centre of the interaction length L_{int}. The RMS width parameter varies with longitudinal distance z (measured from that point) as:

$$\sigma_L = \sigma_0\sqrt{1+\left(\frac{\lambda z}{\pi\sigma_0^2}\right)^2} \tag{G.7}$$

The photon direction is assumed to be perpendicular to the laser wave front whose radius varies with distance as:

$$R_L = z\sqrt{1+\left(\frac{\pi\sigma_0^2}{\lambda z}\right)^2} \tag{G.8}$$

The laser photon density distribution can be expressed in the form:

$$n_L = \frac{1}{c}\frac{P_L}{E_L}\frac{1}{2\pi\sigma_L^2}\exp\left(-\frac{x^2+y^2}{2\sigma_L^2}\right) \tag{G.9}$$

The integral over the momentum variables of both beams can be readily performed due to the small dependence of the total Compton cross-section with the energy (as was already assumed in order to write down Eq. G.5), and the spatial overlap can be calculated numerically for a given straight section and laser beam parameters. Representative numbers are shown in Fig. G.7 and have been calculated assuming an electron beam of constant $\sigma_X = 0.25$ mm and $\sigma_Y = 0.015$ mm, a laser beam with $\sigma_0 = 0.5$ mm and an interaction length of $L_{int} = 5$ m. As can be observed intensities $I_\gamma = 2-5\times10^6$ s^{-1} are obtained per Watt of laser power and

wave lengths in the range $\lambda = 0.25 - 100\mu$m. It should be noticed that although the number of laser photons per Watt is proportional to the wavelength, this effect is counter balanced by the increase in the divergence of the laser beam with wavelength, imposed by the diffraction limit.

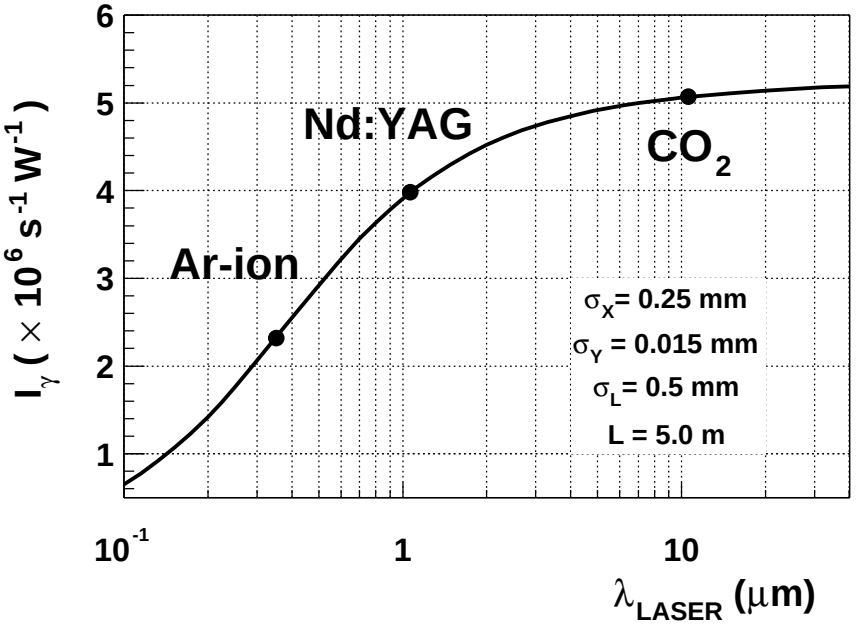

Figure G.7: γ-ray intensity per Watt of laser power as a function of laser wavelength

Nd:YAG laser devices with 100 W CW power are readily available, with conversion efficiencies of about 45 %, 25 % and 10 % for the second, third and fourth harmonics, which would provide beams of $10^7 - 10^8$ gamma rays per second. Still higher powers are available for CO_2 lasers, and intensities larger than 10^9 s^{-1} can be expected. In the case of the OPO source ($\lambda = 1.5 - 12\mu$m, see below), powers of about 10 W are foreseen giving intensities in excess of 10^7 s^{-1}. One possible limit to the ultimately obtainable γ-ray intensity is the removal of electrons from the beam in the scattering process. Electrons which loose less than 90 MeV, equivalent to the ring acceptance $\Delta p/p_0$ (see Table G.1), are kept in the ring in principle, except for multiple scattering effects for very high laser powers. In this situation the γ-ray intensity will be limited rather by the available laser power. For γ-rays above that energy, the electron will eventually hit the vacuum chamber and will be lost. In the topping-up mode electrons are replenished frequently to compensate for the usual losses of intensity in the ring. Assuming a refilling time period of 100 s and that the new source of losses should be limited to a fraction of one percent, say 0.2 %, will impose a limit of about 3×10^7 s^{-1} in the γ-ray intensity obtainable from the installation.

G.4 Gamma-ray beam energy resolution

As was mentioned earlier, due to the strong backward focusing most of the γ-rays produced (between a fraction and the maximum value of the γ-ray energy) are arriving at the measuring station within a radius of few millimeters. On the other hand, most of the measurements performed will require a determination of the γ-ray energy in general with good precision. There are two possible methods to define the energy at an installation of this type: collimation and tagging. The tagging technique requires the determination of the energy of the electron dispersed in the collision in coincidence with the γ-ray or its reaction products. Since the technique requires the detection of the dispersed electron there is a minimum γ-ray energy which can be tagged, related to the synchrotron ring dispersion and the distance of closest possible approach to the electron beam envelope. As will be explained later, this minimum tagged energy is about 150 MeV. The collimation method exploits the angle-energy relation of the scattered photons. It is the only method available for γ-rays with energy below the limit for the tagging technique.

G.4.1 Collimation

The relation between the energy of the outgoing γ-ray and its angle is given by Eq. G.1 and it is shown in Fig. G.4 for a representative case. It should be noted the small values of the angles involved and the strong sensitivity of the energy to the angle. It will be thus possible to define the γ-ray energy by defining their angle with a collimator. Obviously, smaller opening angles procure better energy resolution at the cost of intensity, so a balance between the two must be reached for actual experiments. In addition, since the angular definition also depends on the directions of the colliding electron and photon and the position of their interaction, there is a minimum energy resolution which can be obtained depending on the electron and laser beam angular spread and the collimation geometry. It is possible to obtain a rough estimate of the uncertainty in the γ-ray energy due to the uncertainty in the angles and energies, applying the error propagation formula to Eq. G.1. Fig. G.8 shows results obtained by this method for some typical values of the angular uncertainties in the straight sections of the DBA lattice.

It can be deduced from this figure that collimation as a way of defining the energy is only meaningful when placing the collimator at zero degrees, that is at the maximum possible value of the energy. In this case a variation of the γ-ray energy requires a variation of the electron energy (not feasible at ALBA) or of the laser photon energy. An advantage of the method of collimation at zero degrees is that one can obtain close to 100 % polarized beams (see Fig. G.6).

An accurate estimation of the resolution and intensity that could be obtained when placing a given collimator at a given distance, requires the proper consideration of the possible variations of the parameters in Eq. G.1. We have chosen the Monte Carlo method for this purpose. The electron and laser photon beam distributions are modeled in the same way as was explained before. The parameters of the electron beam vary along the straight sections as is shown in Fig. G.2. A computer code has been written to sample these distributions. For each collision event the scattered electron and γ-ray momenta are sampled from the appropriate Compton differential cross section distribution and weighted by the total cross section. For practical reasons we follow the approach in [10]: first, the laser photon momentum is Lorentz transformed into

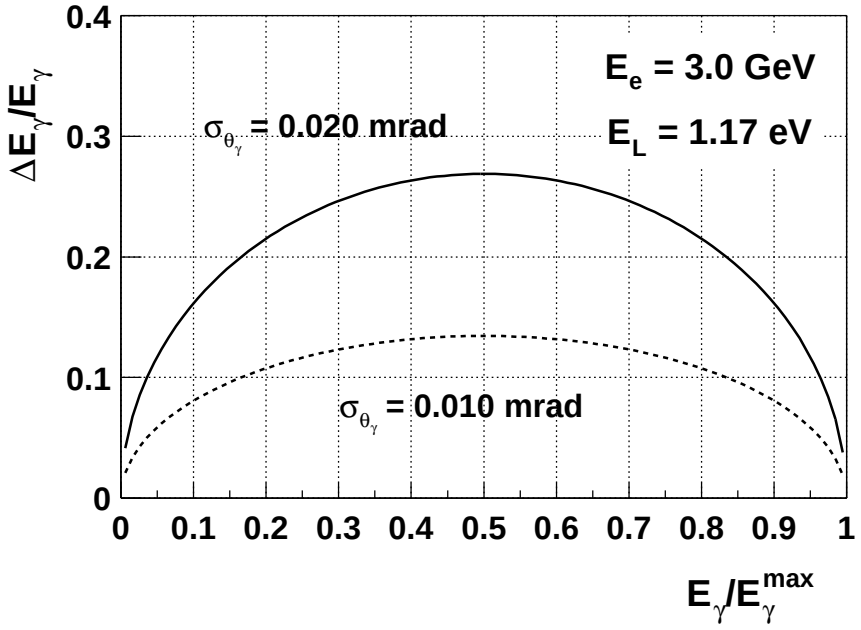

Figure G.8: FWHM relative energy resolution as a function of γ-ray energy for two values of the angular uncertainty.

the incoming electron rest frame, second, the well known Klein-Nishina formula for Compton scattering is sampled [11] to calculate the scattered electron and photon momentum, and third, these momenta are transformed back to the laboratory frame.

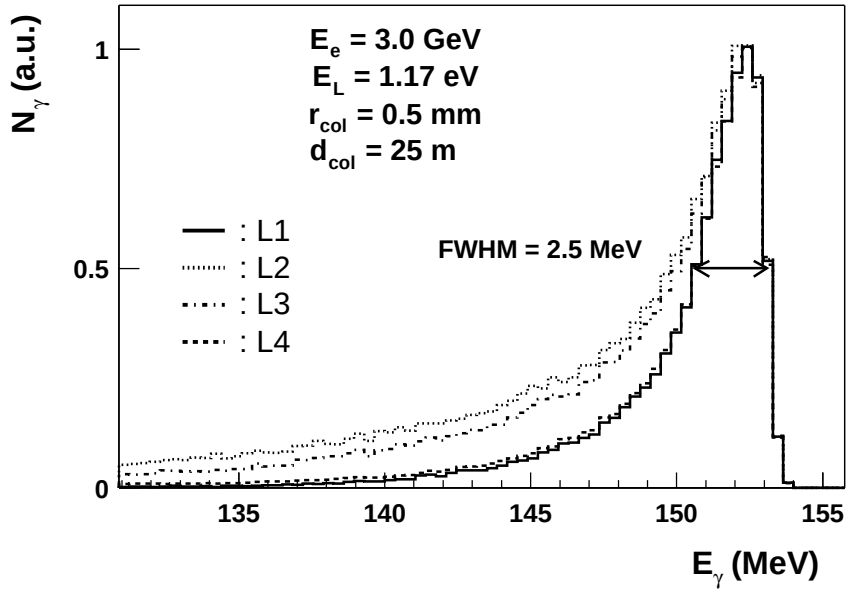

Figure G.9: Collimated γ-ray energy distribution at $\theta_{col} = 0^\circ$ for different straight sections

Fig. G.9 shows the result of the Monte Carlo simulation for a laser photon energy $E_L =$ 1.17 eV (Nd:YAG laser) when a collimator of radius $r_{col} = 0.5$ mm is placed at $\theta_{col} = 0^\circ$ and a distance $d_{col} = 25$ m from the centre of different straight sections. As can be observed the energy distribution is characterized by a low energy tail coming from the distribution of angles, most of the effect being due to the horizontal divergence of the electron beam in this case. The electron energy resolution has a small smearing effect. The low energy tail for straight sections labelled 2 and 3 in Table G.1 and Fig. G.1 and G.2 is unacceptably large, and therefore only straight section 1 (the long one) or 4 (in-between the magnet doublet) are considered as candidates for the γ-ray beam line. The FWHM resolution amounts to $\Delta E_\gamma / E_\gamma = 1.7$ % for both sections. The collimated intensity is 8.3×10^4 s^{-1}W^{-1} (uncollimated intensity: 4.6×10^6 s^{-1}W^{-1}) for the long section and 5.7×10^4 s^{-1}W^{-1} (3.7×10^6 s^{-1}W^{-1}) for the short one, in spite of the factor 3 in length between both sections. This reflects again the effect of the defocussing of the laser beam with longitudinal distance imposed by the diffraction limit.

The simulations were repeated for several collimator openings and laser photon energies for the long straight section (labelled 1). Fig. G.10 shows the relationship between γ-ray energy resolution and intensity for two different laser photon energies, for collimator radii: 0.25, 0.35, 0.50, 0.75 and 1.0 mm. The chosen laser photon energies $E_L = 1.17$ eV (Nd:YAG laser) and $E_L = 0.117$ eV (CO_2 laser) would provide γ-ray energies of $E_\gamma = 152$ MeV and $E_\gamma = 16$ MeV

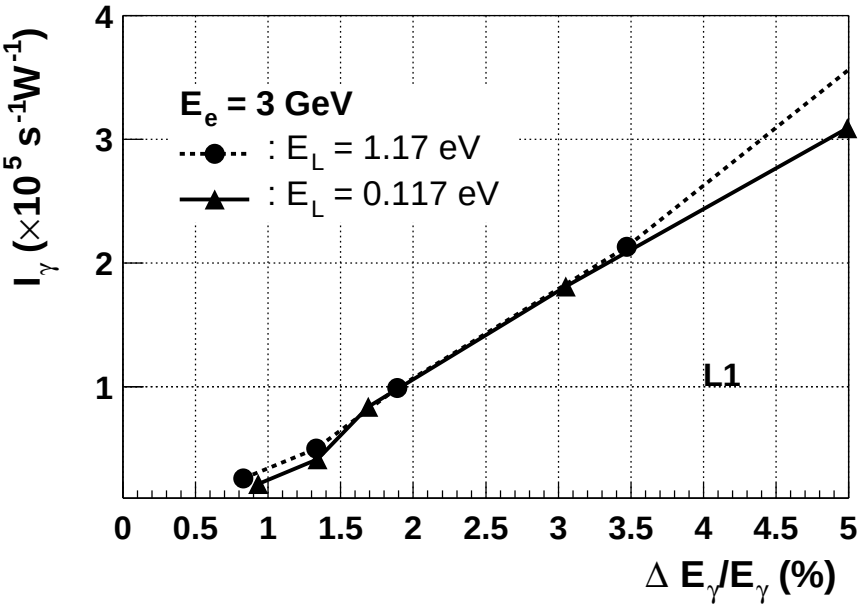

Figure G.10: Relationship between collimated energy resolution and intensity for the long straight section. Each point represents a different collimator opening.

respectively. As can be observed, the relation intensity-resolution is approximately linear. For a given collimator radius the energy resolution and intensity depends little on the laser photon energy. The latter is again consequence of the wavelength dependent defocussing of the laser beam.

From this discussion it can be concluded that the availability of γ-ray beams with good energy resolution (< 2 %) and high intensities ($> 10^5$ s^{-1}) with energies bellow the limit of the tagging technique (150 MeV) requires the use of lasers with variable wave length in the range $1 - 100$ μm and powers of few Watts. Recent advances in the field of OPO (Optical Parametric Oscillators) devices make it feasible to have photon sources with wavelengths $1.5 - 12$ μm and average powers of 10 W. We foresee to use OPO devices (see Appendix H) pumped by a 100W CW Nd:YAG laser and the collimation technique to produce γ-ray beams in the range of energies 15-110 MeV with resolutions of about 1.5 % and collimated intensities of few times 10^5 s^{-1}. We also foresee the use of a 1 kW CO_2 laser to produce an intense (10^7 s^{-1}) and quasi monochromatic 16 MeV γ-ray beam for industrial and medical applications.

G.4.2 Tagging

The tagging technique requires the determination of the energy of the electron dispersed in the collision in coincidence with the γ-ray or its reaction products. From the energy conservation principle the energy of the γ-ray is equal to the energy lost by the electron in the collision (plus the negligible laser photon energy). Given the energies involved, the determination of the scattered electron energy with good precision requires the use of magnetic analysis for the electron momentum, therefore a magnetic spectrometer would be required. Electrons with less than the nominal energy entering the next bending magnet after the collision point will describe an orbit with a smaller radius deviating from the central trajectory towards the centre of the ring. If the electrons deviate enough (that is if the energy loss is high enough) they will separate enough from the beam at the exit of the bending magnet and could be collected by the first stage of a magnetic spectrometer, which would have to be placed inside the ring. This solution can not be realized at ALBA since the booster ring will be placed inside the main ring, concentric with it and at a small distance (about 2 m) leaving no space for the installation of a bulky magnetic spectrometer. The only possibility will be to place a position sensitive counter at the exit of the bending magnet to detect the position of the electron (proportional to its momentum), or in another words to use this section of the ring as a magnetic spectrometer. A clear advantage of this so called internal tagging is the very reduced cost, limited to the tagging detector. Of course the feasibility of this solution depends on the resolving power which can be attained. The energy resolution of the spectrometer depends on the ring lattice optics, which define horizontal beam size (σ_{X_D}) and momentum dispersion (D_X) at the electron detector position. The γ-ray energy resolution which equals the detected electron energy resolution [12] is given by:

$$\sigma_{E_\gamma} = \frac{\sigma_{X_D}}{D_X} E_e = \frac{1}{D_X} \sqrt{\varepsilon_X \beta_{X_D} E_e^2 + \eta_{X_D}^2 \sigma_{E_e}^2} \tag{G.10}$$

where the subscript D on the synchrotron functions indicate that they are evaluated at the detector position. The dispersion D_X distinct from the dispersion function η_X, represent the

dispersion from the collision point (in the straight section) to the detector position (after the bending magnet). This dispersion can be estimated from the synchrotron functions through the relations:

$$D_X = \eta_{X_D} - r_{11}\eta_{X_I} - r_{12}\eta_{X_I'} \quad \text{(G.11)}$$

$$r_{11} = \sqrt{\frac{\beta_{X_D}}{\beta_{X_I}}}(cos(\mu_{X_D} - \mu_{X_I}) + \alpha_{X_I} sin(\mu_{X_D} - \mu_{X_I})) \quad \text{(G.12)}$$

$$r_{12} = \sqrt{\beta_{X_D}\beta_{X_I}} sin(\mu_{X_D} - \mu_{X_I}) \quad \text{(G.13)}$$

where the new optical functions α ($\equiv -\beta'/2$) and μ (phase) have been introduced (see for example [3]). The subscript I refers to the interaction or collision point. These relations can be obtained from the matrix equations for the transport of the dispersion function. Using the optical functions for the DBA cell, the dispersion, beam size and resolution have been calculated assuming collisions at the centre of the interaction length for the different straight sections. In Fig. G.11 these quantities are shown for the long straight section (labelled 1). As can be observed dispersions of about $D_X = 0.37$ m are reached in the central region between the two bending magnets of the doublet. This gives resolutions FWHM ($\equiv 2.35\sigma_{E_\gamma}$) of 5.4 MeV. The resolutions obtained for the other straight sections are comparable. It has to be noticed the contribution of the electron beam resolution ($\sigma_{E_e} = 3$ MeV) to the γ-ray energy resolution, coming through the second term in the square root of Eq. G.10. Better energy resolutions would require a modification of the lattice optics in order to minimize (or zero) the value of the dispersion function at the detector position η_{X_D} (to cancel the contribution from this term), to decrease the betatron function at the detector position β_{X_D}, and/or to increase the dispersion from the interaction to the detection point D_X.

The value calculated in this way represents a first approximation to the resolution which would be obtained. The optical functions utilized correspond to the first order or linear optics of the lattice. In general higher order terms corresponding to the higher order optical aberrations should be considered. Also, proper consideration has to be given to the fact that collisions take place along the whole straight section so that the scattered electrons see different optical elements in their way. Since standard beam transport or ray-tracing codes as TRANSPORT [13] or TURTLE [14] cannot cope with the latter problem a computer code was written to simulate the transport of scattered electrons to the detection point. The momentum of the scattered electrons is Monte Carlo generated from the electron and laser beam parameters in the manner that was explained earlier. The effect of the optical elements (quadrupoles, sextupoles, dipoles) is represented by first and second order beam transport matrices [15]. The result of the simulation performed for the long straight section (labelled 1) is shown in Fig. G.12. The tagging detector is placed halfway between the bending magnets of the DBA doublet and assumed perpendicular to the central trajectory. The energy distribution is shown for different displacements along the tagger detector. For comparison the first order result is also shown. The effect of the distribution of the collisions along the full straight section is to worsen the resolution to a value of 6.8 MeV (FWHM). The second order aberrations introduce a further deterioration of the resolution to

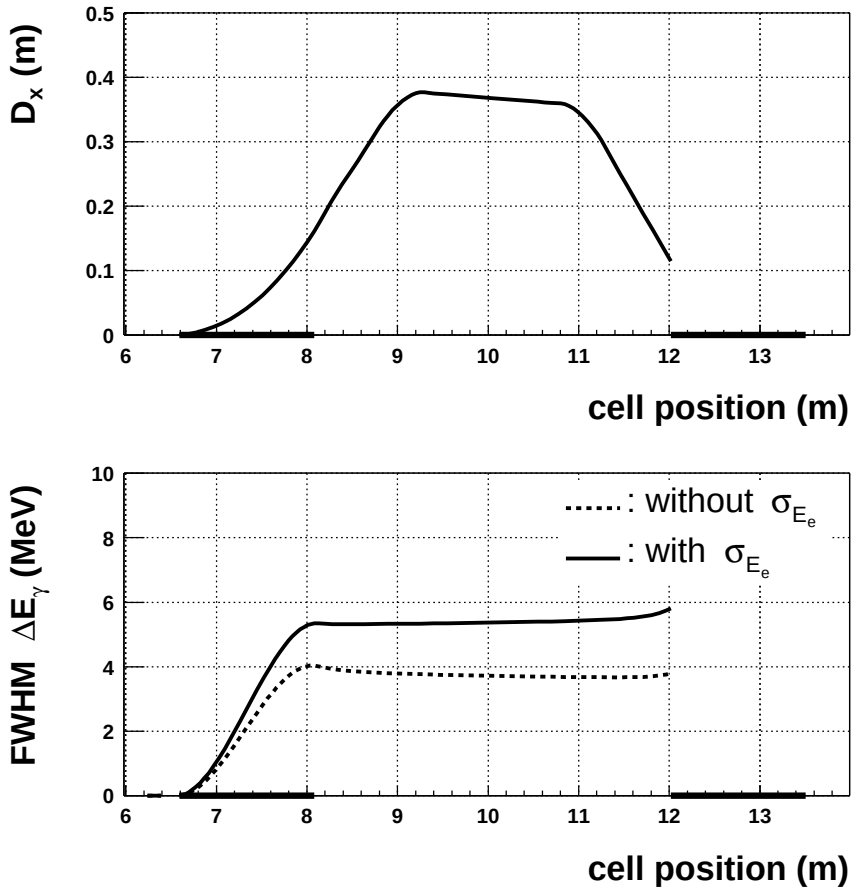

Figure G.11: Dispersion and resolution (FWHM) as a function of tagger position. Collisions take place in the centre of the long straight section. Indicated are the positions of the first and second bending magnets in the cell.

values of about 7.4 MeV.

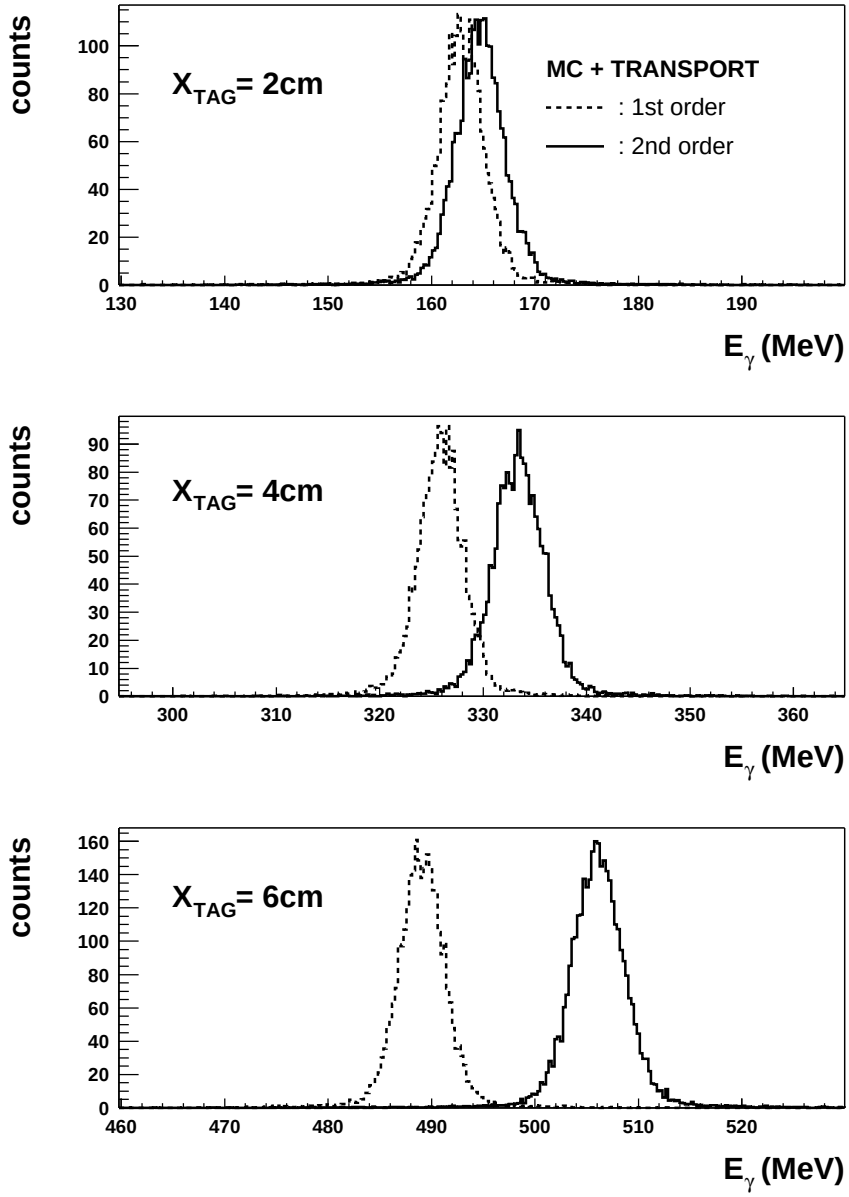

Figure G.12: Energy distribution of γ-rays for three values of the displacement along the tagger. The tagger is positioned halfway between the bending magnets. Collisions take place along the long straight section.

For a value of the dispersion of $D_X = 0.37$ m as obtained in this case, the maximum displacement of the scattered electrons corresponding to the γ-ray energy of $E_\gamma = 530$ MeV will be 6.5 cm.The minimum tagged energy would correspond to the distance of closest approach

which we expect to be in the range of 1.5-2 cm giving 120-160 MeV. This together with the beam size $\sigma_X = 0.28$ mm, $\sigma_Y = 0.017$ mm would set the requirement on tagger detector dimensions and position resolution. We foresee (see Appendix I) the use of 300 μm thick Silicon micro-strip detectors for this purpose, of about 5×1 cm with a strip pitch of 100 μm giving a position resolution of 25 μm. The Si detector will be backed by thin fast plastic scintillator pads which provide the trigger signal for the readout.

The tagging technique is another source of limitation for the achievable γ-ray intensity [10]. At high rates both pile-up signals in the tagger and random coincidences with the measuring detectors introduce spurious events which need to be corrected for and worsen the peak to background ratio. The maximum admissible rate depends on the time resolution and also on the type of experiment. In any case a fast detector with good time resolution is needed for the tagger, as it is the case for the proposed detector. We estimate that the maximum rates that can be handled are on the order of few times 10^7 s^{-1}

Bibliography

[1] "LLS Detailed Design Report", http://www.lls.cells.es/report/report.html

[2] J. Bordas *et al.*, "A Concept for the Spanish Light Source CELLS", Proceedings of the 9th European Particle Accelerator Conference, Lucerne, July 5-9, 2004.

[3] K. Wille, "The Physics of Particle Accelerators", Oxford Univ. Press, 2001.

[4] M. Muñoz *et al.*, "The Lattice for CELLS", Proceedings of the 9th European Particle Accelerator Conference, Lucerne, July 5-9, 2004, and private communication

[5] R.H. Milburn, "Electron Scattering by an Intense Polarized Photon Field", Phys. Rev. Lett. 10, 75 (1963).

[6] F.R. Arutyunian and V.A. Tumanian, "The Compton Effect on Relativistic Electrons and the Possibility of Obtaining High Energy Beams", Phys. Lett. 4, 176 (1963).

[7] E. Feenberg and H. Primakoff, "Interaction of Cosmic-Ray Primaries with Sunlight and Starlight", Phys. Rev. 73, 449 (1948).

[8] I.F. Ginzburg *et al.*, "Colliding γe and $\gamma\gamma$ Beams Based on the Single-Pass e^+e^- Colliders (VLEPP Type)", Nucl. Instr. and Meth. 205, 47 (1983); I.F. Ginzburg, *et al.*, "Colliding γe and $\gamma\gamma$ Beams Based on Single-Pass e^+e^- Accelerators. II. Polarization Effects. Monochromatization Improvement", Nucl. Instr. and Meth. 219, 5 (1984).

[9] P. Mouroulis and J. Macdonald, "Geometrical Optics and Optical Design", Oxford Univ. Press, 1996.

[10] A.M. Sandorfi *et al.*, "High Energy Gamma Ray Beams from Compton Backscattered Laser Light", IEEE Trans. Nucl. Sci. 30, 3083 (1983).

[11] L.M. Garcia-Raffi et al., "Monte Carlo Simulation of Compton Polarimeters", Nucl. Instr. and Meth. A391 (1997) 461.

[12] M. Preger *et al.*, "Monochromatic and Polarized Tagged LADON Gamma Ray Beams", Nucl. Instr. and Meth. A249, 299 (1986).

[13] D.C. Carey et al. *et al.*, "Third Order TRANSPORT with MAD Input", Report FERMILAB-Pub-98/310, Batavia, 1998.

[14] F. Attalah *et al.*, “TURTLE+ (Trace Unlimited Rays Through Lumped Elements)”, Report CENBG-9428, Bordeaux, 1994; D.C. Carey et al. *et al.*, “Decay TURTLE”, Report SLAC-246, Stanford, 1982.

[15] K.L. Brown, “A First- and Second-Order Matrix Theory for the Design of Beam Transport Systems and Charged Particle Spectrometers”, Report SLAC-75, Stanford, 1982.

Appendix H

Optical Parametric Oscillator light source

H.1 Introduction

The generation of gamma-ray radiation by laser backscattering of high-energy electrons in accelerator facilities is a well known technique. A vital component of this technique is the laser system, which must provide an optical beam with the required characteristics in terms of frequency (wavelength, photon energy), optical power, spatial beam quality, as well as compact and practical design for integration with the electron storage rings.

So far, the laser sources for the few such facilities worldwide have been based on conventional Nd:YAG lasers or argon-ion systems. Such lasers operate at a fixed frequency, so they offer no freedom to vary the energy of the optical photons. The ability to freely control the photon energy can offer several advantages and opens up new possibilities for conducting a wide range of novel moderate- to high-energy gamma-ray experiments in accelerator facilities. Here we propose to develop a novel frequency-versatile optical source for the generation of gamma-rays with variable (moderate to high) energies at ALBA. The optical source is based on an optical parametric oscillator (OPO) system operating at wavelengths from 1.5 μm (0.82 eV) up to 12 μm (0.1 eV) in the mid-IR, which will provide gamma-ray energies in the range of $E_\gamma(\text{max}) \sim 15 - 110$ MeV.

Conventional Lasers. Since the invention of the laser in 1960, there have been major advances in the development of a wide variety of laser systems. However, after more than forty years, the vast majority of such conventional systems can operate only at fixed frequencies, hence also providing photons of fixed energy. Examples of such lasers include the widely established Nd:YAG, argon-ion, excimer, He-Ne, semiconductor, and many other types of crystalline and gas lasers.

On the other hand, there has also been significant progress in the development of conventional lasers that are tunable -that is, whose frequency (wavelength) can be varied. Examples of the most established tunable lasers, with their corresponding wavelength range, are shown in Fig. H.1a. However, as can be seen from the figure, the tuning range available to such lasers is restricted to a limited band of a few hundred nanometers at best! In addition, the spectral coverage of these systems is limited mainly to the visible and near-IR. This means that substantial portions of the optical spectrum in the UV, visible and mid-IR can not be accessed, even by

conventional tunable laser systems. To overcome this important obstacle, it is vital to deploy alternative technologies for the generation of tunable optical radiation in new spectral regions, particularly the mid-IR where many applications can benefit.

Optical Parametric Oscillators. A key technology capable of overcoming the limitations of conventional lasers is the OPO. These are novel optical instruments that can provide tunable radiation over an exceptionally wide frequency range from a single device [1]-[5]. They can be configured in compact, portable, and fully solid-state formats, are easy to operate and can deliver high output energies, powers, and efficiencies. Typical conversion efficiencies $> 50\%$ are regularly obtained in a variety of device configurations, which is substantially higher than conventional lasers (such as the Ti:sapphire laser). Another important advantage of OPOs is that they are far less susceptible to thermal effects at high pump powers, since the operating principle is not based on absorption of pump light, as in a laser, but its transmission through the nonlinear gain material.

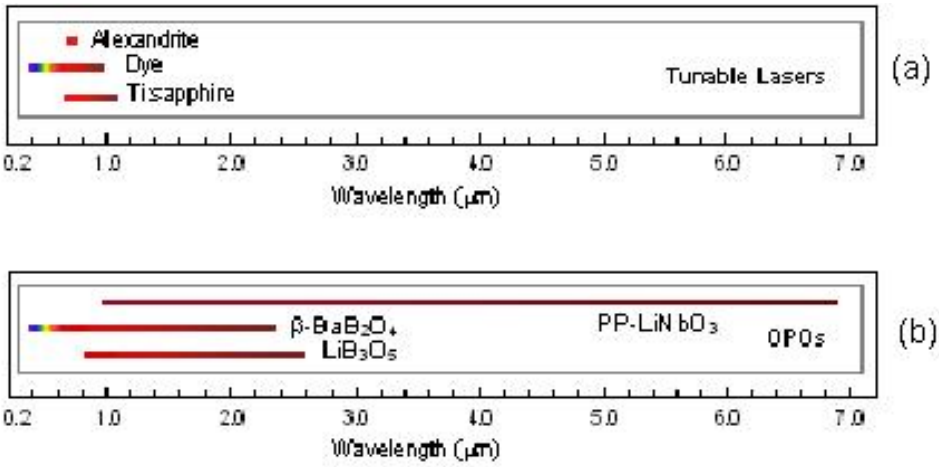

Figure H.1: The tuning range of (a) the most widely established conventional tunable lasers and (b) some OPO systems developed by ME and his team to date.

The above properties make OPOs of great interest and utility for a wide range of applications requiring variable optical frequency and photon energy. Fig. H.1b shows the tuning range of three OPO systems developed by M. Ebrahim-Zadeh (ME) and his research team, which can be compared with the tuning range of existing conventional tunable lasers in Fig. H.1a.

H.2 OPO in the context of ALBA

The unique properties of the OPO highlighted above make it a highly attractive alternative to conventional Nd:YAG or argon-ion lasers for gamma-ray generation in electron accelerator facilities. In the context of ALBA, the development of an OPO system will be an important breakthrough because:

- It will enable the generation of gamma-rays through laser backscattering at ALBA, with tunability control of the γ-ray energy. This will open up new possibilities for novel nuclear physics experiments by scientists from both within and outside Spain.

- The OPO will be able to deliver large optical powers (several watts). Therefore, under similar operating parameters (σ_c, I_e, L, S), the OPO will be able to provide higher gamma-ray intensities through higher optical powers.

- The OPO will deliver an excellent spatial quality in a diffraction-limited optical beam with minimum divergence and suitable cross-section, enabling collimation, manipulation, and propagation over long distances with standard optical elements. The all-solid-state design of the OPO will also ensure excellent output beam stability, with minimum variations in optical power, spatial beam quality, temporal stability, beam size and shape, and beam positioning over long distances. The compact, rugged, and practical design will also ensure convenient integration with the electron beam-line where limited space will be available.

- The OPO represent a new optical instrument, which has not been previously deployed in any other accelerator facilities throughout the world. Therefore, in addition to its usability, it will represent a world-first addition to such a facility, which will also enable novel scientific advances in high-energy accelerator physics.

- The OPO system will be developed by indigenous expertise in Spain.

H.3 Current status

In the current state of technology, OPO devices can cover spectral regions from 400 nm in the visible to 12 μm in the mid-IR in a variety of device configurations and output temporal formats [1]-[5]. Because of the instantaneous nature of electronic susceptibility, the origin of parametric amplification, OPOs are also highly flexible with regard to temporal output and can operate in all time domains. By a suitable choice of pump source, OPO devices can provide optical radiation from the continuous-wave (cw) to pulsed (nanosecond, microsecond), down to ultrafast (picosecond and femtosecond) time-scales. This is not possible with lasers, where the time dependence of the output is strictly determined by the fundamental properties (e.g. upper-state lifetime, fluorescence bandwidth) of the particular laser material.

In the context of ALBA, the most important operating requirements are:

- Wavelength tunable range: this must produce gamma-rays with energies $E_\gamma(\max) <$ 150 MeV.

- Optical output power (cw or average power): this must be as high as possible -several watts.

These two important requirements immediately limit the choice of OPO device configuration to two:

- High-power cw OPOs
- High-average-power, pulsed (nanosecond) OPOs

In Fig. H.2, we summarize the current status of OPO technology in cw device format. As evident, optical output powers of up to 4 W have so far been generated from cw OPOs. This device was pumped by a 13.5 W pump laser [6]. By exploiting the current pump laser technology (where cw pump powers of 100 W that are now available), it should be readily possible to generate substantially higher optical powers of at least 10 W from such cw OPOs. It can also be seen in Fig. H.2 that the spectral coverage of cw OPOs is currently limited to 5 μm in the mid-IR, with the longest wavelength so far generated by ME and co-workers [7]. These systems have been based predominantly on PPLN (periodically-poled $LiNbO_3$) as the nonlinear material. Spectral extension of cw OPOs to wavelengths beyond 5 μm has not yet been demonstrated. However, we are confident that this will be readily possible by using innovative pumping techniques or difference-frequency-generation schemes. A particularly important approach, proposed by ME, is the use of cascaded pumping using a two-stage system, where the output of the first PPLN OPO system acts as the pump for the second OPO system or for a difference frequency generator (DFG) based on ZGP (zinc germanium phosphate) or alternative IR materials. Internal pumping will be used to maximize generated mid-IR output power and efficiency [8]. In this way, spectral extension to at least 12 μm will become possible in cw OPO systems.

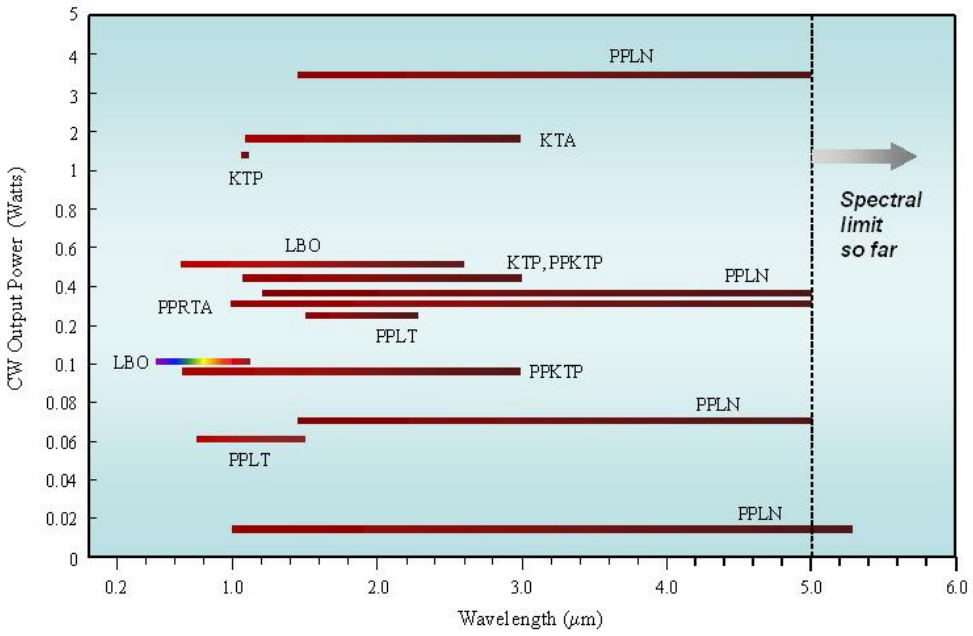

Figure H.2: Survey of the output power performance and spectral coverage of cw OPOs that have been developed to date using various nonlinear materials.

In Figs. H.3 and H.4, we summarize the current status of OPO technology in pulsed

(nanosecond) device format. Fig. H.3 shows the spectral coverage and pulse energy of low-repetition-rate (1 Hz to 100 Hz) devices, while Fig. H.4 contains the performance of high-repetition-rate (1 kHz to 30 kHz) systems. It is clear that tuning to 12 μm has been achieved in low-repetition-rate device formats and average optical powers as high as 10 W have been obtained from high-repetition-rate systems up to 8.5 μm. Such systems have used ZGP as the nonlinear material [9, 10]. The combination of the high-repetition-rate pump laser deployed in [10] with the ZGP geometry used in [9] will allow the generation of optical radiation at an average power of at least 10 W and spectral coverage to at least 12 μm in the mid-IR.

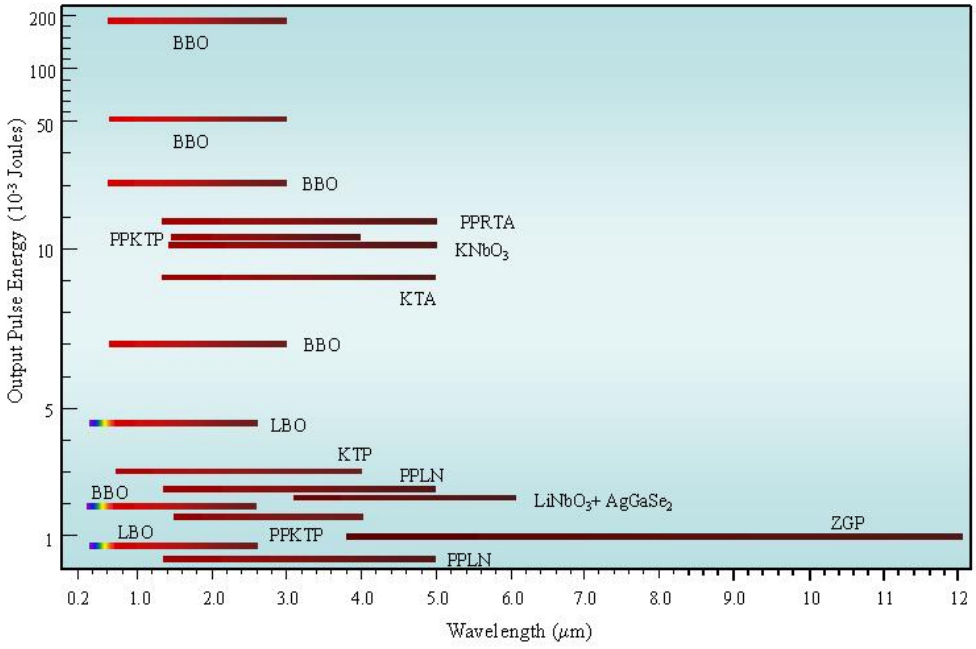

Figure H.3: Survey of the output energy performance and spectral coverage of low-repetition-rate (1Hz-100Hz) pulsed nanosecond OPOs that have been developed to date using various nonlinear materials.

H.4 Proposed program

Based on the current status of OPO technology discussed above, we propose two different approaches for the development of the optical source for ALBA:

1. A high-power cw OPO, with no time structure in the output and a steady state flow of optical photons in time.

2. A high-average-power, high-repetition-rate pulsed OPO, with a nanosecond time structure in the output optical radiation.

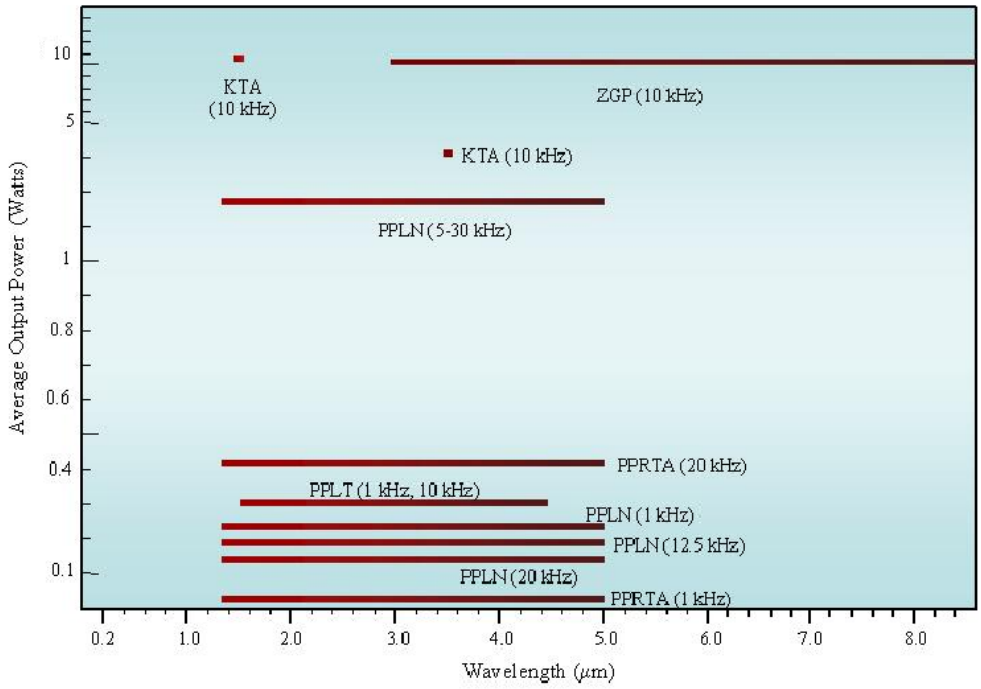

Figure H.4: Survey of the output energy performance and spectral coverage of high-repetition-rate (1kHz-30kHz) pulsed nanosecond OPOs that have been developed to date using various nonlinear materials.

Using either approach, we will provide a practical source of coherent variable-energy photons with the required optical power and photon energy to meet the requirements at ALBA. In either case, the system will be a state-of-the-art instrument operating in the 1.5 to 12 μm wavelength range in the mid-IR, where no other conventional laser sources with similar operating characteristics are available. The OPO will, therefore, be capable of providing optical photons with controllable energies in the range of 0.82 to 0.10 eV to generate gamma-rays with energies in the range $E_\gamma(\max) \sim 15 - 110$ MeV at ALBA. The optical beam will be of the highest spatial quality ($M^2 \sim 1$), with minimum divergence. This will allow diffraction-limited propagation over long distances without significant beam spreading, and will permit collimation and manipulation of the optical beam to the desired characteristics without difficulty. The intensity profile will be Gaussian (TEM_{00}) and the beam diameter at the exit of the OPO instrument will be $\phi \sim 2$ to 5 mm ($1/e^2$ intensity points), depending on the exact focusing and resonator configuration. The instrument will be designed in a compact, rugged and fully solid-state design, which will be capable of being conveniently integrated with the electron beam line at ALBA.

To achieve the required performance parameters, we will use the nonlinear crystals of PPLN as the primary optical gain element. For cw operation, it will be necessary to use a high-power cw Nd:YAG laser, whereas for pulsed operation the OPO will use a high-average-power Q-switched Nd:YAG laser as the pump source. Both lasers will operate at a wavelength near 1.064 μm. By suitable design of the phase-match grating on the PPLN crystal, we will be able

to achieve wavelength tuning over the 1.5-5 μm range from either OPO system, but to achieve wavelength extension above 5 μm and up to 12 μm, we will use ZGP a second-stage OPO or DFG crystal. In order to obtain the high spatial quality in the output beam, the OPO cavity in either system will be designed in a stable resonator. The output beam will also be linearly polarized. The OPO systems will be "user-friendly", requiring some basic training of personnel for day-to-day operation.

H.4.1 High-power cw OPO

1.5-5 μm (0.82-0.25 eV) cw OPO

As highlighted in Sect. 3, and evident from Fig. H.2, in the current status of cw OPO technology, devices with optical powers of up to 4 W and wavelength tuning up to 5 μm have already been demonstrated. Therefore, the implementation of such a cw OPO can be readily achieved using existing technologies. However, we will be able to substantially improve the performance of such systems in terms of optical power by deploying high power laser pump sources that are now commercially available [11]. Specifically, with the use of a 100 W all-solid-state pump laser (ELS, Germany), we will be able to generate cw OPO optical output powers > 10 W over the same wavelength range of 1.5-5 μm. Such a program can be viewed as a Development Project, where much of the research has already been performed and a comprehensive knowledge base already exists. A schematic of the cavity configuration for the proposed high-power cw OPO, which is based on PPLN as the nonlinear material, is shown in Fig. H.5. The predicted performance characteristics of the 1.5-5 μm cw OPO system are summarized in Table H.1. With such an OPO system, gamma-ray energies in the range of $E_\gamma(\max) \sim 35 - 110$ MeV will be generated.

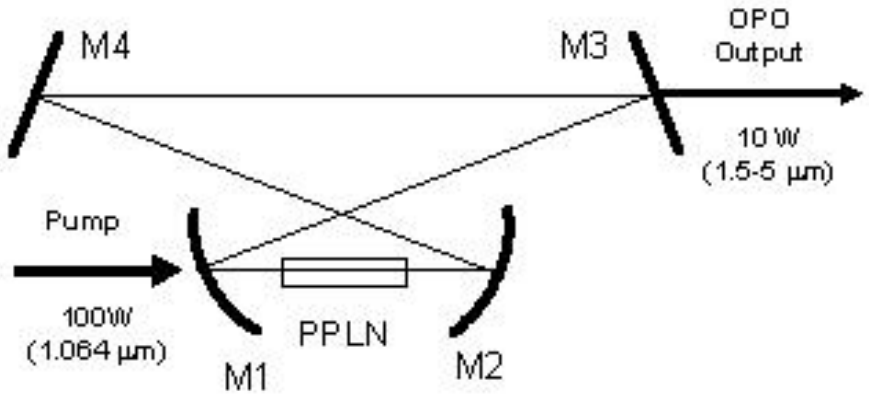

Figure H.5: Resonator configuration for the 1.5-5 μm cw OPO based on a 100-W Nd:YAG laser as the pump source and the crystal of PPLN as the nonlinear gain element. M1-M4 are mirrors. This system will generate gamma-rays with energies in the range $E_\gamma(\max) \sim 35 - 110$ MeV.

Pump Laser	Nd:YAG (cw)
Wavelength	1.064 μm
Output Power	100 W
OPO Design	Singly Resonant (PPLN)
Wavelength Coverage	1.5-5 μm
Photon Energy	0.82-0.25 eV
Output Power	10 W
Spatial Quality	$M^2 \sim 1$
Spatial Profile	Gaussian (TEM_{00})
Polarization	$>$ 99% Linear
Total Footprint	100 $\times$ 150 cm

Table H.1: Characteristics of the cw pump laser and the 1.5-5 μm cw OPO for the generation of gamma-rays with energies of $E_\gamma(\text{max}) \sim 35 - 110$ MeV at ALBA.

1.5-12 μm (0.82-0.1 eV) cw OPO

On the other hand, extension of spectral range of cw OPOs to wavelengths > 5 μm has not yet been demonstrated. However, as noted earlier, we believe that such an extension will be possible with the use of novel cascaded internal pumping schemes, where the radiation from a first PPLN OPO is used as the pump source for a second OPO based on ZGP. A schematic of the possible cavity configuration is shown in Fig. H.6. An alternative approach would be to use the generated radiation from the first OPO to achieve DFG in ZGP within the same OPO cavity, as illustrated in Fig. H.7.

Using a high-power, 100 W cw laser pump source and either of the two approaches, we will be able to generate cw optical radiation at power levels of up to 10 W in the 1.5-12 μm wavelength range in the mid-IR. Such a program for spectral extension of cw OPOs to wavelengths > 5 μm should be viewed as a Research Project, because while such systems have already been demonstrated in pulsed OPOs, they have not so far been applied to cw OPOs.

The design and predicted performance characteristics of the 1.5-12 μm cw OPO system are summarized in Table H.2. With such an OPO system, gamma-rays with energies in the range $E_\gamma(\text{max}) \sim 15 - 110$ MeV will be generated.

H.4.2 High-average-power (0.82-0.1 eV) pulsed OPO

As noted in Sect. 3, and evident from Figs. H.3 and H.4, in the current status of pulsed OPO technology, devices with optical powers of up to 10 W and wavelength tuning up to 12 μm have already been demonstrated. Therefore, the implementation of such a cw OPO can be readily achieved using technologies currently available. Again, such a program in the context of this proposal should be considered as a Development Project, as most of the design and performance parameters are already well established.

The most effective and practical approach for the implementation of such a device is to use

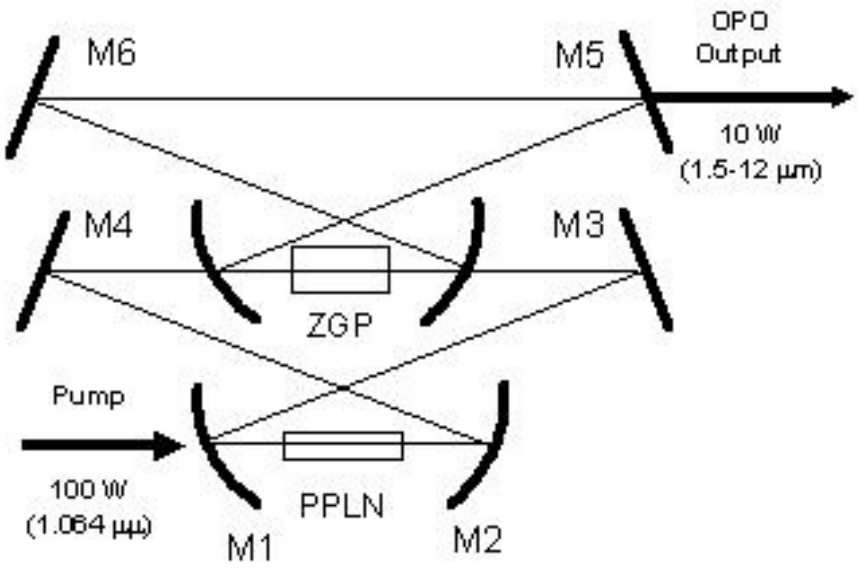

Figure H.6: Resonator configuration for the 1.5-12 μm cascaded intracavity cw OPO using a 100 W Nd:YAG pump laser. The internal radiation generated by the PPLN OPO provides the pump for the ZGP OPO located internal to the first OPO cavity. M1-M6 are mirrors. This system will generate gamma-rays with energies in the range $E_\gamma(\max) \sim 15 - 110$ MeV.

cascaded two-stage pumping, where the output of the first OPO is used as the pump for a second OPO. A high-average-power, Q-switched Nd:YAG laser will be used to pump a PPLN OPO to provide tunable radiation in the 1.5-3.8 μm. This will then be used to pump a second OPO based on ZGP [10] to generate tunable coherent radiation in the 1.5-12 μm range. Because of the high intensities available with pulsed pumping, it will not be necessary to use internal pumping as in cw OPOs (see Fig. H.5), and so external pumping can be readily used. A schematic of the experimental configuration for such a system is shown in Fig. H.8 and the corresponding design parameters and performance characteristics are summarized in Table H.3. With such an OPO system, gamma-rays with energies in the range of $E_\gamma(\max) \sim 15 - 110$ MeV will be generated.

H.5 Summary and future directions

This project is unique in that the coherent optical source will be developed with the expertise available in Spain, with ME having a well-established international track record in the field. It is fully expected that the development of an OPO system for ALBA will bring about an added capability to this facility and, in the long term, will have a major impact on a wide range of nuclear physics applications, not only in Spain, but also at the European and international level.

It is also important to note that while the proposed design relates to the development of OPO systems operating in the mid-IR, alternative designs can also be implemented to provide continuous tuning at longer wavelengths. In particular, spectral regions up to 20 μm (0.06 eV)

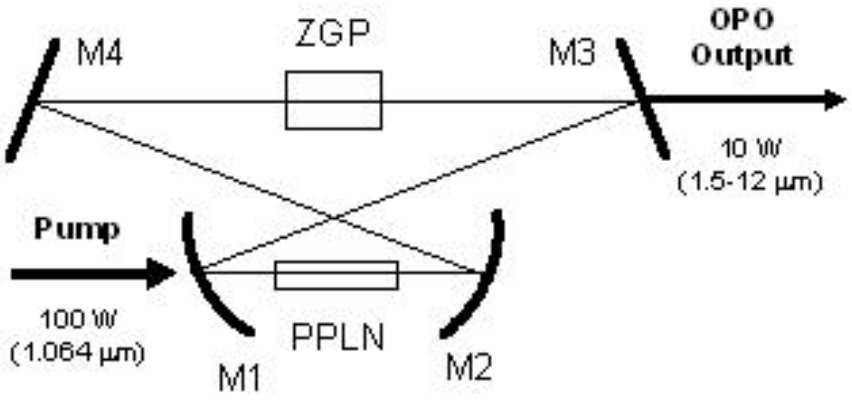

Figure H.7: Resonator configuration for the 1.5-12 μm cascaded intracavity cw OPO using a 100 W Nd:YAG pump laser. The internal radiation generated by the PPLN OPO provides the pump for single-pass DFG in the crystal of ZGP located internal to the OPO cavity. M1-M4 are mirrors. This system will also generate gamma-rays with energies in the range $E_\gamma(\text{max}) \sim 15 - 110$ MeV.

can be accessed using parametric generation techniques [12]. The spectral extension of OPO sources to such long wavelengths could, therefore, be an important subject of future research and development, which will also provide further capabilities for gamma-ray generation at energies $E_\gamma(\text{max}) < 10$ MeV at ALBA. Moreover, alternative designs can also be implemented and integrated into the proposed OPO systems to provide tuning in short wavelength regions, particularly from 400 nm in the visible to 1.5 μm in the near-IR, which can also provide for gamma-rays at energies in the range $E_\gamma(\text{max}) \sim 110 - 400$ MeV at ALBA.

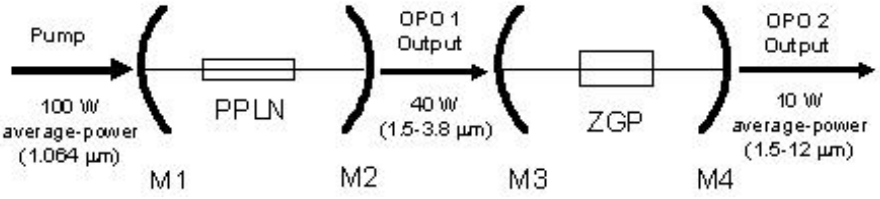

Figure H.8: Resonator configuration for the 1.5-12 μm cascaded external pulsed OPO using a 100-W average-power Nd:YAG pump laser. The output radiation from the PPLN OPO provides the pump for second OPO based on ZGP. M1-M4 are mirrors. This system will generate gamma-rays with energies in the range $E_\gamma(\text{max}) \sim 15 - 110$ MeV.

Pump Laser	Nd:YAG (cw)
Wavelength	1.064 μm
Output Power	100 W
OPO Design	Singly Resonant (PPLN+ZGP)
Wavelength Coverage	1.5-12 μm
Photon Energy	0.82-0.10 eV
Output Power	10 W
Spatial Quality	$M^2 \sim 1$
Spatial Profile	Gaussian (TEM_{00})
Polarization	$>$ 99% Linear
Total Footprint	150 $\times$ 150 cm

Table H.2: Characteristics of the cw pump laser and the 1.5-12 μm cw OPO for the generation of gamma-rays with energies of $E_\gamma(\max) \sim 15 - 110$ MeV at ALBA.

Pump Laser	Nd:YAG (Q-switched)
Wavelength	1.064 μm
Average Power	100 W
Pulse Duration	50-100 ns
Repetition Rate	100 Hz
OPO Design	Singly Resonant (PPLN+ZGP)
Wavelength Coverage	1.5-12 μm
Photon Energy	0.82-0.10 eV
Average Power	10 W
Pulse Duration	50-100 ns
Repetition Rate	100 Hz
Spatial Quality	$M^2 \sim 1$
Spatial Profile	Gaussian (TEM_{00})
Polarization	$>$ 99% Linear
Total Footprint	150 $\times$ 150 cm

Table H.3: Characteristics of the high-average-power pulsed pump laser and the 1.5-12 μm pulsed OPO for the generation of gamma-rays with energies of $E_\gamma(\max) \sim 15 - 110$ MeV at ALBA.

Bibliography

[1] M. Ebrahim-Zadeh, R.C. Eckardt and M.H. Dunn, Eds., ”Optical parametric devices and processes”, Special Issue, J. Opt. Soc. Am. B 16, 1477-1597 (1999).

[2] M.H. Dunn and M. Ebrahim-Zadeh, ”Parametric generation of tunable light from continuous-wave to femtosecond pulses”, Science 286, 1513-1517 (1999).

[3] M. Ebrahim-Zadeh and M.H. Dunn, ”Optical parametric oscillators”, in Handbook of Optics IV, Optical Society of America, McGraw-Hill, USA, 2201-2272 (2000).

[4] M. Ebrahim-Zadeh, ”Optical parametric devices”, in Handbook of Laser Technology and Applications, Institute of Physics Publishing, 1347-1392 (2003).

[5] M. Ebrahim-Zadeh, ”Mid-infrared ultrafast and continuous-wave optical parametric oscillators”, in Solid-State Mid- Infrared Laser Sources, Springer-Verlag Science Series, Topics Appl. Phys. 89, 179-218 (2003).

[6] W.R. Bosenberg *et al.*, Opt. Lett. 21, 1336-1338 (1996).

[7] G.A. Turnbull *et al.*, Opt. Lett. 25, 341-343 (2000).

[8] M. Ebrahim-Zadeh *et al.*, J. Opt. Soc. Am. B 16, 1499-1511 (1999).

[9] K.L. Vodopyanov *et al.*, Opt. Lett. 25, 841 (2000).

[10] K.L. Vodopyanov and P. Schunemann, Opt. Lett. 28, 441 (2003).

[11] For example, 100-W cw Nd:YAG laser available from Electronic Laser Systems (ELS), Germany.

[12] K.L. Vodopyanov, J. Opt. Soc. Am. B 16, 15799 (1999).

Appendix I

Silicon sensors for the tagging system

I.1 Introduction

Semiconductor sensors are widely used in Particle and Nuclear Physics experiments as tracking devices. Charged particles lose energy by ionization processes while crossing the sensor bulk. That energy is used to generate pairs of electrons and holes inside the semiconductor. Electrons and holes have different charge sign therefore they are separated by an electric field which also accelerates them. The movement of those electric charges produces an electrical current which can be detected and produces the detector's signal [1] (see Fig. I.1).

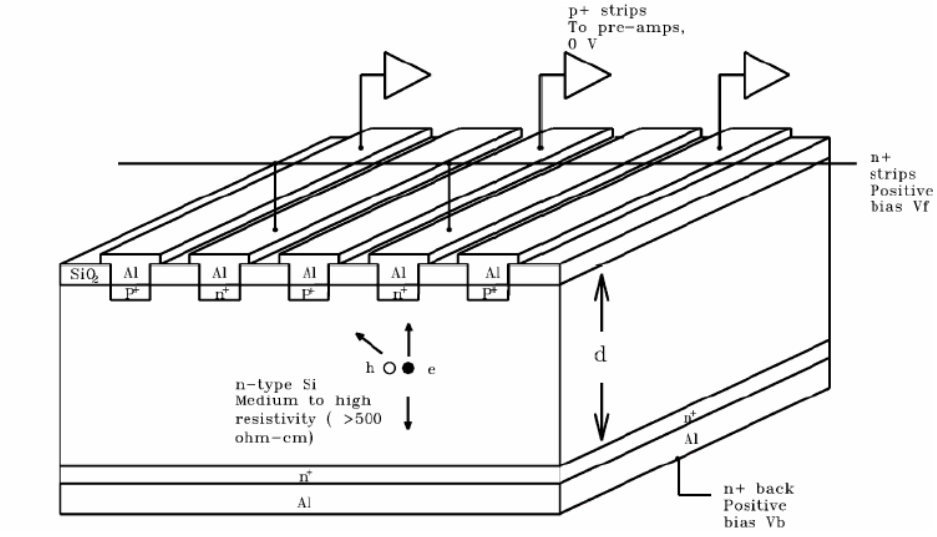

Figure I.1: Schematic view of a silicon microstrip detector. The electric field in the bulk separates the un-like sign electrons and holes and accelerates them. The movement of these charges produces a current detected by the electronics.

There exist several semiconductor materials which can be used in particle detectors as silicon, diamond and GaAs. Silicon sensors are the most in use by far, because of their good

sensing properties, well known and developed technology and affordability. The current particle physics experiments ([2]-[7]) are equipped with up to hundreds of squared meters of silicon sensors, while the very first experiments had just a few squared centimeters [8]. This gives an idea of the impressive development of the silicon sensor technique and that its associated technology is well known.

One of the main advantages of the silicon sensors is that they have a very good spatial resolution. Of course, the spatial resolution depends on the geometric configuration of the sensors. There exist designs where the active areas are strips and designs with active areas in pixels. The spatial resolution of microstrips sensors depends directly on the strip pitch, but it can be better than 20 microns. The spatial resolution of individual sensors can be further improved in a tracking system by combining several layers of sensors.

Silicon sensors are manufactured as plates of several centimeters wide and large but just of the order of 300 microns thick. The charge collecting time is of the order of few nanoseconds. Therefore silicon sensors are an appropriate type of sensors to be used in experiments with a very high trigger and read out rate. In fact, the sensors and their associated electronics developed during the 1990's for the CERN Large Hadron Collider experiments do work at a 40 MHz rate with a typical signal to noise ratio of 12-15 with a shaping time of 25ns. One can obtain a much better signal to noise ratio when using larger shaping times for the signals.

One of the advantages of using thin sensor layers (as for silicon) is a minimization of the multiple scattering effects. Of course it also depends on the incident particle type and on its energy but using layers of 300 micron-thick detectors has the benefit of having a small radiation length.

In recent years there has been also a large development of radiation hard silicon sensors. This development has been motivated specially because of the LHC experiments, where the silicon sensor will operate under extreme radiation levels. The radiation damage in terms of the signal effects are quantified in a signal loss and an increase of the noise. In terms of the operation, the irradiation causes a change in the effective doping concentration, change in the depletion voltage, and a change in the leakage current, which in its turn produces more power consumption, heat dissipation and shut noise [13]. The ability of an irradiated sensor to perform its duty has to be measured in terms of its signal to noise. Nowadays there exist silicon sensors able to operate providing a signal to noise of 10 even after having been irradiated with a dose of 10^{15} 1-MeV-neutrons/cm^2.

All these aspects concerning the properties and operation of the silicon sensors are developed in the following sections.

I.2 Detector design and spatial resolution

As already stated, there are several designs of silicon sensors available. They can be grouped in two main categories: pixels and strips.

Pixels allow to measure the crossing points of charged particles with a good 3D space point spatial resolution, while microstrips just provide a good 2D space point. 3D space points can be measured by using double sided silicon sensors, but this option has to be discarded because

of the problems induced by the radiation damage. Therefore 3D resolution with single sided silicon sensors must be gained by combining several layers of microstrip sensors oriented at different angles.

In principle the spatial resolution of microstrip sensors is just the strip pitch divided by $\sqrt{12}$. So for a typical sensor with a strip pitch of 75 microns one just gets a resolution of 20 microns. It can be further improved by using an analogue readout. With an analogue readout it is possible to give a relative weight to all channels giving signal according to the height of the pulse, and then compute the gravity center, thus producing a more accurate spatial point. But for doing so, the charge must be shared among several channels. So for a detector 5 cm wide instrumented with 512 channels one just needs a 100 microns strip pitch, which gives a spatial resolution better than 30 microns.

It is possible to use microstrip detectors with a pitch strip down to 50 microns. Detectors with a thinner pitch strip are also possible, but some problems arise as for instance, the electric field among strips increases and so does the probability of micro-discharges. This problem can be circumvented by using some specific design and manufacturing process, of the implantation of the dopants in the strip and of the aluminium implant. An immediate consequence of a thinner pitch strip is a considerable increase of the number of readout channels, which in turn requires more electronics, more power consumption and heat dissipation. Of course all these effects have an impact on the final cost.

A disadvantage of the pixel system is that the electronics must be located on top of the active sensor. This means that the electronics will receive the same radiation dose as the sensors. Besides, the additional material increases the multiple scattering, which it may be not an issue in this case, but any specific study has to consider it.

The sensor design for the LHCb experiment consists in two types of geometries, and the sensors have a half-disk shape [5]. There are sensors that are devoted to measure the azimuthal angle, therefore have strips in a radial configuration, while the second type of sensors is meant to measure the radial distance, therefore the strips are segments of circles. Both configurations include also a varying strip pitch in order to achieve a better granularity in the region where the density of particles is supposed to be higher. So complicated strip geometries which match the physics requirements are also possible.

In brief, one must say that 20 microns spatial resolution can be achieved without too much hassle. Better space point resolution can be also achieved at some cost in the detector design, but also considering the electrical insulation among strips.

One can foresee a system with multi layers of silicon sensors as it will provide a redundancy in the system. This redundancy will be much appreciated in case of accidents or problems in one of the layers, as the system could be still operated and the detection of the scattered electrons will not be perturbed. Therefore a system with a double layer separated by a few centimeters can provide a very good and reliable tracking system.

In conclusion a multilayer system of single sided microstrip detectors (of variable pitch if needed) with the electronics located in the outermost part is a very good option for the tracking system.

I.3 Read Out

Another important aspect is the readout electronics. This requires to use a hybrid board with multipurpose functions. The first is to connect the sensor to the bias voltage, the second to support the front end electronics and the connection with the data acquisition system, plus some mechanical support, cooling system and pitch adapter.

In what concerns the readout electronics, the sensors have to be AC coupled to the ASICs, which count with a front end amplifier, shaper and pulse analyzer (discriminator, ADC). The late stage can be performed in many ways depending on the event rate, occupancy and on the available time to integrate the signal. As stated above the LHC systems can operate up to 40MHz with shaping times of 25 ns [9]. This gives enough time between collisions to collect the whole signal but the noise due to the short shaping time is also quite important. In LHC the shaping time must be kept short because of the high density of particles per event. A larger shaping time will reduce the noise, leading to a better spatial resolution, reduced noise occupancy and fake hits. In figure I.2 one can see an schematic view of the processing of the signal from a silicon sensor within a chip.

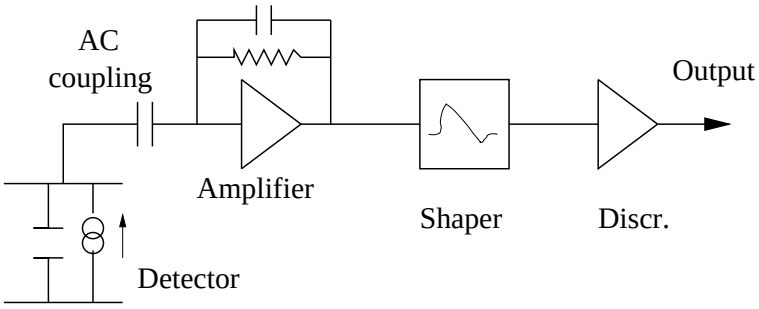

Figure I.2: Schematic view of the processing of the signal from a silicon sensor AC coupled in a chip: amplifying stage, shaping and producing an output.

For tracking systems with a large number of channels it is convenient to use a binary readout system. That means, after the front end amplifier and the pulse shaper the ASICs can integrate a digital part where a threshold can be set in order to transfer only the channel identification of those channels providing signal. However for systems with a small number of channels it is convenient to use an analogue system. That means, the pulse height of all channels are transfered to the data acquisition system. The event size can further be reduced by including some means of zero suppression or DPS (Dynamic Pedestal Subtraction). But keeping the analogue information may help tremendously in an off-line analysis. It may help to determine the center of gravity when a cluster of channels is formed, thus improving the spatial resolution. Matters as common noise are rather better treated off-line than on-line where one can aim for a better grounding scheme and an optimal cable and pipe routing which can be source of common noise. Masking noisy or dead channels can be done either way, on-line or off-line. Gain recalibration can be easily monitored in an off-line system and the channel-by-channel effects can be taken into account.

As the electrons may arrive at any time, and in order to keep the acquisition running all time, one must consider the possibility of running the system in a continuous mode. The signal from a channel is first amplified and then shaped. Considering a 10 MHz triggering rate, and a low occupancy level per channel, one may use a large shaping time, of the order of 100ns. There exist already manufactured chips that can be suitable for this application [10] and even some of them are radiation hard [11]. A large shaping time has the advantage of keeping the noise low, but has the disadvantage that pile-up may occur. So, as far as the occupancy level per channel is low, using a long shaping time is appropriate. Then the discriminator output can be stored either in a pipe-line , in order to be read when a trigger occurs, or stored in a FIFO buffer, that may be filled with two informations: a) the channel identifier and b) the time at which the signal occurred.

There is also the possibility of splitting the channel output in two and one of the signals used then for triggering. This feature already exists in some commercial chips. This offers the opportunity of having a self triggering system, but if one has to consider many channels (e.g. 512) and triggering the readout just if one of the channels triggers the fake trigger rate can be too high. There are methods to keep it low such as using a high level for discrimination, with the disadvantage of maybe cutting out genuine signals, or making coincidences with a scintillator system.

Nowadays submicron chip technology provides at affordable prices a radiation hard technology. Although in this system the readout chips can be located further away from the beams thus keeping radiation damage as low as possible.

In what concerns the data transmission, optical link provides nowadays a reliable means of data transmission, at a low cost and with very small impact in the material budget.

I.4 Radiation hardness

Silicon sensors operating in a high radiation environment suffer from radiation damage. The basic effects of the radiation is a change in the effective doping concentration (see Fig. I.3), which in turn affects the bias voltage, an increase in the leakage current and therefore the noise, the power consumption and the heat dissipation, and the introduction of charge trapping centers, thus reducing the signal [12].

The above are the macroscopic manifestations of the microscopic effects of the radiation damage. The radiation damage appears when an incident particle transfers to a silicon atom enough energy in order to vacate its position in the silicon lattice. The binding energy of a silicon atom is 25 eV. So for a fixed energy, heavier particles as protons and neutrons create more radiation damage than light particle as electrons. The studies of the radiation damage are based in the NIEL hypothesis (Non Ionizing Energy Loss). That means that the damage to the silicon lattice is due to the non ionizing energy lost by incident particles which do not induce a signal but moves silicon atoms from their lattice locations.

As mentioned above when a silicon atom is removed from its position in the silicon lattice it leaves a vacant position behind. As that vacancy can be filled by a neighbouring atom just by thermal excitation, the vacancy moves and therefore the defects in the lattice are mobile. As

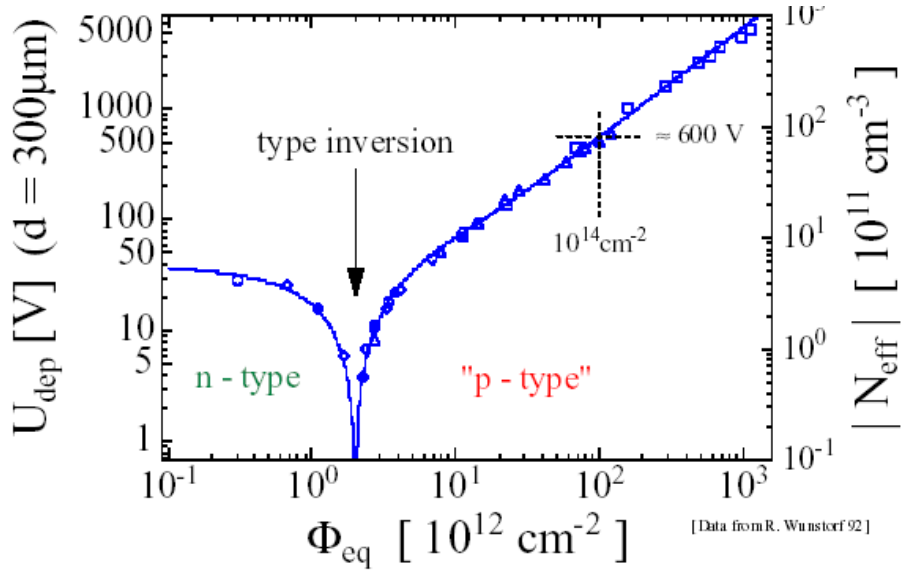

Figure I.3: Change in the effective doping concentration of the silicon sensor bulk as a function of the radiation dose. A substrate with an initial majority of donor states (n-type) becomes a substrate with a majority of acceptor doping states (p-type). Therefore there is an inversion of the bulk type.

defects move around, they can meet and generate more complex defects. The vacancies can react with interstitials, impurity atoms and other vacancies. A particularly harmful state is a divacancy, formed when two vacancies meet. The divacancy or V_2 state is quite stable. As V_2 acts as acceptor state, the Fermi level is moved toward the lower side of the band gap modifying the effective doping concentration and therefore affecting the bias voltage needed to operate the detector. It is also possible to invert the bulk type, from an initial majority of donors (n-type) to a majority of acceptor states (p-type).

Not only V_2 states are formed. The phenomenology of defects is quite complex [13]. There is also the possibility of the vacancies to react with impurities and create more complex structures, as for instance oxygen atoms and create VO or V_2O. There appear also regions where the lattice structure is severely damaged. All these defects may act as effective doping or trapping centers.

The radiation damage has been a matter of concern for the silicon tracking detectors of the LHC experiments (namely ATLAS, CMS, LHCb and ALICE). Therefore during the past years there has been a large development in this area [14][15][16]. It has been seen that the diffusion of oxygen in the silicon bulk improves the radiation tolerance, and that other silicon materials, like Czoralski silicon are also more radiation hard. The LHC experiments have studied mainly the effect of the proton and neutron irradiation, inside what was called the ROSE collaboration, an specific R&D CERN project, which nowadays has its continuation in RD50.

Studies of the radiation damage due to electrons have been carried out inside RD50. The irradiation has been performed using low (15 MeV) and high energy (900 MeV, from the LINAC

injector at Elettra in Trieste) electrons. Those studies performed with radiation doses up to 10^{15} e/cm^2 show that the charge collection efficiency is reduced just by 1-2% for Czoralski and epitaxial silicon and somewhat more for FZ (Float Zone) and DOFZ (Diffusion of Oxygen in Float Zone).

The annealing of the irradiated samples, either at room or at high temperature shows a slight improvement of the macroscopic properties of the irradiated samples. This is seen in a reduction of the effective doping concentration, thus the depletion voltage, a decrease of the leakage current and a slight increase of the charge collection efficiency.

The defects in the surface of the silicon detectors remain to be studied, although it seems that they are less important than the bulk defects. However the presence of a charge accumulation layer in the interface between silicon and the passivated layer has to be taken into account in the design.

A last word must be said on what sort of bulk (n-type or p-type) may be used. It is known that the n-type-bulk detectors are more radiation tolerant. This is due to the fact that in n-on-n silicon the signal is carried by electrons, which have a larger mobility rather than the holes (the signal producers in the p-on-n type sensors). On the other hand, single sided n-on-n detectors need a double side processing in order to prevent short circuits in the back side when the bulk type inversion occurs, therefore they are more expensive than p-on-n detectors. The ATLAS studies have shown that irradiated p-on-n type detectors can be used in the real experiment. Moreover the CNM (Centro Nacional de Microelectronica) in Barcelona has recently produced silicon sensors from a p-type bulk [17]. This presents some operational advantages as the bulk type will not invert during irradiation. Irradiation studies with this sort of sensors are currently being performed.

It must be also said, that if the radiation damage is too large one can consider to replace the tracking system. This is the solution adopted by the LHCb experiment for its VELO (VErtex LOcator) system. During the detector phase design of the LHCb VELO, it has always been assumed that the radiation damage will be so important that the system will last just a couple of years. The VELO system will be located just a couple of centimeters away from the LHC beam axis, therefore the expected dose is to reach 10^{16} protons/cm^2 in a couple of years. The VELO system has the readout chips located in the outermost part of the sensors, just where the radiation dose will be smaller.

Another solution can be adopted. As the incident electrons are expected to be registered in a narrow band of less than 100 μm width, the irradiation will be concentrated in that area, while the rest of the detector will be kept almost brand new. This problem is similar to what happens on the LHCb detectors which are disposed transversal to the beam. Therefore the irradiation dose is anisotropic. The current studies performed with LHCb sensor prototypes irradiated with non-uniform doses show that the non irradiated areas have the expected properties. So one can envisage a system of 5×5 cm^2 which can be slided downwards or upwards and offer a non irradiated active area when the damage to the one in use is too high. A side effect may appear as the electric field may have a transverse component due to a gradient in the effective doping concentration as:

$$\nabla^2 V = \frac{-\rho}{\varepsilon_0 \varepsilon_{Si}} \tag{I.1}$$

being ρ the charge density in the detectors bulk, which may be non-uniform due to a non-uniform irradiation dose. ε_0 and ε_{Si} are the dielectric constant of the vacuum and the factor for the dielectric constant of the silicon (≈ 11).

Bibliography

[1] S. Ramo. *Currents induced by electron motion*. Proc IRE 27(9):584 (1939).

[2] D. Amidei et al. *The silicon vertex detector of the collider detector at FermiLab*. Nucl Inst. and Methods A 350:73 (1994)

[3] D. Mihalcea. *The assembly and testing of the D0 silicon detector*. Nucl. Inst. and Methods A 473:49 (2001)

[4] The ATLAS collab.*ATLAS inner detector Technical design report*. ATLAS TDR 4, CERN/LHC 97-16

[5] J. Libby. *VELO: The LHCb Vertex Detector*. Nucl. Instrum. and Meth. A494:113-119 (2002)

[6] CMS collab. D. Abbaneo *Layout and performance of the CMS silicon strip tracker*. Prepared for 9th Pisa Meeting on Advanced Detectors: Frontier Detectors for Frontier Physics. La Biodola. Isola d'Elba. Italy. 25-31 May 2003. Published in Nucl.Instrum.Meth.A518:331-335 (2004)

[7] ALICE Collaboration (G. Anelli et al.) *The Silicon Pixel Detector (SPD) for the ALICE experiment* Prepared for 17th International Conference on Ultra Relativistic Nucleus-Nucleus Collisions (Quark Matter 2004). Oakland. California. 11-17 Jan 2004. Published in J.Phys.G30:S1091-S1095 (2004)

[8] R. Breedon *The AMY vertex detector* 2nd Workshop on TRISTAN Physics at High Luminosities, Tsukuba, Japan, 24-26 Nov 1993.

[9] W. Dabrowski et al. *Design and performance of the ABCD chip for the binary readout of silicon strip detectors in the ATLAS semiconductor tracker*. IEEE Trans. Nucl. SCi. 47:1843-1850 (2000)

[10] T. Zimmerman et al. *A dead-timeless readout chip for silicon strip detectors*. Nucl. Inst. and Methods A 49:369 (1998)

[11] B. Krieger et al. *A new deep submicron readout IC for the TeVatron Collider at Fermilab*. IEEE Trans.Nucl.Sci.51:1968-1973 (2004)

[12] T.J. Brodbeck et al. *Carrier mobility in irradiated silicon.* Presented at the 5th Conference on Position Sensitive Detectors, London, U.K. September 1999. ROSE/TN/2000-09

[13] E. Fretwurst for the CERN RD50 collab. *Recent advancements in the devlopment of radiation hard semiconductor detectors for the S-LHC.* Submitted to the RESMDD04 conference. Florence. Italy 2004.

[14] G. Lindstrom et al. *Developments for radiation hard silicon detectors by defect engineering. Results by the CERN RD48 (ROSE) collaboration*. Nucl. Inst. and Methods A 465:60-69 (2000)

[15] G. Casse et al. *Comparison between ATLAS forward microstrip detectors made on 6 inch* $\langle 100 \rangle$ *and 4 inches* $\langle 111 \rangle$ *silicon wafers*. Nuovo Cim 112 A: 1253-1259 (1999)

[16] S. Martí i García et al. *A model of charge collection for irradiated* $p^{+}n$ *detectors*. Nucl. Inst.and Methods A 473:128-135 (2000)

[17] G. Casse et al. *First results on charge collection efficiency of heavily irradiated microstrip sensors fabricated on oxygenated p-type silicon*. Nucl. Instrum. and Meth.A 518:340-342 (2004)

Appendix J

Radiation shielding

J.1 Introduction and general considerations

The preliminary technical design of the Spanish Synchrotron Light Source ALBA, described in the ”LLS Detailed Design Report” [1], contains a description of the shielding and a personal safety system for this facility. The main sources of ionizing radiation, taken into account in Ref. [1], are the synchrotron light itself and different groups of secondary radiation which include the gas bremsstrahlung, medium energy neutrons (with energies up to 10 MeV) and high energy neutrons (with energies up to a few hundred MeV).

The construction of the beam line for the production of gamma rays of intermediate energies (up to 530 MeV) and intensities up to 10^9 photons/s at the storage ring of ALBA requires a special scenario for shielding which is different from standard X-ray beam lines and which, therefore, has not been envisaged in the preliminary design of the facility.

The general layout of the gamma ray beam line is given in Fig. J.1. It consists of two hutches housing the equipment plus additional shielding structures. The upstream hutch, adjacent to the front end of the facility storage ring, contains the laser and the optical equipment and a vacuum tube for the γ-ray beam transport. The target, detectors and other experimental instrumentation are situated in the downstream hutch. In the middle part a collimator, a sweep magnet and shielding for reducing the background of neutrons are installed. At the very end of the beam line, the beam dump will be situated. On its way from the front end to the detector the γ-ray beam travels a part of the trajectory inside a vacuum tube and the rest of the path in the air.

All considerations on the radiation safety exposed in Sect. 6.3.1 and Sect. 6.3.2 of [1] are applicable to the γ-ray beam line. In particular, in accordance with the Radiation Standards Directive , 96/29/EURATOM of May 13 of 1996, which has been introduced in Spain by the *Real Decreto* 783/2001, the annual effective dose limit for the general public is 1 mSv, while for employers of the facility over 18 years old the limit is set to 100 mSv in a period of 5 consecutive years, with a maximum dose per year of 50 mSv.

To satisfy these dose limits we will apply the local shielding scheme complemented with the shielding provided by the hutch wall. In the framework of this approach the γ-ray beam line will be equipped with necessary elements for local shielding which include a collimator, a sweep magnet, a beam dump (beam stop), a local shielding module and, as an option, a neutron

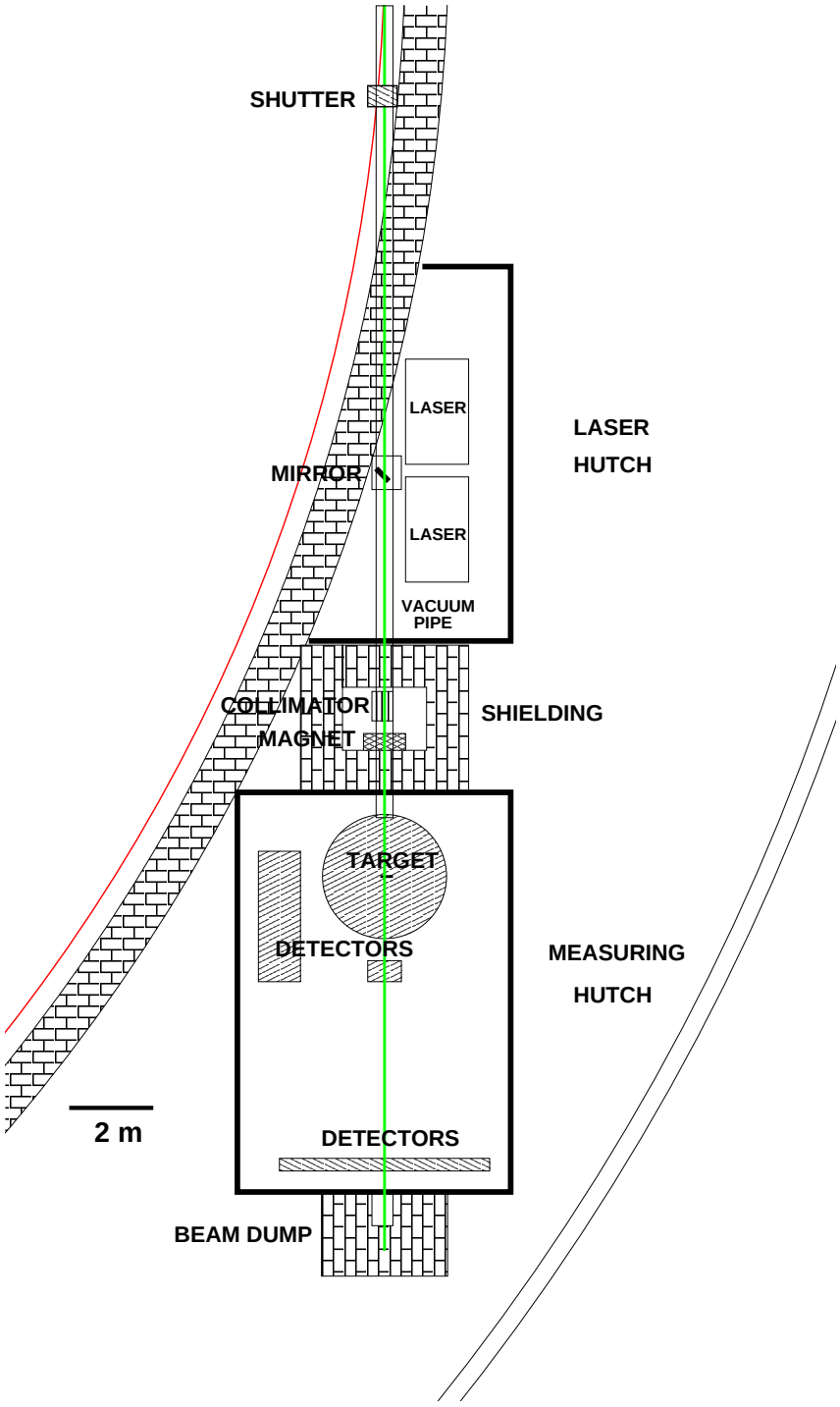

Figure J.1: Schematic lay-out of the gamma-ray line installation, showing the laser hutch, the shielded collimator area, the measuring hutch and the beam dump

absorbing screen. We would like to point out that in this proposal we consider only the ionising radiation associated with the presence of the primary γ-ray beam. The description and some general specifications of the shielding elements and of the hutch are given below. Provided that these elements are correctly designed (this will have to be certified by appropriate safety inspectors during the beam line commissioning) the level of radiation in the areas accessible to personnel when the beam line is in operation should be below the dose limits indicated above. Nevertheless, in accordance with the radiation safety model adopted in the design report [1], we propose that continuous monitoring of radiation level is carried out. These measures should be completed with alarms, interlock systems, areas access rules and emergency shutdown rules, elaborated for this particular beam line, in the same way as it is envisaged in Ref. [1].

Some types of experiments planned at the γ-ray beam line require extremely low background. So, apart from the radiation protection of the personnel, the shielding elements should provide an essential reduction of the flux of neutrons, electrons and positrons produced by the primary γ-ray beam interacting with the elements of the beam line which can enter the experimental zone. For most of the cases the local shielding mentioned above will be sufficient. For the cases when the neutron background is still above the accepted limit additional removable screen absorbing neutrons will be installed.

J.2 Shielding

J.2.1 Sources and types of radiation

As it can be seen in Fig. J.1, after going through the laser beam deflecting mirror the γ-ray photons will successively pass through the following elements:

- γ-ray beam vacuum transport tube
- Collimator
- Sweep magnet
- Vacuum window
- Target
- Detectors
- Beam dump

The secondary radiation due to the interaction of the primary γ-ray beam with these elements can be divided in the following groups:

- Electromagnetic cascade produced inside the front end window, laser mirror and flange of the vacuum pipe. These particles are mainly collimated in the forward direction and may have energies up to 265 MeV. Part of them will pass through the collimator channel and create

a high enough background which may be a problem for certain experiments. To eliminate the electron-positron background we propose to install a sweep magnet equipped with an absorbing shield. The charged particles deviated by the magnet hit a shield where they are absorbed. The magnet must be installed as far as possible from the target.

- The electromagnetic cascade consisting of electrons, positrons and electromagnetic radiation produced inside the collimator. Results of conservative estimates of the dose due to this group of radiation are described below. Its intensity is strongly reduced inside the collimator itself so that the walls of the hutch will be sufficient to reduce the dose outside the hutch below the minimum permitted level.

- Neutrons produced by the primary γ-ray beam inside the collimator. Some estimates of the corresponding dose are presented in the next subsection. The neutron intensity will be reduced by a local shielding and the hutch wall in order to achieve the permitted neutron dose level outside the hutch. To reduce the neutron background in the experimental zone to a required level, an absorbing screen can be installed.

- The electromagnetic cascade (electrons, positrons and photons) and neutrons produced in the core of the beam dump. This radiation will be absorbed by the various layers of the beam dump.

J.2.2 Shielding analysis

The parameters of the collimator, the beam dump core and the sweep magnet will be chosen in accordance with the shielding recommendations given in Ref. [2]. They were confirmed with preliminary studies using the PENELOPE code [3] for numerical simulation of the development of the electromagnetic cascade.

As far as neutron radiation is concerned, a preliminary estimate shows that the neutron annual effective dose at the distance $d = 2$ m from the collimator is of the order of 1 mSv. Therefore, it is necessary to further reduce the neutron flux by a local shielding module surrounding the collimator and the sweep magnet (see Fig. J.1). This local shielding will also help to meet the strict limits on the background level imposed by the experiments.

We also took into account that, since the vacuum transport pipe ends after the laser mirror and before the collimator, the primary photons fly a part of their path between the tube flange and the target in the air. The interaction of the beam with the air may disperse the photons and be a source of radiation. Studies carried in Ref. [2] and our estimates show that the dispersion and attenuation of the γ-ray beam intensity due to the passage through the air are negligible and, therefore, this source of radiation does not present any problem from a radiation protection point of view. Nevertheless, the effect of this interaction on the γ-ray beam quality has to be investigated.

We see that the local shielding elements such as the shielding module, the sweep magnet with its electron-positron shield, the collimator itself and the beam dump should be enough to reduce the dose below the acceptable level. The hutch walls will further reduce the dose

substantially. As an additional option a neutron absorbing screen may be installed to decrease the neutron background, a measure which may be necessary for some types of experiments.

J.2.3 Shielding elements

As it has been already stated in Sect. J.1 in the shielding design two aspects have been taken into account:

1. safe dose outside the hutch

2. reduction of the background in the experimental area.

To satisfy the dose limits indicated above the γ-ray beam line will be equipped with the necessary elements for local shielding inside the hutch. These include the collimator shielding, the sweep magnet with electron-positron shielding and the beam dump. These elements make possible the hutch design proposed in Fig. J.1. In what follows a short description and main parameters of these shielding elements general for the beam line will be given.

The design of shielding elements is based on the analysis described above and on the design parameters of similar beam lines, in particular NSLS [4], SPring-8 [5] and APS [2, 6], with corresponding modifications due to the difference in intensities and energies. Of course, for the technical design of the beam line a more detailed study, supported by calculations and numerical simulations, has to be carried out.

For the **hutch** design we propose to construct its walls out of steel lined with 2 cm thick lead panels. This is the type of hutch used at the SPring-8 facility [7]. Since at the laser electron beam line of SPring-8 photons of energies ranging from 1.5 GeV to 3.5 GeV are produced, it is clear that our proposal is conservative and prudent enough. In fact, it will be sufficient to construct walls of such lead thickness only at certain sectors of the hutch, where the flux of secondary photons and neutrons, according to more detailed calculations which are to be done, is more intense.

The **collimator** is a cylinder of radius of ~ 5 cm and of length of ~ 30 cm made out of lead. The collimating channel, coaxial with the cylinder axis, is of variable diameter smaller than 3 mm. The collimator can also be manufactured of rectangular cross section. In any case it must have the shielding thickness at least 5 cm in the direction orthogonal to the beam and of 30 cm in the longitudinal direction. This is enough to reduce considerably the electromagnetic cascade in transversal directions and to practically suppress it in the forward direction. If necessary, the collimator can be equipped with two collars, an upstream collar and a downstream one, in order to reduce the effect of beam miss steering and hitting the upstream or downstream edge (see Ref. [2]). The decision concerning the collars and their sizes will depend on the results of the detailed study of the radiation production.

The main function of the **sweep magnet** is to protect the target from converted electrons and positrons which pass through the collimator channel. Its layout is presented in Fig. J.2. The particles are deviated vertically by the magnetic field and are absorbed by an electron-positron shield. The layout is similar to the one used at the SPring-8 facility (see Ref. [5]). We propose to use a magnetic field which can be varied from a minimum value of 0.1 kGauss up to 4 kGauss.

With this range of the field and the length of the magnet of 50 cm, as it is indicated in Fig. J.2, all electrons and positrons with energies between 1 MeV and 265 MeV will hit the electron-positron shield and will not pass through its aperture. The value of the field is supposed to be chosen in an optimal way for each experiment, depending on the energy of the primary γ-ray beam. The magnet collimator and the electron-positron shield are made out of lead and have dimensions indicated in Fig. J.2.

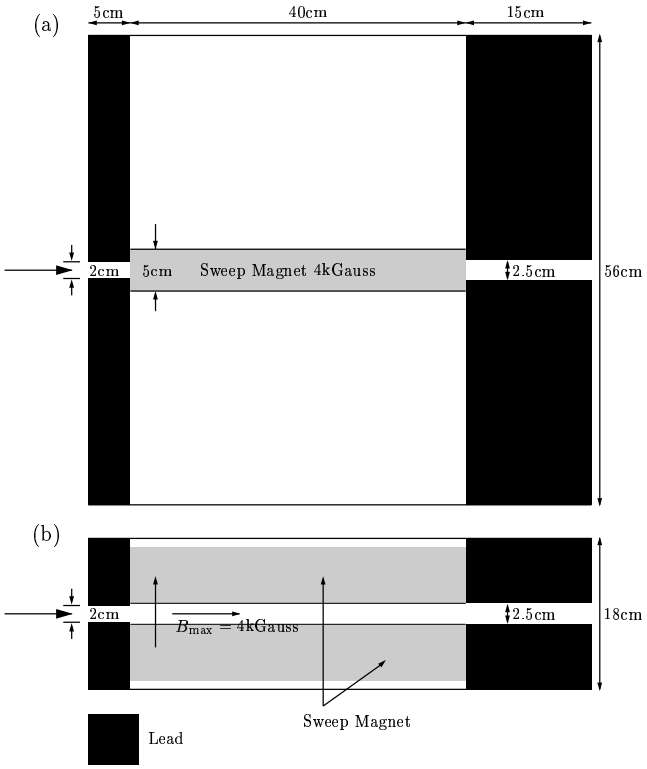

Figure J.2: Sweep magnet layout,(a) lateral cross section, (b) top cross section.

The collimator and the sweep magnet are surrounded by a **shielding module**. Its approximate dimensions are shown in Fig. J.1. As it was explained above, its main function is to reduce/absorb the neutrons flux produced in the collimator and possibly in the sweep magnet collimator. The walls of the module are proposed to be made out of concrete. Additional screens of a hydrogenated material with a low Z neutron absorber, like borated polyethylene, can be placed inside.

The **beam dump** layout, its dimensions and the materials used are shown in Fig. J.3. Here we relay on the designs proposed for other facilities, in particular for the SPring-8.

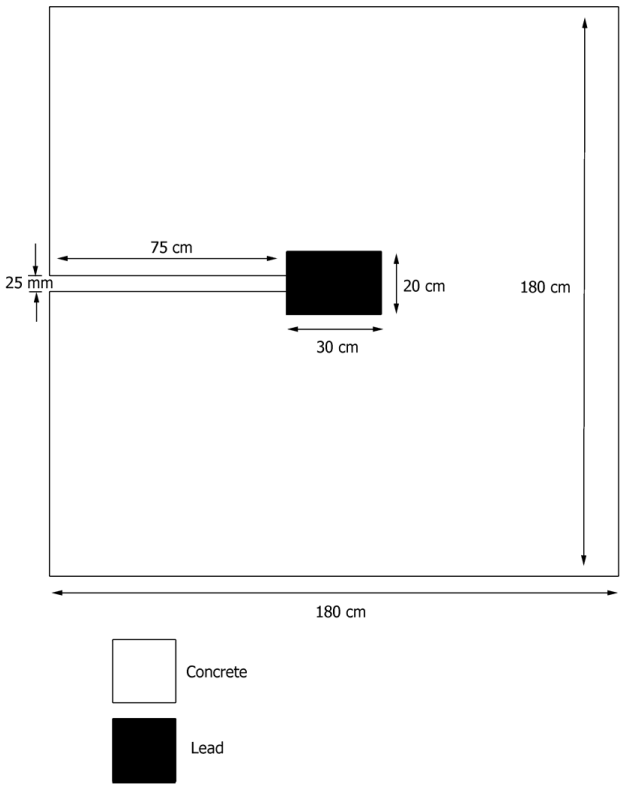

Figure J.3: Beam dump layout, lateral cross section.

J.3 Conclusions

Our conclusion is that the dose limits adopted for the technical design of the facility ALBA (see Sect. 6.3.1 of Ref. [1]) and cited in Sect. J.1 can be satisfied with the proposed design of the hutch and local shielding elements, namely the shielding module, the sweep magnet with its electron-positron shield, the collimator and the beam dump. The proposed elements are sufficient to reduce the dose below the safe level outside the hutch during the operation mode of the beam line. As an additional option a neutron absorbing screen may be installed to further reduce the neutron background for some types of experiments.

This conclusion is based on our analysis, described in Sect. J.2.2, and on the shielding design solutions at similar existing beam lines.

As we have already stressed in different occasion, a detailed design study is needed in order to specify the final parameters of the shielding elements.

Bibliography

[1] ”LLS Detailed Design Report”, LLS, 1997; available at http://www.cells.es

[2] P.K. Job, D.R. Haeffner and D. Shu, ”Bremsstrahlung Scattering Calculations for the Beam Stops and Collimators in the APS Insertion-Device Beamlines”, ANL/APS/TB-20.

[3] F. Salvat, J.M. Fernández-Varea and J. Sempau, ”PENELOPE, A Code System for Monte Carlo Simulation of Electron and Photon Transport”. OECD Nuclear Agency, 2003; available at http://www.nea.fr

[4] P.M. Stefan, updated by W.R. Casey and N.F. Gmur, ”Preparation of Beamline Bremsstrahlung Shielding Anamorphic Drawings”, 2004.

[5] Y. Asano, T. Nakano, T. Hotta and Y. Ohashi, ”Shielding Design Calculations for Laser Electron Beamline of SPring-8” *J. of Nucl. Science and Techn.*, Suppl. **1** (2000) 217-221.

[6] P.K. Job, ”Guidelines for Beamline and Front-End Radiation Shielding at the Advanced Photon Source”, ANL/APS/TB-44, 2003.

[7] ”SPring-8: Facility Design 1991”, SRRC, 1991.

Appendix K

Users of the gamma-ray beam line

The construction of the gamma-ray beam line at ALBA represents the opportunity to have the first installation dedicated to experimental nuclear physics activities in Spain.

Historically, the development of accelerators facilities traditionally associated to nuclear physics research in Europe and the rest of the world, never took place in Spain, hampering the development of experimental nuclear physics and its numerous applications.

The development of experimental nuclear physics in Spain during the last 18 years has been associated to the use of several installations mainly in Europe but also in the U.S.A. During this time the community has grown from a marginal representation to the present situation with groups at UPC Barcelona, U. Huelva, CIEMAT Madrid, IEM (CSIC) Madrid, U. Autnoma Madrid, U. Complutense Madrid, U. Santiago de Compostela, U. Sevilla and IFIC (CSIC-U. Valencia), with several collaborations established between them. This internationally recognized community is actively participating in the research program of ISOLDE and nTOF at CERN, G.S.I-Darmstadt, LNL-INFN Legnaro, CRC Louvain-la-Neuve, among others, as is reflected in the list of few selected publications included at the end. The construction of the gamma-ray beam line will help to strengthen the collaboration between the groups, at the national level. It will also reinforce their weight in the international context, through the development of new specific know-how and the establishment of new collaborations. Not only these, it will stimulate the growth of the groups and the creation of new ones. To this respect, it should be pointed out here that there exist a sizeable number (around 35) of excellent young researchers which have been formed in the recent years, within the Spanish groups or even independently within foreign groups, or are just conducting their PhD work outside of Spain which could be attracted by the new opportunities that the installation will offer. These benefits are not restricted alone to the basic nuclear physics community but will extend also to its applications and, as is the case here, to part of the astrophysics community. In Table K.1 we give a list of the senior researchers which are proposing to conduct experiments at the gamma-ray beam line. To this list we should add approximately twice the number of postdocs and students. The role of theoretical nuclear physicists is particularly important to the successful planning and interpretation of the experiments. As it happens, the Spanish community working in nuclear theory in general, and in the physics with electromagnetic probes in particular, is well reputed internationally. A list of the theoreticians directly interested in the experiments is given in Table K.2 and a brief selection of

their publications is also included in the list at the end. Last, but not least, the proposed gamma-ray beam line has the conditions to attract the interest of foreign users in particular Europeans, to perform experiments complementary to those feasible at other facilities.

Table K.1: Experimental physicists proposing measurements at the beam line.

Name	Position	Center
M. Amor Duch	Investigador	Instituto de Técnicas Energéticas Univ. Politecnica Catalunya, Barcelona
J. Benlliure	Profesor Titular	Departamento de Física de Partículas Univ. de Santiago de Compostela
M.J.G. Borge	Investigador CSIC	Instituto de Estructura de la Materia C.S.I.C., Madrid
F. Calviño	Profesor Titular	Departament de Física i Enginyeria Nuclear Univ. Politecnica Catalunya, Barcelona
D. Cano-Ott	Investigador CIEMAT	Departamento de Fisión Nuclear CIEMAT, Madrid
D. Cortina	Investigador RyC	Departamento de Física de Partículas Univ. de Santiago de Compostela
I. Durán	Catedrático	Departamento de Física de Partículas Univ. de Santiago de Compostela
J.M. Espino	Profesor Titular	Departamento de Física Atómica, Molecular y Nuclear, Univ. de Sevilla
L.M. Fraile	Profesor Contratado Doctor	Departamento de Física Atómica, Molecular y Nuclear, Univ. Complutense Madrid
J.E. García-Ramos	Profesor Titular	Departamento de Física Aplicada Univ. de Huelva
J. Gómez-Camacho	Profesor Titular	Dpto. de Física Atómica, Molecular y Nuclear , Univ. Sevilla
M. Gómez-Santamaría	Profesor Contratado Doctor	Departamento de Física Aplicada Univ. de Huelva
E. González-Romero	Investigador CIEMAT	Departamento Fisión Nuclear CIEMAT, Madrid
D. Guirado	Facultativo	Hospital Clínico Univ. “San Cecilio” Granada
M. Hernanz	Investigador CSIC	Institut d’Estudis Espacials de Catalunya, Barcelona
J. Isern	Profesor Investigación CSIC	Institut d’Estudis Espacials de Catalunya, Barcelona
A. Jungclaus	Investigador RyC	Departamento de Física Teórica Univ. Autónoma de Madrid
Yu. Kubyshin	Profesor Agregat	Instituto de Técnicas Energéticas Univ. Politecnica Catalunya, Barcelona
I. Martel	Profesor Titular	Departamento de Física Aplicada Univ. de Huelva

Table K.1: Experimental physicists proposing measurements at the beam line (Cont.)

Name	Position	Center
T. Martínez	Investigador CIEMAT	Departamento Fisión Nuclear CIEMAT, Madrid
F. Pérez-Bernal	Profesor Contratado Doctor	Departamento de Física Aplicada Univ. de Huelva
F. Pizarro	Profesor Titular E.U.	Departamento de Física Aplicada Univ. de Huelva
A. Poch	Profesor Titular E.U.	Departament de Física i Enginyeria Nuclear Univ. Politecnica Catalunya, Barcelona
J. Rodríguez-Quintero	Profesor Titular	Departamento de Física Aplicada Univ. de Huelva
B. Rubio	Investigador CSIC	Instituto de Física Corpuscular C.S.I.C.-Univ.Valencia
J. Sempau	Investigador	Instituto de Técnicas Energéticas Univ. Politecnica Catalunya, Barcelona
J.L. Taín	Científico Titular CSIC	Instituto de Física Corpuscular C.S.I.C.-Univ.Valencia
O. Tengblad	Investigador CSIC	Instituto de Estructura de la Materia C.S.I.C., Madrid
J.M. Udías	Profesor Titular E.U.	Dpto. de Física Atómica, Molecular y Nuclear Univ. Complutense de Madrid
J.J. Vaquero	Investigador RyC	Hospital Gral. Univ. “Gregorio Marañón” Madrid
M. Vilches	Facultativo	Hospital Clínico Univ. “San Cecilio” Granada

Table K.2: Theoretical physicists related to the proposed experiments.

Name	Position	Center
J.E. Amaro	Profesor Titular	Departamento de Física Moderna Univ. Granada
M. Anguiano	Investigador RyC	Departamento de Física Moderna Univ. Granada
J.A. Caballero	Profesor Titular	Dpto. de Física Atómica, Molecular y Nuclear, Univ. Sevilla
M. Centelles	Profesor Titular	Dept. d'Estructura i Constituents de la Matèria, Univ. Barcelona
F. Fernández	Catedrático	Departamento de Física Univ. Salamanca
J.M. Fernández-Varea	Profesor Titular	Dept. d'Estructura i Constituents de la Matèria, Univ. Barcelona
A.M. Lallena	Catedrático	Departamento de Física Moderna Univ. Granada
F.J. Llanes-Estrada	Prof. Contratado Doctor	Departamento de Física Teórica I Univ. Complutense de Madrid
G. Martínez-Pinedo	Investigador	Institut d'Estudis Espacials de Catalunya Barcelona
E. Moya de Guerra	Profesor Investigación CSIC	Instituto de Estructura de la Materia CSIC, Madrid
J.M. Nieves	Profesor Titular	Departamento de Física Moderna Univ. Granada
J.A. Oller	Profesor Titular	Departamento de Física Univ. Murcia
E. Oset	Catedrático	Departamento de Física Teórica Univ. Valencia
A. Parreño	Investigador RyC	Dept. d'Estructura i Constituents de la Matèria, Univ. Barcelona
A. Polls	Catedrático	Dept. d'Estructura i Constituents de la Matèria, Univ. Barcelona
J.M. Quesada	Profesor Titular	Dpto. de Física Atómica, Molecular y Nuclear, Univ. Sevilla
A. Ramos	Profesor Titular	Dept. d'Estructura i Constituents de la Matèria, Univ. Barcelona
F. Salvat	Catedrático	Dept. d'Estructura i Constituents de la Matèria, Univ. Barcelona

Table K.2: Theoretical physicists related to the proposed experiments (Cont.)

Name	Position	Center
A. Valcarce	Profesor Titular	Departamento de Física Univ. Salamanca
X. Viñas	Catedrático	Dept. d'Estructura i Constituents de la Matèria, Univ. Barcelona

List of some selected publications.

1. U. Abbondanno *et al.*, Phys. Rev. Lett. 93, 161103 (2004).
2. F.M.O. Al-Dweri, A.M. Lallena, M. Vilches, Phys. Med. Biol. 49, 2687 (2004).
3. M. Anguiano, G. Co', A.M. Lallena, S.R. Mokhtar, Ann. Phys. (N.Y.) 296, 235 (2002).
4. P. Armbruster *et al.*, Phys. Rev. Lett. 93, 212701 (2004).
5. P. von Ballmoos *et al.*, Proceed. of the SPIE, vol. 5168, pp. 482-491 (2004) (SPIE: International Society for Optical Engineering).
6. P. von Ballmoos *et al.*, New Astronomy Reviews 48, 243 (2004).
7. D. Cortina-Gil *et al.*, Phys. Rev. Lett. 93, 062501 (2004).
8. C. Fernández-Ramírez, E. Moya de Guerra, J.M. Udías, Proc. 6^{th} Workshop on Electromagnetically Induced Two-Hadron Emission, Pavia, Italy (2003).
9. H.o.U. Fynbo, Y. Prezado *et al.*, Phys. Rev. Lett. 91, 082502 (2003).
10. T. Frick, S. Kaiser, H. Müther, A. Polls, D.R. Entem, R. Machleidt, Phys. Rev. C 65, 034316 (2002).
11. E. Galindo *et al.*, Phys. Rev. C 69 024304 (2004).
12. C. García-Recio, M.F.M Lutz, J. Nieves, Phys. Lett. B 582, 49 (2004).
13. H. Garcilazo, E. Moya de Guerra, Nucl. Phys. A 562, 521 (1993).
14. H. Garcilazo, A. Valcarce, F. Fernández, Phys. Rev. C 64, 058201 (2001).
15. M.V. Green *et al.*, Comput. Med. Imaging and Graphics 25, 79 (2001).
16. H. Jeppesen *et al.*, Nucl. Phys A 738, 511 (2004).
17. A. Jungclaus *et al.*, Phys. Rev. C 67 034302 (2003).
18. K. Langanke, G. Martínez-Pinedo, Rev. Mod. Phys. 75, 819 (2003).
19. K. Langanke, G. Martínez-Pinedo, P. von Neumann-Cosel, A. Richter, Phys. Rev. Lett. 93, 202501 (2004).
20. P. Lava, M.C. Martínez, J. Ryckebusch, J.A. Caballero, J.M. Udías, Phys.Lett. B 595, 177 (2004).
21. F.J. Llanes-Estrada, E. Oset, V. Mateu, Phys. Rev. C 69, 055203 (2004).

22. F.J. Llanes-Estrada, Proc. Workshop on e+ e- in the 1-GeV to 2-GeV Range: Physics and Accelerator Prospects - ICFA Mini-workshp - Working Group on HIgh Luminosity e+ e- Colliders, Alghero, Sardinia, Italy (2003).

23. C. Merlet, X. Llovet, F. Salvat, X-Ray Spectrom. 33, 376 (2004).

24. E. Nacher *et al.*, Phys. Rev. Lett. 92, 232501 (2004).

25. J. Nieves, J.E. Amaro, M. Valverde, Phys. Rev. C 70, 055503 (2004).

26. S.K. Patra, M. Centelles, X. Vias, M. del Estal, Nucl. Phys. A 703, 240 (2002).

27. Y. Prezado *et al.*, Phys. Lett. B 576, 55 (2003).

28. J.M. Quesada *et al.*, Comp. Phys. Comm. 153, 97 (2003).

29. J.M. Quesada *et al.*, Phys. Rev. C 67, 067601 (2003).

30. J. Sempau, J.M. Fernández-Varea, E. Acosta, F. Salvat, Nucl. Instr. Meth. Phys. Res. B 207, 107 (2003).

31. S. Strauch, S. Dieterich, *et al.*, (The Jefferson Lab E93-049 Collaboration), Phys. Rev. Lett. 91, 052301 (2003).

32. J.J. Vaquero *et al.*, IEEE Trans on Nuclear Science 48, 1440 (2001).

33. J. Vijande, P. Gonzalez, H. Garcilazo, A. Valcarce, Phys. Rev. D 69, 074019 (2004).

34. L. Weissman *et al.*, Phys. Rev. C 70, 024304 (2004).